Self-Assembled Host-Guest Thin Films for Functional Interfaces

Christine Julia Erdy

Thesis submitted to the faculty of Virginia Polytechnic Institute and State University
In fulfillment of the requirement for the degree of

Masters of Science
In
Chemical Engineering

Advisory Committee:

Stephen M. Martin, PhD., Chairman
Richey Davis, PhD.
William Ducker, PhD.

December 8, 2008
Blacksburg, VA

Keywords: Langmuir-Blodgett film, self-assembled monolayer, surface modification, host-guest films, X-ray diffraction, specular reflectivity

Self-Assembled Host-Guest Thin Films for Functional Interfaces

Christine Erdy

(ABSTRACT)

The functionalization of surfaces has received attention because the process allows the design and tailoring of substrate surfaces with a new or improved function. 'Host-guest' thin film complexes are composed of 'host' molecules attached the substrate surface, either through physisorption or covalent bonds, with cavities for the inclusion of desired 'guest' molecules for the functionalization of the surface. Two methods for fabricating functional 'host-guest' thin films were investigated: Langmuir-Blodgett (LB) deposition and self-assembly monolayer (SAM). Langmuir films were created at the air-water interface using octadecanesulfonic acid (C18S) as the amphiphilic 'host' molecules separated by hydrophilic guanidinium (**G**) spacer molecules, which created a cavity allowing the inclusion of desired 'guest' molecules. Surface pressure-area isotherms of the (**G**)C18S, with and without guests, are characterized by the lift-off molecular areas and are use to determine the proper deposition surface pressure. 'Host-guest' Langmuir films are deposited onto silicon substrates using the LB deposition technique. The LB films were then subjected to stability testing using different solvents over increasing periods of time. Grazing-angle incidence X-ray diffraction (GIXD), specular X-ray reflectivity (XRR) and transfer ratio measurements were used to characterize the crystallinity, film thickness, overall film stability and film coverage. The GIXD data revealed that the crystallinity of the deposited film varies with the 'guest' molecules and

can be disrupted by the functional group on the 'guest' molecule through hydrogen bonding. After modeling the XRR data using StochFit, it was discovered that the more polar solvent, tetrahydrofuran (THF), removed the film completely while the nonpolar solvent, hexane, compacted the thin film and increased the electron density. With transfer ratios around 0.95 to 1.05, the deposited films were homogenous.

The second method used was self-assembly monolayers, which differs from Langmuir films in that they are created by a spontaneous chemical synthesis from immersing a substrate into a solution containing an active surfactant. Octadecyltrichlorosilane (OTS) was used initially as a molecule to study the self-assembled monolayer procedure. To study a 'host-guest' self-assembled monolayer system, a compound is being synthesized from 9-bromoanthracene. This compound would already contain the cavity necessary for the inclusion of 'guest' molecules. The solution that contained OTS was composed of a 4:1 mixture of anhydrous octadecane: chloroform. Silicon substrates with a deposited oxide layer were hydroxylated for the surfactant binding chemical reaction to occur. The OTS SAMs were exposed to the same stability tests as the LB films. Surface contact angle measurements were taken of the OTS SAMs before and after the stability tests. The contact angle prior to the stability tests was 110° (±2°). The contact angle after immersion in THF was 101° (±2°) while the contact angle resulting from immersion in hexane was 105° (±2°). From the contact angle measurements, the degradation of the OTS SAMs was less extensive than that of the (**G**)C18S LB films.

Acknowledgements

First, I would like to thank the faculty and staff of the Chemical Engineering Department at Virginia Tech for their support both academically and financially. I cannot fully express how grateful I am for the opportunities Virginia Tech has given me.

I would like to individually thank Dr. Stephen Martin for his knowledge, encouragement, and patience in helping make this project possible. His guidance allowed me to make the most of my stay at Virginia Tech and to create work of which I am proud of. Without his advocacy I could not have accomplished the goals I had set while at Virginia Tech.

In addition, I would like to thank Dr. Davis and Dr. Ducker for being on my defense committee. Also, a special thanks goes out to Eric Stonehill for all the help he provided in the lab during the Summer and Fall 2008 semesters.

I would like to thank Stanford University for permitting me to use the beamlines at Stanford Synchrotron Radiation Laboratory (SSRL), which is part of the Stanford Linear Accelerator Center (SLAC) facility. I would like to extend a special thanks to Mike Toney at Stanford University for his help analyzing diffraction data from SSRL. The advice and knowledge he shared with me made completing this work possible.

Finally, I would like to thank my family, my mom and dad, Kathy and Jim, for their support, patience and love. I would also like to thank Rebecca, my sister, and the many close friends, Darryl, Jose, Gaby, etc who have always supported me over the years.

Table of Contents

List of Abbreviations

Chloroform	$CHCl_3$
Cholestearyl stearate	C18chol
Grazing Incidence X-ray Diffraction	GIXD
Guanidinium ion	G
Langmuir-Blodgett	LB
Magnesium	Mg
Nuclear Magnetic Resonance	NMR
Octadecane	C18
Octadecanesulfonic acid-sodium salt	NaC18S
Octadecanol	C18OH
Octadecyltrichlorosilane	OTS
Poly(tetrafluoroethene)	PTFE
Self Assembled Monolayer	SAM
Specular X-ray Reflectivity	XRR
Stanford Linear Accelerator Center	SLAC
Stanford Synchrotron Radiation Laboratory	SSRL
Thin Layer Chromatography	TLC

List of Figures

List of Tables

1. Introduction

Interest in the functionalization of substrates from deposited 'host-guest' thin films stemmed from the potential for these interfaces to interact selectively with the surrounding environment. All the chemical structures used in this chapter were created using ChemSketch [1] and the schematics were created using Canvas 11.0 [2].

1.1 Amphiphilic Molecules

Amphiphilic molecules are typically chosen as monolayer-forming materials. They are insoluble in water and are composed of two distinct regions: a hydrophilic, or "water-loving," head group that prefers to be immersed in water, and a hydrophobic, or "water-hating," long alkyl chain tail that prefers to reside in the air or in a nonpolar solvent. A classic example of an amphiphile is stearic acid ($C_{17}H_{35}CO_2H$).

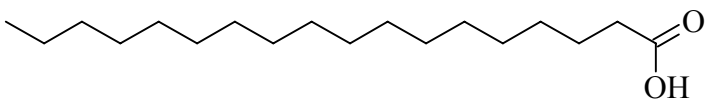

Figure 1.1. Schematic of the molecular structure of stearic acid. The long hydrocarbon tail is hydrophobic while the carboxylic acid head group is hydrophilic.

As seen from Figure 1.1, the long hydrocarbon chain ($C_{17}H_{35}$-) is hydrophobic and the carboxylic acid head group (-CO_2H) is hydrophilic. The hydrophilic head group will dissociate in water and become negatively charged [3]. It is because of this hydrophobic and hydrophilic nature of an amphiphile, they are likely to be located at interfaces such as between air and liquid, which is the reason they are called surfactants or surface active materials.

The amphiphilic molecule is usually mixed with a water-immiscible solvent. Some necessary properties for a solvent are: it must dissolve an adequate quantity of the monolayer material (concentrations of 0.1-1 kg m^{-2}) [4]; it must not react chemically with the material or dissolve the subphase [4]; finally the solvent must evaporate within a reasonable period so no trace remains in the condensed monolayer [4] and the solvent must have a positive spreading coefficient [5]. The spreading coefficient is a measurement of the work done by spreading of a liquid over an area of another liquid. If the spreading coefficient is greater than zero, the liquid spreads completely, whereas if it is less than zero, the drop does not spread completely [5].

1.2 Langmuir Monolayer

To form a Langmuir monolayer, a solution is prepared by dissolving amphiphiles in a volatile organic solvent. When the solution is spread over the subphase, the solvent evaporates leaving a monolayer of the amphiphiles above the surface, as indicated in Figure 1.2, with the hydrophilic groups inside the subphase and hydrophobic groups above the subphase.

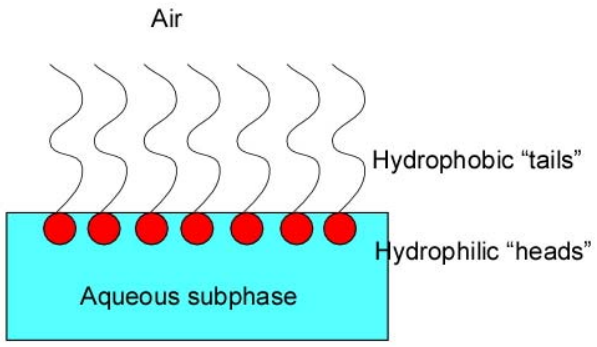

Figure 1.2. Schematic illustrating a Langmuir monolayer. It should be noted that it is a common convention to represent the hydrophilic 'head' group as a circular dot and the hydrophobic 'tail' group as a straight line; however, these do not adequately represent the relative sizes of the sections.

Specialized equipment is needed for the formation of Langmuir films and their subsequent deposition. The subphase container needed for monolayer formation is referred to as a Langmuir or Langmuir-Blodgett trough. Since the material used for the trough comes into direct contact with the subphase, there are requirements for the material used, such as the material must be inert, must not release impurities into the subphase, hydrophobic in nature, withstand organic solvents and easy to shape to aid fabrication [6]. For this reason, polytetrafluoroethylene (PTFE) or its co-polymers are used.

Movable barriers are an integral piece of the trough. The barriers allow for control over the pressure applied to the monolayer. They are also made from PTFE or its co-polymers. There are two basic types of barrier systems used: constant perimeter barrier and movable barrier. In a constant perimeter trough, the surface pressure is increased by varying the shape of the perimeter while keeping its length constant [7]. A disadvantage of this system is that the rollers are required to operate within the active area, creating potential sites for entrapment of the monolayer and possible sources of particulate contamination [8]. In the moving barrier system, the surface pressure is increased by a movable barrier which decreases the actual size of the active area [7]. The movable barrier system is the most popular LB trough.

1.3 Surface Pressure – Area Isotherms

The single most important indicator of the monolayer properties of a material is given by a plot of the surface pressure as a function of the area of subphase surface available to each molecule [6]. The plot is known as a surface pressure – area isotherm and is often abbreviated as “isotherm”. It results from the compression of the

amphiphiles, forming a two-dimensional monomolecular layer on the subphase that is held together by Van der Waals forces [7]. During compression, the changes in the surface pressure are monitored using a Wilhelmy plate. The procedure for using the Wilhelmy plate involves the plate being completely wetted by the subphase liquid and measuring the change in force due to surface tension while remaining stationary. Figure 1.3 shows a schematic of a rectangular Wilhelmy plate.

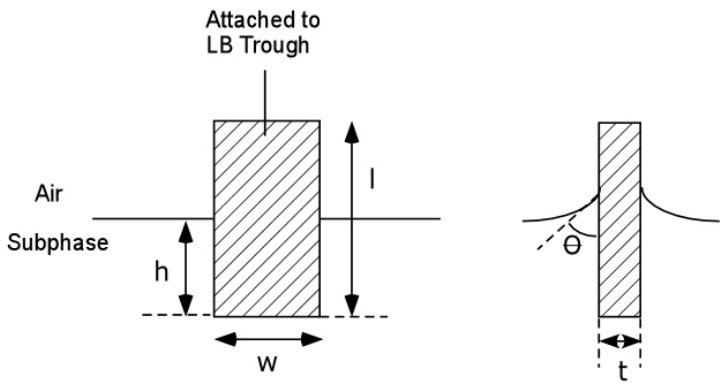

Figure 1.3. Schematic of a front and side view showing the dimensions for this rectangular Wilhelmy plate. The forces acting on the plate consist of gravity and surface tension pulling down and buoyancy pushing upward.

The forces acting on the plate are gravity and surface tension pulling down and buoyancy, due to displaced water, pushing upwards [4]. For a rectangular plate of dimensions l, w and t (as seen in Figure 1.3), and of material of density ρ_P, immersed to depth h in a liquid density of ρ_L the net downward force, F, is given by Equation 1.1

$$F = \rho_P glwt + 2\gamma\left(t + w\right)\cos\theta - \rho_L gtwh \qquad (1.1)$$

where γ is the surface tension of the liquid, θ is the contact angle on the solid plate and g is the gravitational constant [6]. The surface tension can be defined as the reversible work done in creating unit area of new surface [9]. The change in surface tension, $\Delta\gamma$

(mN m^{-1}), on a stationary Wilhelmy plate that is completely wetted by the subphase, so $\theta = 0$ and the $\cos(0) = 1$, is represented by the following equation [4]:

$$\Delta\gamma = \Delta F / 2(t + w) \tag{1.2}$$

If the plate is thin such that $t \ll w$, then

$$\Delta\gamma = \Delta F / 2w \tag{1.3}$$

There are two disadvantages of using the Wilhelmy balance. The first problem is keeping the contact angle constant. As the surface pressure increases, so does the possibility of depositing monolayer molecules onto the plate, changing the value of the contact angle. The second problem is possible contamination of the plate resulting from reusing the plate for multiple experiments. This can be easily avoided if a fresh plate is used for each new experiment, thus minimizing contamination from previous runs.

Initially, when the solution containing the amphiphilic molecules is first deposited, the molecules are very spread out; therefore, their interactions are small. Under these conditions, the monolayer has relatively little impact on the surface tension. As the barriers of the trough start to compress, the surface area available to the monolayer decreases which has an impact on the surface tension as the molecules exert repulsive forces on each other. The change in surface pressure (Π, mN m^{-1}) can be represented by the following equation:

$$\Pi = \gamma - \gamma_0 \tag{1.4}$$

where γ is the surface tension in the absence of a monolayer and γ_0 the value with the monolayer present [6]. The change in the surface pressure is then plotted against the change in area per surfactant (nm^2 $surfactant^{-1}$). The resulting isotherm contains

information on stability of the monolayer at the air-water interface, the reorientation of molecules in the two-dimensional system, phase transitions and conformational transformations[3]. The deposition conditions are also characterized from the surface pressure – area (Π – A) isotherm of the monolayer.

From the isotherm, a number of distinct regions become apparent that indicates the phase changes experienced by the monolayer at its molecules change orientation. Figure 1.4 illustrates the phase transitions typically seen from a Π – A isotherm of stearic acid on a subphase of 0.01 M HCl. This figure was adapted from Figure 2.7 on page 114 in An Introduction to Ultrathin Organic Films: from Langmuir-Blodgett to Self-Assembly by Abraham Ulman.

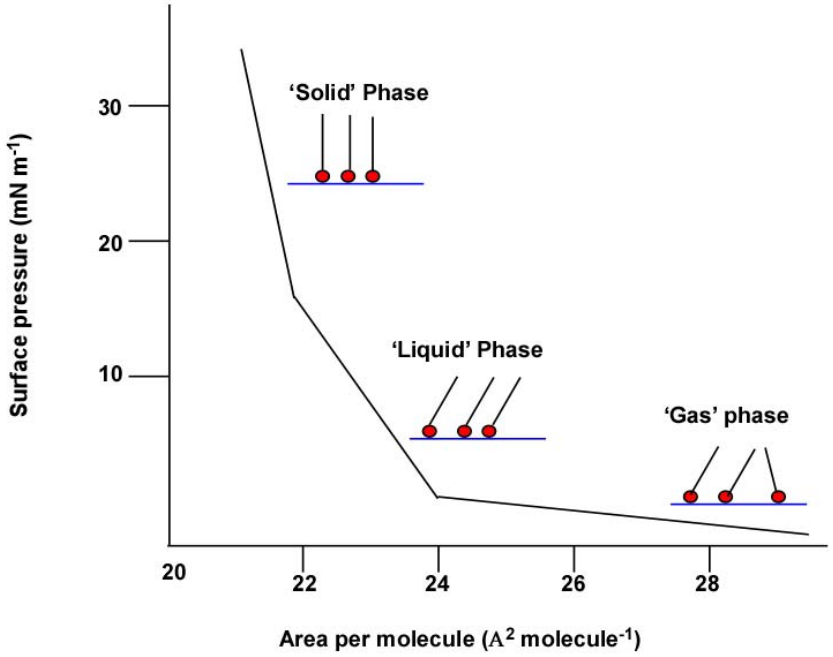

Figure 1.4. A schematic of surface pressure (Π) vs. area per molecule (A) for stearic acid on a subphase of 0.01M HCl [3]. The area per molecule in the 'gas' phase is large; therefore, the surface pressure is low because ideally there should be no interaction between molecules. As the barriers start to compress, the first transition observed is from the 'gas' to the 'liquid' state at ~ 24Å^2. When the barriers compress the film even further, a second transition is seen from the 'liquid' to 'solid' state at ~ 21Å^2. At this stage, the molecules are closely packed and uniformly oriented.

Prior to compression, the hydrophobic chains of monolayer molecules were distributed near the subphase. As the barriers being to compress, the hydrophobic chains are lifted from the subphase and the monolayer is in its 'gaseous' state, represented by the first labeled phase in Figure 1.4. In this state the molecules are far enough apart that they exert little force on one another [4].

As the barriers continue to move towards each other, the spacing between molecules decreases and a second phase transition occurs, which can be seen from Figure 1.4 when the slope becomes steep and linear in form. The monolayer has entered what is known as its 'liquid' state, which is generally called the 'expanded' monolayer phase. The hydrocarbon chains in the film are in a random rather than a uniform orientation, with their polar groups in contact with the subphase [4]. From the isotherm for stearic acid on a subphase of 0.01M HCl, this phase transition occurs at a surface area of approximately $24 Å^2$ $molecule^{-1}$.

As the molecular area available to the molecules is reduced even further, another abrupt change in the slope becomes apparent in the isotherm. This is due to the monolayer entering into a 'solid' or 'condensed' phase. In the 'solid' phase, there is a transition to an ordered solid-like arrangement of the molecules [6]. A schematic of the molecular orientation during this phase is shown in Figure 1.4. At this stage, the area per molecules for a single stearic acid is approximately $21 Å^2$. This is the ideal phase for film deposition to occur.

As the film is compressed past the 'solid' phase, the monolayer collapses due to mechanical instability and a sharp decrease in the surface pressure is observed [6]. The surface area at which the collapse begins usually depends on the rate of film

compression. During this phase transition, the monolayer molecules may ride on top of each other and form disordered multilayers.

A wealth of useful information about molecular sizes and intermolecular forces can be obtained from studies of monolayers on the water surface, but the great resurgence of interest in this area of science has been largely due to the fact that films can be transferred from the water surface onto a solid substrate using what has become universally known as the Langmuir-Blodgett (LB) technique [6].

1.4 Langmuir-Blodgett Deposition

While a wealth of useful information about molecular sizes and intermolecular forces can obtained from studies of monolayers at the water surface, the deposition of these films onto solid substrates have received a considerable amount of scientific attention because the technique may ultimately lead to new materials with tailored properties [10]. Throughout the thesis, the term Langmuir film refers to the molecular film at the air-liquid interface while the term Langmuir-Blodgett (LB) films is used to denote monolayers transferred from the liquid-gas interface onto a solid substrate. The molecules within the LB film adhere to the substrate through physisorption where the atoms adhere to the surface through weak intermolecular forces such as Van der Waals forces. This monolayer and multilayer arrangement was first discussed by Irving Langmuir in 1917 [11] and further pioneered by Katherine Blodgett [12] in 1935.

A conventional method for film deposition is known as the vertical deposition where the monolayer of amphiphiles at the air-water interface is deposited by the displacement of a vertical plate [3]. Figure 1.5 illustrates the deposition of a monolayer onto a solid substrate from the air-water interface.

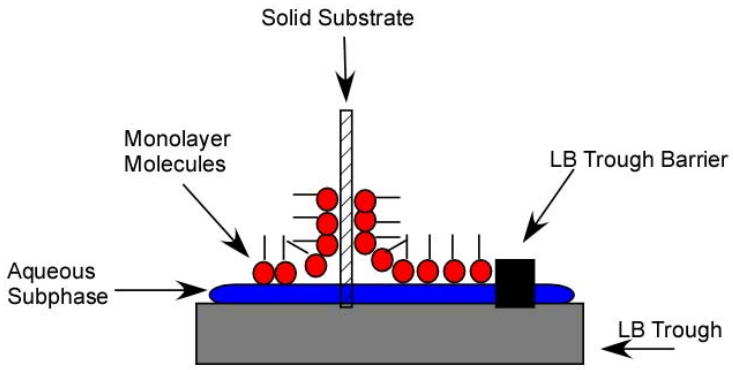

Figure 1.5. A schematic showing the vertical deposition of monolayer molecules from the air-water interface onto a vertical substrate. If the substrate is hydrophilic, the monolayer is deposited as the substrate is retracted from the subphase with the polar head groups being physisorbed to the substrate. If the substrate is hydrophobic, the monolayer is deposited as the substrate is being immersed in the subphase with the molecules nonpolar tail groups being physisorbed to the substrate. This figure was adapted from Figure 2.10 in An Introduction to Ultrathin Organic Films: from Langmuir-Blodgett to Self-Assembly.

Hydrophilic substrates, such as glass or silicon, are the most commonly used substrate for LB deposition. The hydrophilic substrate is first lowered into the subphase before the monolayer is spread. After the monolayer is spread and compressed, the substrate is raised out of the subphase, thus depositing the first layer. During this deposition process, the surface pressure is kept constant. On the other hand, if the substrate is hydrophobic, the substrate is lowered into the subphase after the monolayer has been spread and compressed, thus deposition will start on the first immersion into the subphase.

Once the first layer is deposited, three different types of multilayers are possible: X, Y and Z types. If it is only possible for subsequent depositions to occur as the substrate is being immersed into the subphase, it is known as an X type [6]. If a monolayer is deposited each time the substrate traverses the air-water interface, it is known as a Y type. Z type is the third type of film deposition where the monolayer can

only be deposited onto the substrate during the upstroke. Figure 1.6 illustrates the X, Y and Z type depositions.

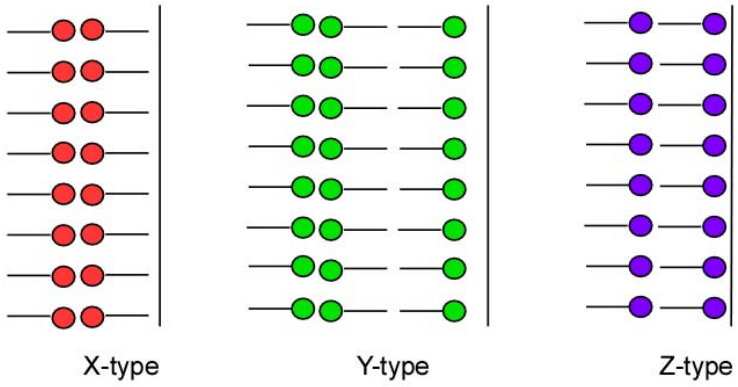

Figure 1.6. Structure of X and Z types monolayer depositions and Y type multilayer deposition. An X type is created if it is only possible for subsequent depositions to occur as the substrate is being immersed into the subphase. A Y type is created if a monolayer is deposited each time the substrate traverses the air-water interface. A Z type is created when the monolayer can only be deposited onto the substrate during the upstroke.

A simple method to characterize the coverage of the monolayer film on the substrate surface is the deposition (transfer) ratio,

$$\tau = A_L / A_S \qquad (1.5)$$

where A_L is the decrease in the area occupied by the monolayer on the subphase surface and A_S is the coated area of the solid substrate [6]. Transfer ratios significantly outside the range 0.95 to 1.05 suggest poor film homogeneity [4]and a transfer ratio equal to 1 implies that the two-dimensional density of the monolayer does not change upon its transfer onto a solid substrate [13]. LB studies have shown that higher transfer ratios can be achieved with close-packed, condensed-phase monolayers compressed to surface pressures exceeding the main monolayer phase transition pressure [13].

Factors that can affect the transfer ratio include changes in surface pressure, deposition velocity, substrate wettability and roughness, pH and temperature of the subphase and interaction with counterions [13]. The speed at which the substrate is withdrawn from the subphase can also affect the transfer ratio. It is important not to raise the substrate through the floating monolayer faster than the rate at which water drains from the solid [4]. The drainage of water is due to the adhesion between the monolayer and substrate. It is normal to transfer the initial monolayer onto a solid substrate relatively slowly: speeds of 10μm s^{-1} to a few mm min^{-1}.

1.5 Self-Assembled Monolayers

The other most common method for forming functional host-guest thin films is known as the self-assembled monolayer (SAMs) technique, which differs from the LB technique in that the LB technique produces films through physisorbed monolayers while SAMs produce films through chemisorbed monolayers which form relatively stronger molecule-substrate bonds. SAMs are distinguished from ordinary surfactant monolayers by the fact that one end of the molecule, generally the hydrophilic one, is designed to have a favorable and specific interaction with the substrate surface [14]. SAM molecules can be divided into three sections: a head group, alkyl chain and a terminal functional group. This structure is illustrated in Figure 1.7

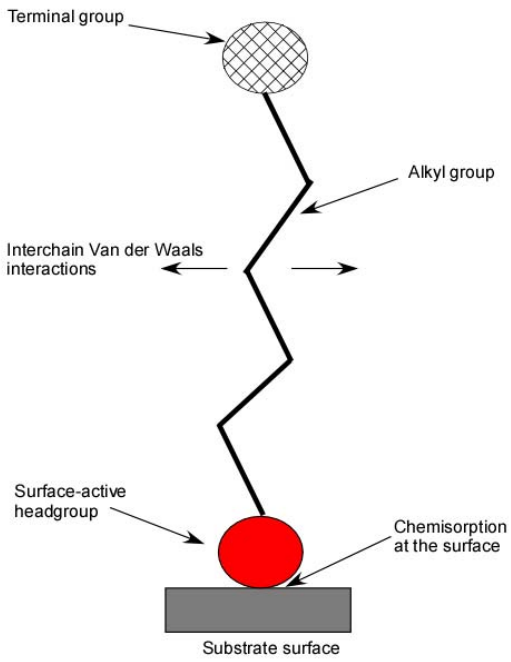

Figure 1.7. A schematic illustrating the different sections of a self-assembled monolayer deposited on a solid substrate. The head group forms the chemical bond with surface atoms of the substrate. The alkyl chain experience inter-chain Van der Waals interactions, which could aid in the ordering of the molecules. The terminal group can be many different functional groups to obtain a specific surface activity.

As stated earlier, the bond that forms between the head group of the surfactant molecule and the substrate is through chemisorption. The very strong molecular-substrate interactions result in an apparent pinning of the head group to a specific site on the surface through a chemical bond [3]. The head group is primarily composed of either a sulfur or silicon group, thus forming alkanethiols and alkylsilanes, respectively. For an alkanethiol, the monolayer undergoes a sulfur-gold (Au) interaction that binds it to the gold-coated surface forming a polar covalent bond, while an alkylsilanes experiences a silicon-hydroxylated surface interaction and forms a covalent Si-O bond. The energies associated with the chemisorption are at the order of tens of kcal/mol (e.g. ~40-45 kcal/mol for thiolate on gold) [3]. This exothermic formation of covalent bonds of

molecule to surface is similar to the pressure exerted by the Langmuir trough barriers in that it is the spontaneous adsorption that brings molecules close together.

The second molecular part is the alkyl chain as illustrated in Figure 1.7. As a result of the spontaneous molecular adsorption of the head groups to the substrate, the molecules are brought close enough together to allow for short-range Van der Waals forces interactions between the alkyl chains. The energies associated with this interchain Van der Waals interactions are on the order of a few (<10) kcal/mol [3]. These interactions could assist in the formation of ordered molecular structures, which depends on the pinning density of the head group [15]. Depending on surface coverage, the alkyl chains will have a tilt from the surface normal where the higher the packing density, the lower the tilt angle [15].

The third molecular part is the terminal functional group. The chemical functionality and packing structure of the terminal groups determine the outermost surface structure and interfacial properties of SAMs [16].

Two-dimensional molecular organization is a key ingredient for SAM stability and function [14]. There is an evolution of molecular order as adsorption progresses and surface coverage increases. The very early stages of adsorption can be pictures as isolated adsorbed molecules, conformationally disordered and randomly distributed on the substrate [14]. The final film involves close-packed adsorbate molecules with relatively uniform molecular orientation and confirmation.

In typical procedure for deposition of an alkylsilane SAM, a hydroxylated surface is immersed in a solution of alkyltrichlorosilane in an organic solvent. SAM formation includes a diffusion process of the reacting molecule to the surface and an adsorption

process at the surface [17]. During adsorption, Si-Cl bonds react with the OH groups present on the surface of the substrate and with trace water to form a network of Si-O-Si bonds [3]. The driving force for this self-assembly is the in situ formation of polysiloxane, which is connected to surface silanol groups (-SiOH) via Si-O-Si bonds [18].

The first part of the process to occur is physisorption of the molecules at the hydrated substrate surface followed by hydrolysis. Hydrolysis occurs in the presence of the adsorbed trace water layer on the substrate surface resulting in the highly polar trihydroxysilane $-Si(OH)_3$ [15]. The OH groups now attach to the Si atoms in the substrate surface to which the water was previously bound [19] by forming covalent bonds with the hydroxyl groups on the surface followed by a condensation reaction [15].

The procedure to form an alkanethiol SAM is differs slightly from that of an alkylsilane SAM. A fresh, clean, hydrophilic gold substrate (which is the typical substrate used) is immersed into a dilute solution of the organosulfur compound in an organic solvent [3]. It is generally believed that the adsorption process takes place by elimination of the terminal hydrogen atom and that the thiol is bound to the gold by a true valence bond [19].

Although thiols on gold and silanes on silicon are the most prominent examples, they are no the only self-assembling systems [17]. Various substrates other than gold and silicon oxide are capable of binding SAMs such as silver, copper, palladium and metal oxides. Also, organic molecules alcohols, amines, organic acids or isocyanides have been used as SAM molecules [17].

1.6 Surface Characterization

This section covers various methods used to analyze and characterize the deposited thin films. Grazing incidence X-ray diffraction (GIXD) and specular X-ray reflectivity (XRR) are methods used to determine the thickness and structure of LB films and SAMs. Contact angles were used to determine the coverage of the SAMs.

1.6.1 X-ray Diffraction

X-rays interact weakly with matter, and this gives them a number of advantages: multiple scattering can often be neglected (unlike electrons), and X-rays penetrate significant distances (typically of the order of 0.1 to 10 mm, depending on the material and the X-ray energy), allowing them to obtain microscopic structural information averaged over a large ensemble of atoms or molecules [20].

The smallest region that completely describes the crystalline pattern is known as the unit cell [MSE 62]. The lengths of the unit cell edges along the x, y, and z axes, respectively, are labeled a, b, and c. The angles between the axes are α, β, and γ with α between b and c, β between a and c, and γ between a and b [21].

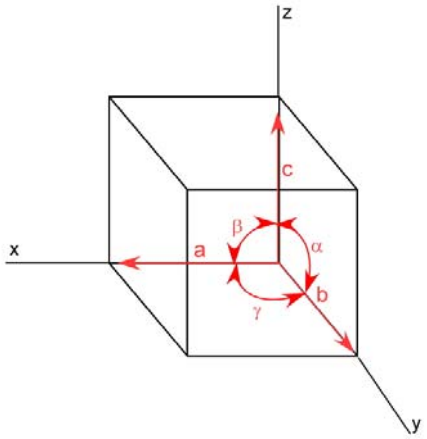

Figure 1.8. Schematic that represents the unit cell of a three-dimensional crystal. The lengths of the unit cell edges along the x, y, and z axes, respectively, are labeled a, b, and c. The angles between the axes are α, β, and γ with α between b and c, β between a and c, and γ between a and b.

Since the angles between the axes are not always at right angles, crystals belong to seven possible systems, characterized by the geometry of the unit cell [4].

Table 1-1: The seven basic crystal systems.

System	Relationship among Lattice Parameters
Triclinic	$a \neq b \neq c$; $\alpha \neq \beta \neq \gamma \neq 90°$
Monoclinic	$a \neq b \neq c$; $\alpha = \gamma = 90$; $\beta \neq 90°$
Orthorhombic	$a \neq b \neq c$; $\alpha = \beta = \gamma = 90°$
Tetragonal	$a = b \neq c$; $\alpha = \beta = \gamma = 90°$
Hexagonal	$a = b \neq c$; $\alpha = \beta = 120°$ $\gamma = 90°$
Rhombohedral	$a = b = c$; $\alpha = \beta = \gamma \neq 90°$
Cubic	$a = b = c$; $\alpha = \beta = \gamma = 90°$

Many planes can be drawn through the lattice points of a crystal structure and diffraction of X-rays by the crystal can be treated as reflections of the X-ray beam by these planes [4]. Miller indices can be used in any of three ways: to designate a set of

lattice planes, a particular member of the set, or the face of a macroscopic crystal parallel to the set [21]. The most common notation for lattice planes is h, k, and l.

When there is constructive interference from X-rays scattered by the atomic planes in a crystal, a diffraction peak is observed [22]. The condition for constructive interference from planes with spacing d is given by Bragg's law:

$$2d \sin\theta = n\lambda \qquad (1.5)$$

where θ is the angle between the atomic planes and the incident (and diffracted) X-ray beam [22]. The process of reflection can be viewed involving a fixed incident beam, in which case reflection occurs from planes set at the angle θ with respect to the beam and generates a reflected ray deviating through 2θ [21]. Thin films can also consist of many grains or crystallites having a distribution of orientations [22]. Therefore, diffraction can occur from any crystallite that has the right orientation. The diffracted X-rays emerge as cones about the incident beam with an opening angle of 2θ, creating a "powder" diffraction pattern [22].

It is more common to look at diffraction patterns using a reciprocal lattice. So, Bragg's law can be arranged to take the form of

$$\sin\theta = \frac{n\lambda}{2}\left(\frac{1}{d}\right) \qquad (1.7)$$

showing that sin θ is inversely proportional to *d*. Since sin θ is a measure of the deviation of the diffracted beam from the direct beam, it is evident that structures with large *d* will exhibit compressed diffraction patterns [21]. To help the analysis of diffraction data, a direct relationship between sin θ and d is needed; therefore, a reciprocal lattice can be created based on 1/*d*, which varies directly with sin θ.

The reciprocal lattice can be defined as follows: Consider normals to all possible direct lattice planes (h, k, l) to radiate from some lattice point taken as the origin [21]. Terminate each normal at a point at a distance $1/d_{hkl}$ from the origin, where d_{hkl} is the perpendicular distance between planes of the set (hkl) [21]. The set of points so determined constitutes the reciprocal lattice [21].

1.6.2 Grazing Incidence X-ray Diffraction

A method restricting the penetration depth to the surface region is a prerequisite for all surface diffraction/scattering experiments, which can be achieved by using grazing angles of incidence [23]. The grazing incidence geometry is surface selective meaning it largely avoids scattering from the substrate and does not require a transparent substrate [20]. The grazing incidence x-ray diffraction (GIXD) method is a hybrid technique that is based on diffraction and on the extreme surface sensitivity of incident x-rays close to the critical angle [24]. GIXD also employs the phenomenon of total external reflection from the surface occurring for angles of incidence smaller or equal to the critical angle, α_C [25].

The refractive index, n, of matter for X-rays in the 1 Å wavelength range is give by

$$n = 1 - \delta - i\beta \qquad (1.6)$$

where $\delta = \rho r_0 \lambda^2 / 2\pi$ with ρ is the electronic density, λ is the wavelength and r_0 is the Bohr radius of the electron (2.82 x 10^{-13} cm) [25]. The term β is equal to $-\mu / 2\kappa$ where μ is the linear absorption coefficient, however, for X-rays of wavelength ≈ 1 Å, absorption is small and $\beta << \delta$ [23].

As n < 1, for angles of incidence α_i less than or equal to the critical angle α_C, which is defined as $\alpha_C = \cos^{-1}(n) = (2\delta)^{1/2}$, total reflection occurs [23]. The incident wave is totally reflected, while the refracted wave becomes evanescent travelling along the surface [25]. Since the amplitude of the evanescent wave decays exponentially with depth, it cane be diffracted by a crystalline thin film lying on the surface [25] and provide information on its inplane structure [23].

For a two-dimensional crystal, diffraction occurs if there is two-dimensional crystalline order of sufficiently long range [26]. Only the a and b vectors of the unit cell are considered, for a two-dimensional crystal, the diffraction is governed by Bragg's law and the horizontal component q_{xy} of the scattering vector in the plane must coincide with a reciprocal lattice vector q_{hk} where

$$q_{xy} = 2\pi d^* = 2\pi\left(ha^* + kb^*\right) \qquad (1.7)$$

where d* is the reciprocal of the interplanar spacing d, a* and b* are the reciprocal vectors of the unit cell axes a and b, and h and k are integers that represent the Miller indices of planes with a space $d_{hk} = 1/d^*_{hk}$ [23]. The conditions needed for diffraction to occur in a two-dimensional crystal are illustrated in Figure 1.9.

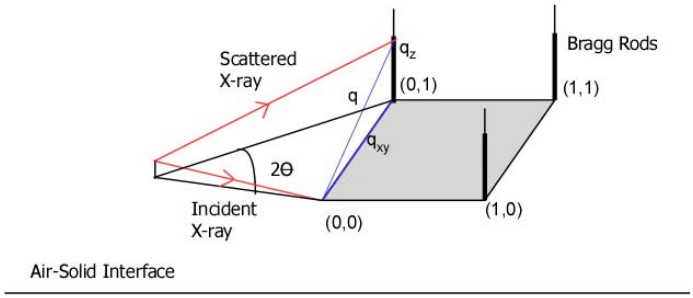

Figure 1.9. Schematic illustrating conditions needed for diffraction to occur for a two-dimensional crystal. It requires that the horizontal component q_{xy} of the scattering vector must coincide with a reciprocal lattice vector q_{hk} where $q_{xy} = 2\pi d^* = 2\pi\left(ha^* + kb^*\right)$ [26].

The two reciprocal lattice vectors a* and b* are parallel to the monolayer plane and a* is orthogonal to b [26]. Thus $\left|a^*\right| = 2\pi / \left(a\sin\gamma\right)$ and $\left|b^*\right| = 2\pi / \left(b\sin\gamma\right)$ where γ is the angle between a and b [26].Since there are no selection rules or restrictions on the scattering vector component q_z along the film normal, the Bragg scattering extends as continuous rods [23]. The angular positions of the Bragg peaks, corresponding to $q_{hk} = \left(4\pi/\lambda\right)\sin\alpha_{hk}$, yields the repeat distance $d_{hk} = 2\pi/q_{hk}$ for the 2-D lattice structure [25].

In the GIXD setup, the angle of incidence of the incoming X-ray beam and outgoing angles of the beam are kept below the critical angle while the diffraction pattern is recorded. This limits the penetration depth in the range of 50 – 100 Å thus removing the X-ray scattering due to the substrate [23]. The x-rays then probe the interplanar spacing of vertically inclined lattice planes [24]. The resulting pattern of Bragg rods is recorded by continuously increasing the scattering angle, 2θ.

Several different types of information may be extracted from the measured profiles: the angular 2θ positions of the Bragg rods yield the repeat distance

$d = 2\pi/q_{xy}$ for the 2-D lattice, Bragg peaks may be indexed by the two Miller indices h, k to yield an a and b unit cell [23] as well as the area of the unit cell, $A_{cell} = ab\sin\gamma$ [26]. Specific forms of the equation $d = 2\pi/q_{xy}$ are possible for the two-dimensional crystal system, as seen in the Table 1-2.

Table 1-2: Two-dimensional crystal systems.

Crystal System	**Unit Cell Parameters**	**d-spacing**
Hexagonal	a = b; γ = 120°	$d = a\left[\left(h^2 + k^2 + hk\right)\right]^{-1/2} 3^{1/2}/2$
Rectangular (centered)	a ≠ b; γ = 90°	$d = \left[\left(h^2/a^2 + k^2/b^2\right)\right]^{-1/2}$
Rectangular	a ≠ b; γ = 90°	$d = \left[\left(h^2/a^2 + k^2/b^2\right)\right]^{-1/2}$
Square	a = b; γ = 90°	$d = \left[\left(h^2 + k^2\right)/a^2\right]^{-1/2}$
Oblique	a ≠ b; γ ≠ 90°	$q_{xy} \approx k\left[\left(1 + \cos^2\left(\alpha_f\right) - 2\cos\left(\alpha_f\right)\cos\left(2\theta_{xy}\right)\right)\right]^{1/2}$

There are disadvantages to using grazing incidence because it works well only with very smooth surfaces and at grazing angles most of the incoming X-ray beam is wasted [20]. For example, assuming an incident angle of 0.1° and a surface dimension of 1 cm, only a 2μm slice of the X-ray beam will fall on the surface; the rest either hits the side or passes over the sample [20]. This is fixed by using a beam that is both compact and collimated, where the X-rays stay parallel and spreads slowly as it propagates, which is provided by synchrotron sources [20]. Also, the diffraction data from a 2-D monolayer

only produces a few Bragg rods due to the very limited amount of matter intercepting the X-ray beam and due to crystalline disorder [26].

1.6.3 Specular X-ray Reflectivity

Specular X-ray reflectivity (XRR) is one of many X-ray techniques that is available for the study of thin films and it offers some unique advantages for working at the small-length scales that are becoming technologically important [27]. Among these are high spatial sensitivity (with roughness and thickness resolution that can be 0.1 nm), high penetration (for measuring buried interfaces or in ambient processing atmospheres), and a nondestructive capability for studying real-time processes [27]. Like other X-ray techniques, in XRR measurements consist of monitoring the intensity of an X-ray beam reflected from a surface relative to the intensity of the incident beam, as a function of the scattering transfer vector, K, defined as $K = k_{\text{reflected}} - k_{\text{incident}}$ [27]. The scattering geometry of specular X-ray reflectivity is illustrated in Figure 1.10. Since the wave vector transfer is only in the z-direction, normal to the interface, $Q_x = Q_y = 0$ where x and y are in the plane of the interface and $Q_z = \left(4\pi/\lambda\right)\sin(\alpha)$ where Q_z is the z component of the wave-vector transfer of the scattered radiation, λ is the X-ray wavelength (Å) and α is the angle of incidence [28].

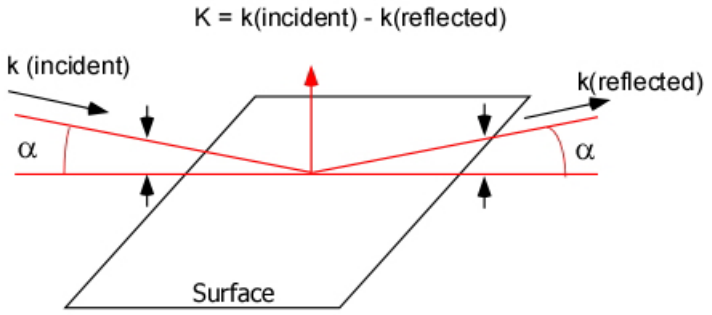

Figure 1.10. Schematic that illustrates the scattering geometry for specular x-ray reflectivity. The scattering transfer vector, K, is normal to the substrate surface; therefore, no information about in-plane structure is obtained.

Specifically, specular reflectivity probes the electron density normal to the interface and averaged over the region of the X-ray footprint on the sample [28]. This is because the reflectivity technique probes smaller magnitudes of K and the incident and reflected angles are equal so that K is oriented for probing structures normal to the surface [27]. This orientation is visualized in Figure 1.10. Reflectivity data consists of measurements of the X-ray intensity measured just before the X-ray strikes the surface [28]. The data is further modified by subtracting a background measured slightly off the specular condition by averaging intensity values at wave vector transfer $Q = \left(0, \Delta Q_y, Q_z\right)$ and $Q = \left(0, -\Delta Q_y, Q_z\right)$ [28]. The reflectivity for an ideal surface is commonly called the Fresnel reflectivity, denoted by the symbol R_F is given by the following equation:

$$R_F = \left(\frac{2Q_Z}{Q_C}\right)^{-4} = \left(\frac{2\left(4\pi/\lambda \sin(\alpha)\right)}{\left(4\pi/\lambda \sin(\alpha_C)\right)}\right)^{-4} \quad (1.8)$$

where λ is the X-ray wavelength (Å), α is the angle of incidence and α_C is the critical angle for total external reflection below which the incident ray is totally reflected from the surface [27].

For nonideal surfaces, scattering results deviate from the Fresnel reflectivity. Als-Nielsen presented a derivation of the results from specular reflection from nonideal surfaces as:

$$R(Q_Z) = \left(\frac{2Q_Z}{Q_C}\right)^{-4} \left|\int \rho'(z) \exp(iQ_z z)\, dz\right|^2 \quad (1.9)$$

where $\rho'(z)$ is the electron density gradient normal to the surface, the term in front of the integral is the Fresnel reflectivity and the integral is the Fourier transform of the electron density gradient normal to the interface [27]. Also, $\rho'(z)$ is the average value of electron density along the z direction and contains no information about the nature of the interface in the x,y-plane [27].

Although X-ray reflectivity spectra contain information about layer thickness and composition, the primary ability of XRR measurements has been in the evaluation of surface and interfacial roughness [27]. Surface roughness, σ, is a measurement of the texture of the surface. The variation of surface height as a function of lateral position by

$$H(r) = h(r) - \langle h \rangle \quad (1.10)$$

where H is the deviation of the surface height, h, from the average value, $\langle h \rangle$, as a function of the lateral position vector, r [27]. The mean square surface roughness is the most basic characterization of the surface profile, given by

$$\sigma^2 = \frac{1}{r_{\max}} \int_0^{r_{\max}} H(r)^2 dr \qquad (1.11)$$

which does not integrate over all r because all information would be lost about the lateral structure of the surface [27].

1.6.4 Contact Angle Measurements

Wetting of liquid on solid surface is a topic of fundamental interest for widespread technological applications [29]. Young's equation is the basis for a quantitative description of the wetting phenomena by relating the contact angle to the interfacial tensions γ_{SG}, γ_{LG}, γ_{SL} [17]:

$$\gamma_{LG} \bullet \cos(\theta) = \gamma_{GS} - \gamma_{SL} \qquad (1.12)$$

The angle, θ, between the solid surface and the tangent to the liquid surface at the line of contact with the solid is known as the contact angle [5]. Figure 1.11 depicts the contact angle created by the interfacial tensions. The contact angle originates from the balance between cohesive forces, forces between liquid molecules, and adhesive forces, forces between liquid molecules and the surface [5].

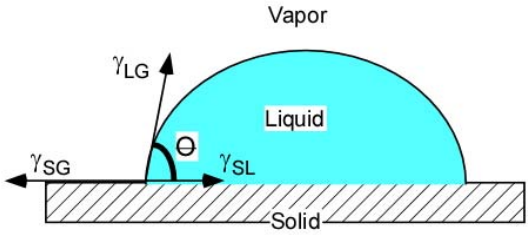

Figure 1.11. A schematic depicting the forces present at the triple interface for a drop of liquid on a solid substrate. If $\theta < 90°$, the liquid is said to wet the solid; if $\theta = 0$, there is complete wetting; if $\theta > 90°$, the liquid does not wet the solid.

Wetting of the surface is determined by the contact angle, if $\theta < 90°$, the liquid is said to wet the solid; if $\theta = 0$, there is complete wetting; if $\theta > 90°$, the liquid does not wet the solid [5]. A surface that has polar groups on it will have a high affinity for water; therefore, will have a strong adhesive force and a low contact angle with water. However, if the surface has non-polar groups on it, it will have a low affinity for water, thus having a low adhesive force and a high contact angle. These surfaces are respectively called hydrophilic and hydrophobic. Clean silicon surfaces are completely hydrophilic ($\theta = 0°$), while the coated surfaces are hydrophobic (not wetted by water, $\theta > 0°$) [3]. This technique is surface sensitive; therefore, the contact angle can be used to detect the presence of films, coatings, or contaminants with a surface energy different from that of the underlying substrate [30]

A review of Langmuir-Blodgett films and self-assembled monolayers is presented here with particular emphasis on the host-guest thin-film systems. Chosen monolayer components as well as the deposition technique employed to generate the deposited thin film are reviewed. Also, potential applications of Langmuir-Blodgett films and self-assembled monolayer thin film systems are discussed.

1.7 Literature Review of Langmuir-Blodgett Films

1.7.1 Background

Langmuir-Blodgett films have received a great deal of attention from the scientific community because the technique can lead to materials with tailored properties. These properties are the result of the arrangement of the amphiphiles with specific 'head' and/or 'tail' groups. Langmuir and Blodgett first studied the detailed structure of fatty acid multilayers obtained by depositing multilayers on a glass slide and investigated the detailed condition for producing such films [31]. However, Langmuir and Blodgett were not the first to engineer this at a molecular level. The Chinese developed an ink that was a suspension of carbon particles in a protein solution which was spread on a water surface to allow a protein monolayer to form. This monolayer was then deposition on paper using the horizontal lift technique [32].

1.7.2 Host-Guest Structures

One of the unique characteristics of LB films is the ability of some organic molecules to display crystalline two-dimensional frameworks which can be used to serve as 'host' films with defined cavities for the inclusion of complementary 'guest' molecules. To clarify the previous sentence, if a crystalline monolayer on water is

composed of two different amphiphile, A and B, which separate into different domains and complement each other, ordered arrays of ABABABAB can occur [23].

In this thesis, guanidinium ions were used as 'spacer' molecules to create the cavities necessary for the inclusion of 'guest' molecules. These ions were dissolved in the deionized water subphase, which then interacted with the 1-octadecanesulfonic acid-sodium salt 'host' film by separating the hydrocarbon chains, thus forming a cavity. A similar method was reported using phenylethylamine as the spacer between the hydrocarbon chains in pentadecylmandelic acid monolayers [33].

Another way to form the cavity necessary for the inclusion of 'guest' molecules is to use a sterically hindering 'host' molecule. A group at the Tokyo Institute of Technology looked at a LB host-guest monolayer containing a phthalocyanines (Pcs) 'host' monolayer system. This system has attracted interest because its space cavity on a water surface can form homogeneous host-guest monolayers. They found that the plane area of the C_{18}PcCu ring was 3.0 nm^2 which should be overlapped with an area of 1.6 nm^2 of eight alkoxy substituents, which left 1.4 nm^2 for the cross-sectional area for guest hydrocarbons molecules [34]. They found that a uniform monolayer was formed using octadecane as a guest at a mixing ratio of $C_{18}H_{38}$:Pc = 7:1.

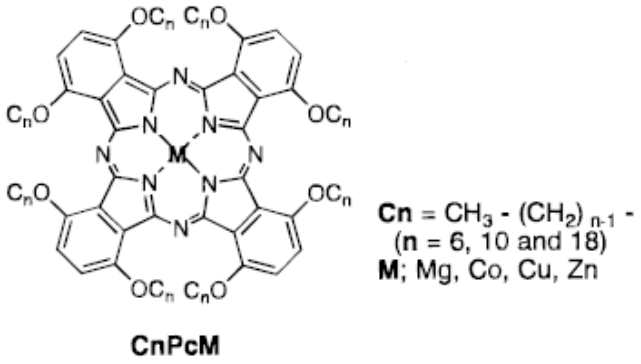

Figure 1.12. Structure of octaalkoxyphthalocyanine metal complex, which has been used as the 'host' molecule in a LB 'host-guest' monolayer, is illustrated. This system has attracted interest because its space cavity on a water surface can form homogeneous host-guest monolayers.

1.7.3 Characterization Techniques

Characterization of a monolayer's molecular structure at surfaces has been an important subject in order not only to understand fundamental interfacial properties but also to gain control of the thin film properties at the molecular level [35]. Identification of the morphology of a Langmuir-Blodgett film and a self-assembled monolayer can be accomplished using a number of analytical techniques. To acquire information about the fabricated LB and SAM films, we used grazing incident X-ray diffraction and specular reflectivity at the Stanford Linear Particle Accelerator in addition to contact angle measurements at Virginia Tech. We had particular interest in using the gathered data to determine the crystal structure, unit cell parameters and thickness of the deposited monolayers.

Previous work done by Dr. Martin investigated the structure of the guanidinium - octadecanesulfonic acid-sodium salt system, G(C18S), at the air-liquid interface. By using the GIXD at HASYLAB in Hamburg, Germany, it was determined that the octadecanesulfonic acid-sodium salt sites were separated by 7.2 – 7.5 Å due to the

guanidinium ions, which allowed the cavities needed for inclusion of the guest molecules which included: octadecane (C18) and cholesteryl stearate (C18chol). For the guest-free G(C18S) system, it was found that the crystals had a rectangular structure with unit cell parameters of a = 5.0 Å, b = 10.2 Å, and $\gamma = 90^{o}$, $A_{cell} = 51.0$ Å^2, with a tilt of 26°. GIXD data of the 1:1 molar mixture of G(C18S):C18 revealed a hexagonal crystal with unit cell parameters of a = 4.97 Å, $\gamma = 120^{o}$, $A_{cell} = 51.0$ Å^2. From the Bragg rods produced by the G(C18S):C18chol, the peaks were indexed as rectangular structure with a = 10.0 Å, b = 7.5 Å, and $\gamma = 90^{o}$ in which the molecules were not tilted.

Using these techniques is common when determining the structure of the film. One group from Northwestern University looked at the structure of monolayer and multilayer LB films of lead stearate monolayer using X-ray diffraction and reflectivity. Since only one peak was seen from the diffraction data for the monolayer LB film of lead stearate, the monolayer has a hexagonal structure and the nearest-neighbor distance was 4.75 Å (19.54 Å^2/molecule), and has an estimated a film thickness around 20 Å determined from the reflectivity data [10].

Another method, which was not used in the study of out thin films, is scanning tunneling microscopy (STM). In STM, the probe is used to measure the value of current which passes between it and the sample where the probe doesn't touch the surface so electron have to pass from the tip to the sample or vice versa by tunneling [36]. Through STM, the topography, or surface structure, can be observed.

1.7.4 Potential applications of LB films

A wide variety of applications exist for Langmuir-Blodgett films because one of the ability to deposit organic layers with an ultrafine control of the layer thickness [37]. Langmuir and Blodgett filled many patents based on their discovery and research with a specific application in mind: skeletonized films. As stated in one of Katherine Blodgett's patents: "An important aspect of my present invention consists in the provision of stratified films in which there are numerous voids…a factor which is significant in respect to the utility of skeleton films…Practically, this feature may be employed in various ways in image reproduction devices." [38]. However, they predicted that there would be a wide range of applications available. In that same patent, Blodgett also stated that the films could be used for optical purposes since film thickness could be controlled [38]. In a later patent, Langmuir proposed the idea of using the skeleton films as a sensor [37]. So, no mater what the commercial prospects are for these films, there is no doubt in the applicability of LB films in fundamental research.

In keeping with the thought of a sensor application, a Russian research group in 2004 presented the idea of using Langmuir Blodgett films as piezoelectric sensor modifiers prepared from β-cyclodextrin (CD). They compared the results of the CD modified sensor to a normal sensor coated in arachic acid (AA, 10 monolayers) and found that the response time of the CD modified sensor was 3-5 times shorter (1-3 minutes against 10-15 minutes for the coating technique) and the detection limit was 2-5 times lower [39].

1.8 Literature Review of Self-Assembled Monolayers

1.8.1 Background

Progress in exploring Langmuir-Blodgett films has led to the perception that the technical application of LB films is hampered by some inherent disadvantages of these films, e.g. the domain structure of the layers, the defect structure covering the region resulting from pinholes and larger inhomogeneities in the film structure [40]. This in addition to the lengthy time scale needed for the film deposition to occur. The self-assembly technique was developed to form structured, ordered monolayer and multilayer systems from adsorption in the liquid phase. With this knowledge in mind, we investigated and compared the stability of the thin films fabricated by these techniques by exposing the thin films to the harsh environments, which included highly polar solution, acidic and basic solutions and varying salt concentrations for different amount of time. In order to observe the effect the environments had on the structure of the films, the films were placed on the GIXD; XRR; or contact angles were taken. The results of these stability tests are discussed in-depth in Chapter 4.

1.8.2 Host-Guest Structures

In the host-guest structures, the 'host' molecules have been seen to interact specifically with complementary 'guest' molecules and form noncovalent host-guest pairs. Supramolecular host-guest interactions have been exploited for the assembly of receptor-functionalized molecules or particles onto interfaces with molecular recognition abilities [41]. In this thesis, we were interested in the synthesis and characterization of

immobilized self-assembled monolayers with 'host' molecules that had a premade cavity for 'guest' molecule inclusion. To this end, we embarked on the study of using sterically hindering 9-bromoanthracene derivative, 9-octadecyl,10-trichlorsilanthracene, as 'host' molecule. The procedure used to synthesize this compound can be found in Chapter 4.

Other research groups have also investigated the use of 'host' molecules with preexisting cavities. One such example is the use of cyclodextrin. Cyclodextrin, which is a cyclic oligosaccharides, posses an interior hydrophobic cavity that can include a variety of guest species and have been widely used in the study of redox-responsive sensors for environmental and biomedical applications [42].

Another noted method is known as the insertion process. It was first documented in 1997 from a group from the School of Science and Engineering at the University of Saitama, Japan [43]. This method was successfully used by another group from Japan that fabricated a SAM consisting of 4-(2-(4-(acetylthio)phenyl)ethynyl)benzoic acid and butanethiol [44]. After cleansing in a "piranha" solution, the gold substrate used was first immersed in a 1mM ethanol solution of butanethiol for 24 hrs. The substrate was then washed with ethanol, deionized water and dried using nitrogen. It was then reimmersed in a 1mM 4-(2-(4-(acetylthio)phenyl)ethynyl)benzoic acid THF solution containing concentrated sulfuric acid. From observing peaks corresponding to carbon (284.0 ev), oxygen (531.5 eV) and sulfur (161.9 eV) from X-ray photoelectron spectroscopy, the successful preparation of a mixed SAM was confirmed [44].

1.8.3 Potential Applications of SAMs

Self-assembled monolayers have a considerable amount of interest for electrochemical applications. Because of the components of a SAM molecule, the head

group that binds to the substrate and the tail group that constitutes the outermost surface, molecular "devices" carrying active units can serve as electrodes, biosensors, molecular machines, or molecule electronic components and devices [45].

A group from the Republic of Korea fabricated an oligophenylethynylene containing conjugated structure as a bioreceptor in prostate specific antigen immunosensor. The mixed SAM consisting of oligophenylethynylene thiol and butanethiol was fabricated because the biomolecule is effectively immobilized owing to the high ordered structure of the SAM molecules [44].

Molecular electronics involves the replacement of a wire, transistor or other basic solid-state electronic element with one or a few molecules[46]. One technique that that is used in the mechanical controllable break junction for recording the current through a single molecule can be accomplished in four steps: 1) a gold wire was coated with a SAM of the molecular wires, which is composed of benzene-1,4-dithiolate; 2) the wire is then pulled until cleavage results in metal tip formations; 3) any volatile components are allowed to evaporate while the tips are slowly moved together until the onset of conductance where one molecule bridges the gap between the two tips [46].

The next section outlines the main objectives of this thesis which are based on the fabricated LB and SAM films in such a way to optimize 'guest' molecule inclusion and overall film stability.

1.9 Thesis Objectives

1) The first objective of this work is to characterize the structure of the deposited guanidinium organomonosulfonate host Langmuir-Blodgett and alkyltrichlorosilane self-assembled monolayer films using grazing incidence X-ray diffraction and specular reflectivity data. With this data, we can determine the unit cell parameters, unit cell area, film thickness and crystal structure.

2) The second objective is to determine the effect of different environments on the stability of the LB and SAM films. Specifically, we investigated whether the placement of the films in highly polar solvents, acidic and basic solutions, and deionized water resulted in changes in film thickness and crystal structures.

3) The third objective of this thesis is to show how to synthesize anthracene derivates for use in alkyltrichlorosilane self-assembled monolayer. With these derivatives, we investigated whether sterically hindered molecules can create defined cavities for the inclusion of complementary 'guest' molecules.

The following chapters detail the experimental work that relates to these objectives.

1.10 References for Chapter 1

1. *ACD/ChemSketch*. 2008, Advanced Chemistry Development, Inc (ACD/Labs). p. Chemical drawing program.

2. *Canvas*. 2008, ACD Systems of America. p. Create, Enhance and Share Technical Illustrations.

3. Ulman, A., *An Introduction to Ultrathin Organic Films: from Langmuir-Blodgett to Self-Assembly*. 1991, Boston: Academic Press, Inc.

4. Petty, M.C., *Langmuir-Blodgett Films: An Introduction*. 1996, New York: Cambridge University Press.

5. Barnes, G. and I. Gentle, *Interfacial Science: An Introduction*. 2005, Oxford: Oxford University Press.

6. *Langmuir - Blodgett Films*, ed. G. Roberts. 1990, New York: Plenum Press.

7. Ray, A.K. and C.A. Hogarth. *Langmuir-Blodgett films: technology and applications*. 1994. London, UK: IEE.

8. Miller, L.S., et al., *A new type of Langmuir-Blodgett trough.* Journal of Physics E: Scientific Instruments, 1988. **21**: p. 163-167.

9. Venables, J., *Introduction to surface and thin film processes*. 2000, Cambridge: Cambridge University Press.

10. Malik, A., et al., *Structures of head-group and tail-group monolayers in a Langmuir-Blodgett film.* Physical Review B, 1995. **52**(16): p. R11654.

11. Langmuir, I., *THE CONSTITUTION AND FUNDAMENTAL PROPERTIES OF SOLIDS AND LIQUIDS. II. LIQUIDS.* J. Am. Chem. Soc., 1917. **39**(9): p. 1848-1906.

12. Blodgett, K.B., *Films Built by Depositing Successive Monomolecular Layers on a Solid Surface.* J. Am. Chem. Soc., 1935. **57**(6): p. 1007-1022.

13. Angelova, A. and R. Ionov, *Langmuir-Blodgett Film Organization Resulting from Asymmetrical or Partial Types of Monolayer Transfer: Comparison for Amphiphiles of Different Geometrical Shapes.* Langmuir, 1996. **12**(23): p. 5643-5653.

14. Schwartz, D.K., *MECHANISMS AND KINETICS OF SELF-ASSEMBLED MONOLAYER FORMATION.* Annual Review of Physical Chemistry, 2001. **52**(1): p. 107.

15. Aswal, D.K., et al., *Self assembled monolayers on silicon for molecular electronics.* Analytica Chimica ACTA, 2005. **568**(1): p. 84 - 108.

16. *Thin Films: Self-Assembled Monolayers of Thiols*, ed. A. Ulman. Vol. 24. 1998, San Diego: Academic Press.

17. Butt, H.J., K. Graf, and M. Kappl, *Physics and Chemistry of Interfaces*. 2006, Weinheim: Wiley-VCH Verlag GmbH & Co.

18. Ulman, A., *Formation and Structure of Self-Assembled Monolayers.* Chem. Rev., 1996. **96**(4): p. 1533-1554.

19. Tredgold, R.H., *Order in Thin Organic Films*. 1994, Cambridge University Press: Cambridge, UK.

20. Dutta, P., *Grazing incidence X-ray diffraction.* Current Science, 2000. **78**(12): p. 1478 - 1483.

21. Stout, G.H. and L.H. Jensen, *X-ray Structure Determination: A Practical Guide*. 2 ed. 1989, New York: John Wiley & Sons.

22. *Encyclopedia of Materials Characterization: Surfaces, Interfaces, Thin Films*. Materials Characterization Series, ed. C.R. Brundle, C.A.J. Evans, and S. Wilson. 1992, Boston: Butterworth-Heinemann.

23. Kuzmenko, I., et al., *Design and Characterization of Crystalline Thin Film Architectures at the Air-Liquid Interface: Simplicity to Complexity.* Chem. Rev., 2001. **101**(6): p. 1659-1696.

24. Birkholz, M., *Thin Films Analysis by X-ray Scattering*. 2006, Weinheim: Wilwy-VCH Verlag GmbH & Co. KGaA.

25. Alonso, C., et al., *Grazing Incidence X-ray Diffraction Studies of Thin Films at The air-liquid Interface.* Mat. Res. Soc. Symp. Proc., 2001. **678**.

26. Plaut, D.J., *Structural characterization of crystalline ternary inclusion compunds at the air-water interface*. 2004, University of Minnesota.

27. Chason, E. and T.M. Mayer, *Thin film and surface characterization by specular X-ray reflectivity.* Critical Reviews in Solid State and Materials Sciences, 1997. **22**(1): p. 1-67.

28. Li, M., D.J. Chaiko, and M.L. Schlossman, *X-ray Reflectivity Study of a Monolayer of Ferritin Proteins at a Nanofilm Aqueous-Aqueous Interface.* J. Phys. Chem. B, 2003. **107**(34): p. 9079-9085.

29. Lin, C.-T. and K.-L. Lin, *Contact angle of 63Sn-37Pb and Pb-free solder on Cu plating.* Applied Surface Science, 2003. **214**(1-4): p. 243-258.

30. Li, H., *Relationship between molecular structure and surface properties of self-assembled monolayers*, in *Chemistry*. 2004, Virginia Tech: Blacksburg.

31. Kuhn, H., *Present status and future prospects of Langmuir-Blodgett film research.* Thin Solid Films, 1989. **178**(1-2): p. 1-16.

32. Terada, T., R. Yamamoto, and T. Watanabe, *Experimental studies on colloid nature of Chinese black ink.* Institute of Physical and Chemical Research -- Scientific Papers, 1934. **23**(482): p. 173.

33. Kuzmenko, I., et al., *Formation of Chiral Interdigitated Multilayers at the Air-Liquid Interface Through Acid-Base Interactions.* Science, 1996. **274**(5295): p. 2046-2049.

34. Matsuzawa, Y. and K. Ichimura, *Host-guest monolayers of octaalkoxyphthalocyanatocobalt with nematic liquid crystals at the air-water interface.* Materials Science and Engineering: C, 1999. **8-9**: p. 47-52.

35. Kim, Y.-H., et al., *Electrochemistry of Langmuir-Blodgett and self-assembled monolayers of pyrrole derivatives.* Thin Solid Films, 1999. **352**(1-2): p. 138-144.

36. DeRose, J.A. and R.M. Leblanc, *Scanning tunneling and atomic force microscopy studies of Langmuir-Blodgett films.* Surface Science Reports, 1995. **22**(3): p. 73-126.

37. *Langmuir-Blodgett Films*, ed. G. Roberts. 1990, New York: Plenum Press.

38. Blodgett, K.B., *Film structure and method of preparation*, G.E. Company, Editor. 1940: United States of America. p. 5.

39. Shtykov, S.N., et al., *Use of Langmuir-Blodgett films as modifiers for piezoresonance sensors.* Journal of Analytical Chemistry, 2007. **62**(5): p. 119-121.

40. Arndt, T., H. Schupp, and W. Schrepp, *Self-assembled and Langmuir-Blodgett films of thiocarbaminates: A comparative study.* Thin Solid Films, 1989. **178**(1-2): p. 319-326.

41. Ling, X.Y., et al., *An in Situ Study of the Adsorption Behavior of Functionalized Particles on Self-Assembled Monolayers via Different Chemical Interactions.* Langmuir, 2007. **23**(20): p. 9990-9999.

42. Ju, H. and D. Leech, *Host-Guest Interaction at a Self-Assembled Monolayer/Solution Interface: An Electrochemical Analysis of the Inclusion of 11-(Ferrocenylcarbonyloxy)undecanethiol by Cyclodextrins.* Langmuir, 1998. **14**(2): p. 300-306.

43. Nishida, N., et al., *Formation and Exchange Processes of Alkanethiol Self-Assembled Monolayer on Au(111) Studied by Thermal Desorption Spectroscopy and Scanning Tunneling Microscopy.* Japanese Journal of Applied Physics, 1997. **36**: p. 2379-2385.

44. Lee, J.B., et al., *Fabrication of an electrically conductive mixed self-assembled monolayer and its application in an electrochemical immunosensor.* Ultramicroscopy, 2008. **108**(10): p. 1352-1355.

45. Weidner, T., et al., *Self-assembled monolayers of ruthenocene-substituted biphenyl ethynyl thiols on gold.* Journal of Electroanalytical Chemistry, 2008. **621**(2): p. 159-170.

46. Tour, J.M., *Molecular Electronics. Synthesis and Testing of Components.* Acc. Chem. Res., 2000. **33**(11): p. 791-804.

2. Experimental Setup Langmuir-Blodgett Monolayers

In this section the experimental procedures followed to create both 'guest free' and 'host-guest' Langmuir-Blodgett films are discussed with particular emphasis on the preparation of the monolayer solution and deposition techniques. All the chemical structures presented in this chapter were created using ChemSketch [1].

2.1 Subphase Preparation

The subphase was prepared by dissolving guanidinium carbonate ions (**G**) in the deionized water. The water used was deionized through a Millipore system to a resistivity of 18.2 MΩcm.

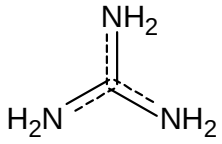

Figure 2.1. Chemical structure of guanidinium carbonate ion (**G**), which is used as the spacer molecule between the "host" film molecules because it interacts with the hydrophilic head group. The aqueous subphase has a concentration of 10-2 M of guanidinium carbonate ions.

The guanidinium acted as "spacer" molecule between host molecules to create an inclusion gap where the guest molecules can interdigitate into. They formed the inclusion gap by interacting with the 1-octadecanesulfonic acid-sodium salt 'host' and separating the hydrocarbon chains. A target subphase concentration of 10^{-2} M was attained by adding guanidinium ions (0.38 – 0.41g, mmol, Sigma Aldrich) to deionized

water (210 mL). The subphase solution was then sonicated for 5 minutes to ensure all guanidinium ions dissolved and dispersed uniformly in the deionized water.

2.2 Host-Guest Monolayer Solution Preparation

Chloroform was the solvent of choice for creating the monolayer solution for specific reasons: it completely dissolved the monolayer molecules and needed a short amount of time to evaporate from the liquid surface due to its high vapor pressure, 160 mmHg at 20°C.

The host molecule chosen for these experiments was 1-octadecanesulfonic acid-sodium salt (S). Figure 2-1 shows the structure of this molecule.

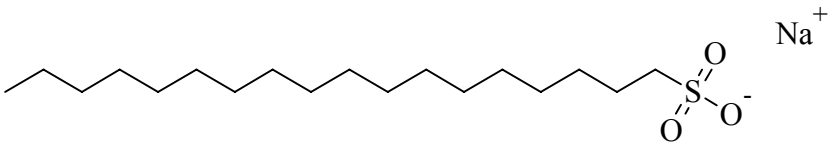

Figure 2.2. A schematic representing the molecular structure of 1-octadecanesulfonic acid-sodium salt molecule (C18S), which was used as the "host" film component. It was chosen as the "host" molecule because it is known to form stable Langmuir monolayers.

This molecule was picked as the host film due to its ability to form stable Langmuir films because it is insoluble in water.

Multiple potential guest molecules were investigated over the course of the project. One criterion that all guest molecules were required to meet was the molecule had to contain an eighteen carbon chain. This requirement ensured that the 'guest' molecules were similar in structure to the 'host' film. Octadecane (C18) was chosen because it represents a simple alkane chain without a functional group. The other guest molecules were chosen to see how the size and components of the functional groups

altered the structure and stability of the host film. The molecular structure and abbreviations for each guest molecule investigated are listed in Table 2-1.

Table 2-1: Langmuir-Blodgett films guest molecules

Name (Symbol)	**Molecular Structure**
Octadecane (C18)	
1-Octadecanol (C18OH)	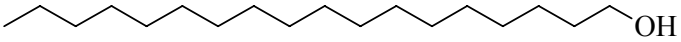
2-Hydroxystearic acid (2-HSA)	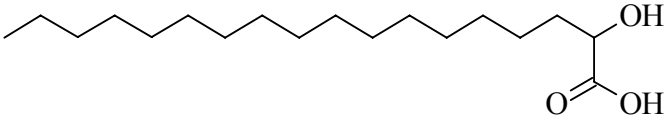
Naphthyl stearate (Naph)	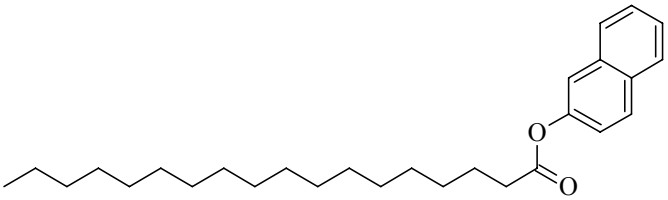
Cholesteryl stearate (Chol)	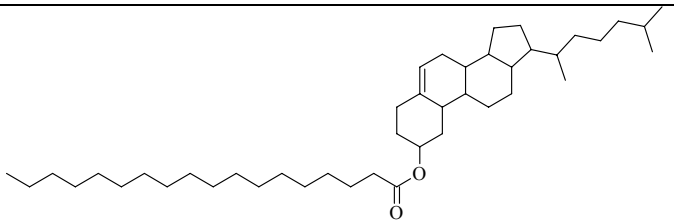

The target solution of 1-octadecanesulfonic acid-sodium salt in chloroform was 0.1 mg/mL, so for a solution containing 10 mL of chloroform, 1 mg of 1-octadecanesulfonic acid-sodium salt was needed. The required concentration of the 'host-guest' solution was a 1:1 molar mixture. The steps taken to create the host-guest

solution started with the creating of "stock solutions" of each molecule where the masses of the molecules and the chloroform used were noted. Next, the concentration of the "stock solution" of the NaC18S mixture was determined in grams/(mL of chloroform). Conversion from grams to moles of NaC18S using its molecular weight (356.54 g/mol) was an important step since the host-guest mixtures were on a 1:1 molar basis. With the known molar quantity of NaC18S in the "stock solution", the necessary mass of the guest stock solutions could also be determined using the molecular weights of each molecule. The calculated quantities for each host-guest solution were then weighed out from their respective "stock solutions" to a clean labeled vial containing 10 mL of chloroform. All solutions were sonicated for 20 minutes afterward to ensure good mixing. An example of these calculations can be seen in Appendix A – Sample calculation for 1:1 molar LB film solution.

2.3 Substrate Preparation

The substrate used for film deposition was silicon wafers 100 mm in diameter with one polished side from WaferWorld. There was no oxide layer deposited on these wafer. The wafers were cut into rectangular pieces measuring 1.5 x 2.5 cm long using a diamond-tipped stylus giving a total area of 3.75 cm^2. In order to calculate the actual area immersed and deposited on, the following formula was used,

$$Area = 2 * [Width + Thickness] \times [(Bottom - Top) - Meniscus] \qquad (2.1)$$

where the Width of the silicon slide was 1.5 cm (15 mm), the Thickness was negligible, the Bottom was 2.5 cm (25 mm), and the Top was typically between 1 to 1.5 cm (10 to 15 mm) below the top edge of the slide. It was assumed that the meniscus radius was 0.4 cm (4 mm). This provided at least between 1.8 and 3.3 cm^2 (180 to 330 mm^2) of available

surface for monolayer deposition to occur on. The calculated value of the substrate area was then entered into the LB program. The reduction in area available for deposition resulted from the area covered by the clamp used to dip the substrate in and out of the subphase and the meniscus radius. Knowing the deposition area allows the determination of accurate transfer ratios.

Since removal of any organic contaminant was essential for monolayer formation, the cut silicon slides were sonicated in chloroform for 10 minutes and dried prior to use.

2.4 Film Deposition

The cleanliness of the Langmuir trough was essential to monolayer film formation. Chloroform was used as the initial cleaning agent to remove any organic molecules on the trough's surface. A chemwipe was lightly doused with chloroform and then rubbed across the surface of the trough and the barriers. Next, the trough was filled with deionized water, which was then drained to further remove containments (e.g. dust, lint, etc). To determine if the trough was clean, a test isotherm was performed. The trough was refilled with deionized water and the Wilhelmy plate was lowered so it touched the surface of the water. Once the plate stabilized, the pressure reading was zeroed and the barriers were closed at a rate of 35 mm/min. If surface pressure remained below 1 mN/m during the isotherm, the trough was clean and ready for use.

Since the monolayer undergoes a phase change when it is compressed, knowing where to begin film deposition was essential. A test isotherm was performed without film deposition for every 'host-guest' monolayer solution. Useful information was gathered from these isotherms, such as the lift-off area for the monolayer, the surface pressure corresponding to the close-packed condensed phase, and the surface pressure at

which the monolayer collapsed. The lift-off area corresponds to the area per sulfonate at which a noticeable pressure increase occurs.

As the silicon slide was lowered into the subphase, the speed it moved was unimportant because it did not affect the monolayer transfer. However, on withdrawal through the floating monolayer it was important not to raise the substrate faster than the rate at which the aqueous subphase drained. This drainage is a result of the adhesion between the monolayer being transferred and the material on the substrate which acts along the line of contact and so drives out the water [2]. To maintain a constant surface tension, the "pressure control" option in the trough program was used while the slide was being withdrawaled at a speed of 5 mm/minute. Once removed from the subphase, the slides were allowed to dry. The slides were then placed on the GIXD and XRR

2.5 Stability Tests

The 'host-guest' LB films that exhibited diffraction peaks on the GIXD were subjected to stability tests. The solvents used were hexane, a 20% tetrahydrofuran: hexane mixture, a 40% tetrahydrofuran: hexane mixture, pure deionized water, and salt solutions with concentrations of 10^{-4} to 10^{-2} M. Three milliliters of each solvent were placed in 10 mL vials that had been cleaned using chloroform to remove any organic contaminants and washed using soap and deionized water. The slides were vertically lowered into the vials and remained immersed in the solvents for time periods that varied from 30 minutes to 5 hours. Upon removal from the solvents, the slides were placed on the specular X-ray reflectivity machine and data was recorded. The results of the stability tests are reported in Chapter 4.

2.6 Reference

1. *ACD/ChemSketch*. 2008, Advanced Chemistry Development, Inc (ACD/Labs). p. Chemical drawing program.

2. Petty, M.C., *Langmuir-Blodgett Films: An Introduction*. 1996, New York: Cambridge University Press.

3. Experimental Setup for Self-Assembled Monolayers

In this section, the experimental procedures used in the fabrication of the octadecyltrichlorosilane self assembled monolayers and the synthetic process followed in the creation of 9-octadecyl,10-trichlorsilanthracene are discussed. All the chemical structures in this chapter were created using ChemSketch [1].

3.1 Substrate Preparation

For the formation of self assembled monolayers, silicon wafers (100), 150 mm in diameter with a deposited dioxide layer were ordered from WaferNet. The dioxide layer was essential to form the hydroxide groups (-OH) needed during the chemisorption process. Individual slides were cut from the silicon wafers to a dimension of 1.0 cm x 2.5 cm, giving a total deposition area of 2.50 cm^2.

The slides were then cleaned by first sonicating them with chloroform to remove any organic containment on the surface. Next, the slides were immersed in a "piranha" solution of 30% hydrogen peroxide (H_2O_2) and concentrated sulfuric acid (H_2SO_4) in a 2:1 volume mixture for 10 minutes at room temperature. The "piranha" solution was a strong oxidant and reacted violently with organic materials, so small quantities were created and then immediately diluted with water for proper disposal. The "piranha" solution created the reactive hydroxyl groups (-OH) on the surface of the silicon wafer.

The slides were then rinsed with deionized water for 5 minutes to remove any "piranha" solution from the slide. A vacuum oven was then used to fully dry the slides to remove any water left over from the rinsing step. This minimized the possibility of cross linking between the molecules during the self-assembly. Once the slide was fully dried and allowed to cool to room temperature, it was ready for use. Figure 3.1 illustrates the above procedure.

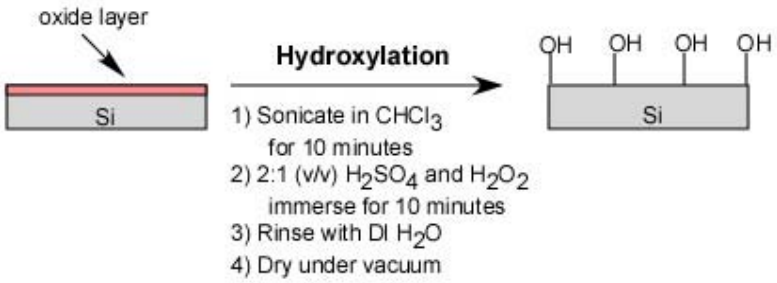

Figure 3.1. Illustration of the procedure used to hydrolyze the silicon oxide wafers used for alkylsilane SAM depositions. The most important step was the immersion of the slides into the H_2SO_4 and H_2O_2 solution, which is also known as a "piranha" solution.

3.2 Octadecyltrichlorosilane Self-Assembled Monolayer

For this project, the alkyltrichlorosilane of choice was n-octadecyltrichlorosilane [$C_{18}H_{37}SiCl_3$, OTS]. OTS was chosen because it has been shown to form closely-packed monolayer films with approximately vertical alkyl chain axes forming an organic-ambient interface composed of chain terminating functional groups (e.g. CH_3 for OTS) [2]. Figure 3.2 represents the molecular structure of OTS.

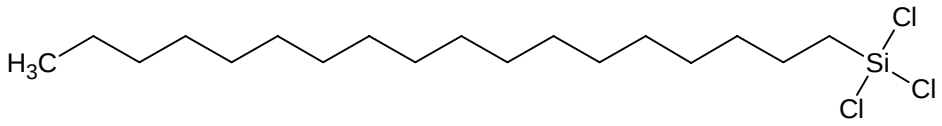

Figure 3.2. Here is a representation of the structure of octadecyltrichlorosilane (OTS). OTS was used because other research groups have documented a procedure for deposition and have recorded contact angles.

The chemicals used in the SAM process were standard solvent grade except the hexadecane and chloroform were anhydrous (Sigma Aldrich). The OTS SAM solution was a 0.5 mM of OTS (Sigma Aldrich, 94% purity) in a 4:1 volume mixture of hexadecane and chloroform. Once the OTS solution was formed, it was heated to between 28-30°C, which is the reported transition temperature where OTS forms a SAM film. The dried hydroxylated silicon dioxide slide was then immersed in the OTS solution for 20 – 30 minutes. Afterward, the SAM was first rinsed and immersed for 5 minutes in methanol and then deionized water. Upon removal from the deionized water, the SAM was dried in the vacuum oven. Contact angle measurements were performed on the SAM and are reported in Chapter 4 of the thesis.

3.3 9-octadecyl,10-trichlorsilanthracene Synthesis

The synthesis of 9-octadecyl,10-trichlorsilanthracene can be divided into three major parts. The first part is the synthesis of 9-octadecylanthracene using a Grignard reagent and 9-bromoanthracene. The second part is the attachment of bromine to the para position of 9-octadecylanthracene. The last part is the replacement of bromine with trichlorosilane on 9-octadecyl,10-bromoanthracene. All syntheses, unless otherwise noted, were done in an atmosphere of oxygen-free nitrogen using the Schlenk technique. Also, commercially available reagents from Sigma Aldrich were used as received unless otherwise noted. The ^{1}HNMR predictions for all the end products were done using mNova [3]. The actual ^{1}HNMR were done using the equipment available in the Chemistry Department of Virginia Tech.

3.3.1 Synthesis of 9-octadecylanthracene

. For the synthesis of 9-octadecylanthracene, the procedure used was adapted from the procedure laid out by Shaopeng Wang in "Amphiphilic Anthracyl Crown Ether. A Langmuir and Langmuir-Schaefer Films Study" was followed [4]. The synthesis took place in two steps: 1) the synthesis of a Grignard reagent using 1-bromooctadecane and magnesium; 2) reaction between the Grignard reagent from the first step and 9-bromoanthracene to synthesize 9-octadecylanthracene.

3.3.1.1 Synthesis of Grignard Reagent from 1-bromooctadecane

The first step was the creation of the Grignard reagent, 1-octadecylmagnesium bromide. Its chemical structure is illustrated in Figure 3.3.

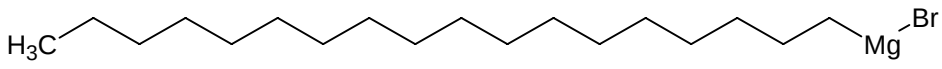

Figure 3.3. The chemical structure of octadecylmagnesium bromide, which was used as a Grignard reagent in the synthesis of 9-octadecylanthracene with 9-bromoanthracene, is represented in this figure.

The procedure to create the Grignard reagent started with cleaning a 250 mL three neck flask by purging with nitrogen gas and flame drying under vacuum three times. Then magnesium (Mg, 0.2019 g, 8.3 mmol, 99% pure) and two iodine crystals were placed in the three neck flask, which was then purged and dried under nitrogen. The iodine crystal was used as an initiator. Next, 1-bromooctadecane (1.349 g, 4.046 mmol) was dissolved in anhydrous diethyl ether (40 mL) in a dropping funnel, which was also purged with nitrogen gas and flame dried under vacuum prior to use. Once all the 1-bromooctadecane was dissolved in the diethyl ether, 5 mL of the solution was added to the three neck flask containing the magnesium and iodine. This reaction was carried out

on the Schlenk line to avoid exposure to air and water. The mixture was slightly heated using a heating mantle to the just below the boiling point of anhydrous diethyl ether (34.6°C) to help initiate the exothermic reaction. The remaining 1-bromooctadecane and diethyl ether solution was then added dropwise over an hour. After the addition was complete, the mixture was refluxed with stirring for 4 hours and then cooled to room temperature. Figure 3.4 illustrates the reaction pathway used to create the Grignard reagent.

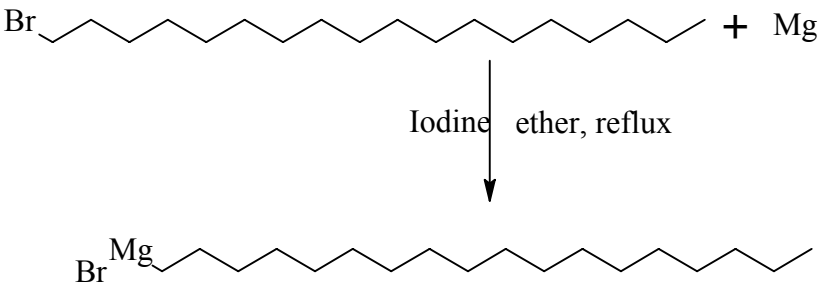

Figure 3.4. This schematic shows the synthesis of Grignard reagent octadecylmagnesium bromide. This Grignard reagent was then reacted with 9-bromoanthracente to create 9-octadecylanthracene.

3.3.1.2 Synthesis of 9-octadecylanthracene from Grignard Reagent and 9-bromoanthracene

The second part in creating 9-octadecylanthracene was the reaction between the Grignard reagent made in the previous steps, 1-octadecylmagnesium bromide, and 9-bromoanthracene. In a separate three neck flask, which was purged with nitrogen gas and flame dried under vacuum three times prior to use, [1,3-bis(diphenylphosphino)-propane]dichloronickel(II), ($Ni(dppp)Cl_2$, 0.07 g, 0.129 mmol), and 9-bromoanthracene (1.007 g, 3.96 mmol, 94%) were dried under vacuum for an hour. The mixture was then dissolved using anhydrous diethyl ether (20 mL). 1-Octadecylmagnesium bromide was

transferred to a dropping funnel using a cannula and added to the 9-bromoanthracne mixture over 10 minutes while stirring. The nickel complex reacted immediately with the Grignard reagent, and the resulting tan reaction mixture was allowed to warm to room temperature while stirring. An exothermic reaction starts within 30 minutes, and the anhydrous diethyl ether began to reflux. This reaction was carried out on the Schlenk line to avoid exposure to air and water and refluxed overnight. A schematic of the synthesis of 9-octadecylanthracene is illustrated in Figure 3.5 .

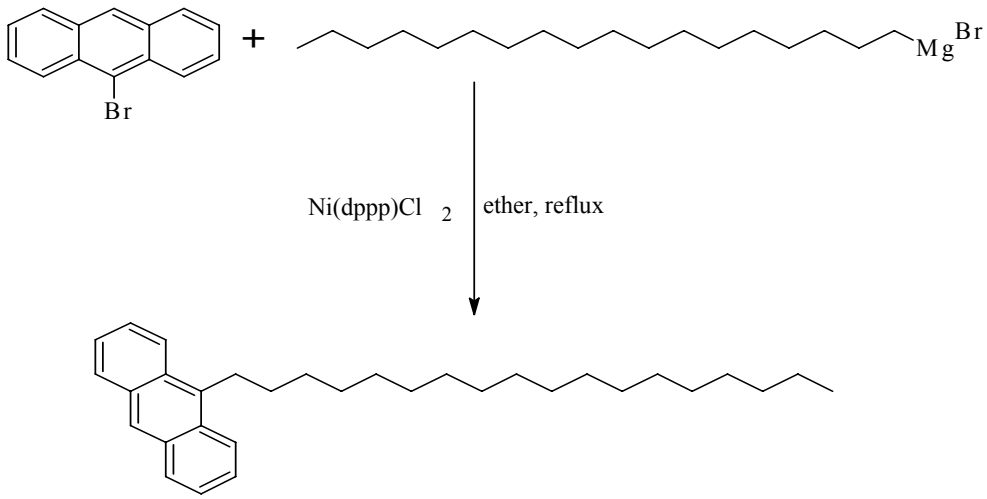

Figure 3.5. A schematic that illustrates the synthetic pathway used to create 9-octadecylanthracene from 9-bromoanthracene and 1-octadecylmagnesium bromide.

After cooling, the reaction was quenched by adding 10 mL of 3% hydrochloric acid (HCl, 37%) solution. The aqueous and organic phases were separated in a separatory funnel using three 40 mL portions of diethyl ether. The combined organic extracts were washed first with of saturated sodium carbonate in DI water (50 mL) and then brine (50 mL). Magnesium sulfate ($MgSO_4$) was then used to dry the washed extracts. The remaining solvent was evaporated using the rotary evaporator.

A thin layer chromatography (TLC) was performed in order to identify what compounds were created during the synthesis. The TLC was performed on the product

and starting materials, 1-bromooctadecane and 9-bromoanthracene, in order to identify spots of interest from unreacted starting material.

a TLC analysis indicated that the reaction mixture consisted of three components. In order to identify the possible products from unreacted starting material, a TLC was taken of 9-bromoanthracene and 1-bromooctadecane. Figure 3.6 illustrates the TLC values for the crude solution and the starting materials.

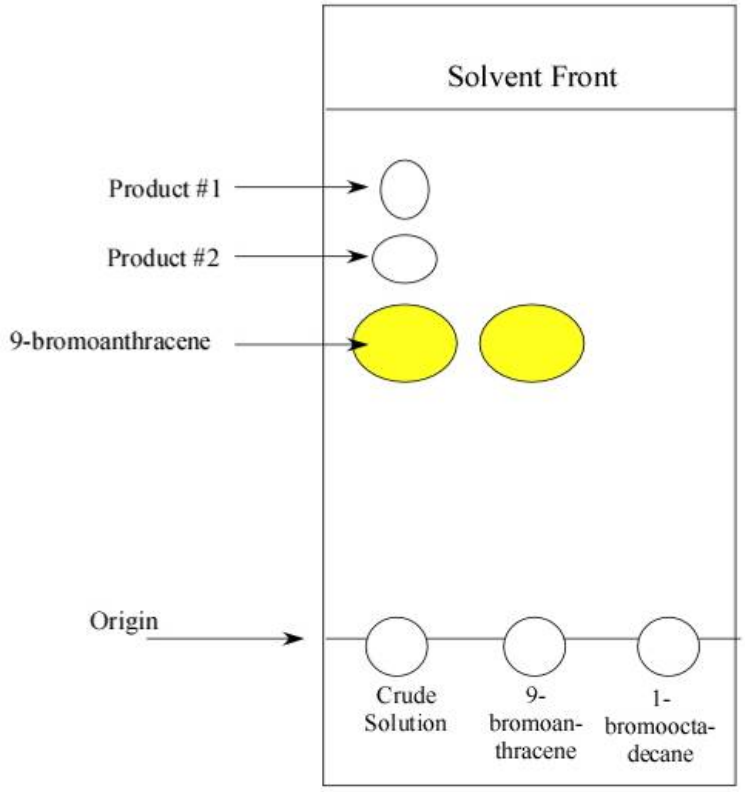

Figure 3.6. A schematic of the TLC taken of the crude product solution and the starting materials, 9-bromoanthracene and 1-bromooctadecane, using an eluting solution of 5% ethyl acetate: hexane solution is illustrated. The spot for 9-bromoanthracene appeared in the crude product TLC, indicating that some of the starting material did not react.

From the comparison of the TLC results using a 5% ethyl acetate eluting solution for the crude product solution and the starting materials, one spot was identified as unreacted 9-bromoanthracene because it had the same retention factor, R_f value, of 0.473.

The first product had a R_f value of 0.727 and the second product had a R_f value of 0.709, indicating that the first product was slightly less polar than the second product, which could be due to the absence of the anthracene rings. Once the TLC spots were identified, flash column chromatography was performed on the product solution first using a 5% ethyl acetate/hexane solution, then a 2.5% mixture to separate the 9-octadecylanthracene from the other products. Upon separation of the two products using column chromatography, ^{1}HNMR spectroscopic analysis was performed. The ^{1}HNMR analysis of the first product indicated the absence of a ringed structure due to the lack of the higher order shifts in the protons attributed to ringed structures. Figure 3.10 illustrates a possible molecular structure of the first product.

Figure 3.7. The proposed molecular structure of the first possible product formed during the synthesis of 9-octadecylanthracene. It was created from a reaction between two 1-bromooctadecane molecules.

The predicted ^{1}HNMR for 9-octadecylanthracene is δ_H ($CDCl_3$), 0.99 (-CH_3, 3H), 1.33 (-CH_2-, 30 H), 1.73 (-CH_2-, 1H), 2.97 (-CH_2-Aromatic, 2H), 7.50 (2H), 7.51 (2H), 8.03 (2H) 8.11 (2H) and 8.29 (1H). The actual ^{1}HNMR for 9-octadecylanthracene is δ_H (399 MHz, $CDCl_3$), 0.82 (-CH_3, 3H), 1.33 (-CH_2-, 30 H), 1.74 (-CH_2-, 1H), 3.52 (-CH_2-Aromatic, 2H), 7.19 (2H), 7.43 (2H), 7.93 (2H) 8.21 (2H) and 8.43 (1H). ^{1}HNMR analysis of the second possible product indicated the presence of a ringed structure from the higher order shifts in the protons, which are attributed to ringed structures and the successful attachment of the carbon chain to the 9-bromoanthracene from the lower order shift attributed to carbon chains.

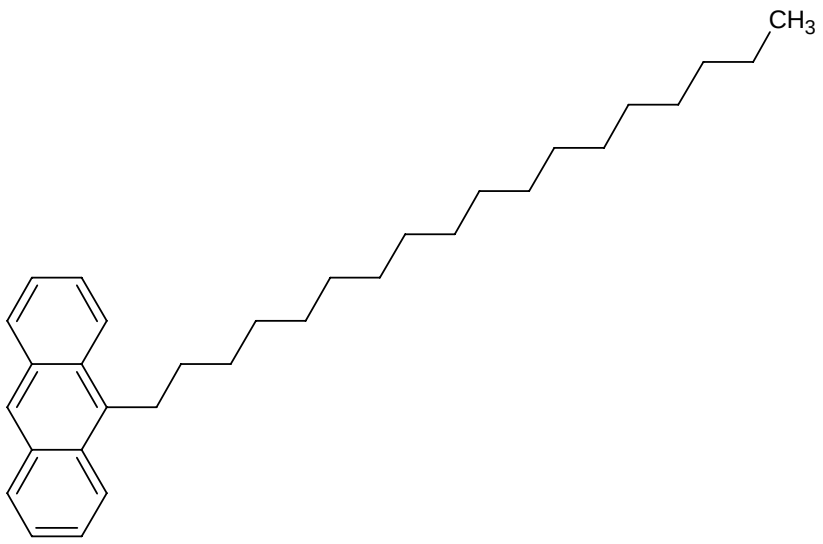

Figure 3.8. A schematic illustrating the desired product from reacting 9-bromoanthracene with 1-octadecylmagnesium bromide.

The percent yield of 9-octadecylanthracene was determined to be 4.83%, which is drastically low. This is the result of the creation of a side product that is more energetically favorable and not all the starting material reacting.

3.3.2 Synthesis of 9-octadecyl,10-bromoanthracene

For the synthesis of 9-octadecyl,10-bromoanthrance, the procedure laid out by Osman Cakmak in "Synthesis of new anthracene derivatives" found in the *Journal of Organic Chemistry* was followed [5].

Bromine shows an ability to discriminate among the different types of hydrogen atoms. It tends to substitute itself for a hydrogen atom in the para positions of an aromatic compound, which is known as an "aromatic substitution". With this knowledge, the bromination of 9-octadecylanthracene was done using two equivalent of molecular bromine using dimethyl chloride (CH_2Cl_2) as the solvent. A 250 mL three-

neck flask was cleaned prior to the reaction. The 9-octadecylanthracene (0.0816g, 0.1894 mmol) made in the previous section was dissolved in dimethyl chloride (5 mL) and added to the three neck flask. The flask was placed in an ice bath to cool the solution to 0°C. Two of the three necks were capped using a septum while the third neck had a device attached to it to absorb the hydrogen bromide (HBr) that would be produced as a side product. The device consisted of glassware that contained cotton and sodium hydroxide (NaOH) pellets. A solution consisting of bromide (Br_2, 9.74μL, 0.1894 mmol) in dimethyl chloride (0.5 mL) was added to the three neck flask while being protected from light. The reaction was carried out in the dark for an hour to avoid the bromination of hydrocarbon chains, which occurs in the presence of light. After an hour, any remaining dimethyl chloride was removed using the rotary evaporator. The residue that was formed was dissolved in hot chloroform and allowed to stand at room temperature for a day. Figure 3.9 illustrates the synthetic pathway used to attach the bromine in the *para* position of 9-octadecylanthracene.

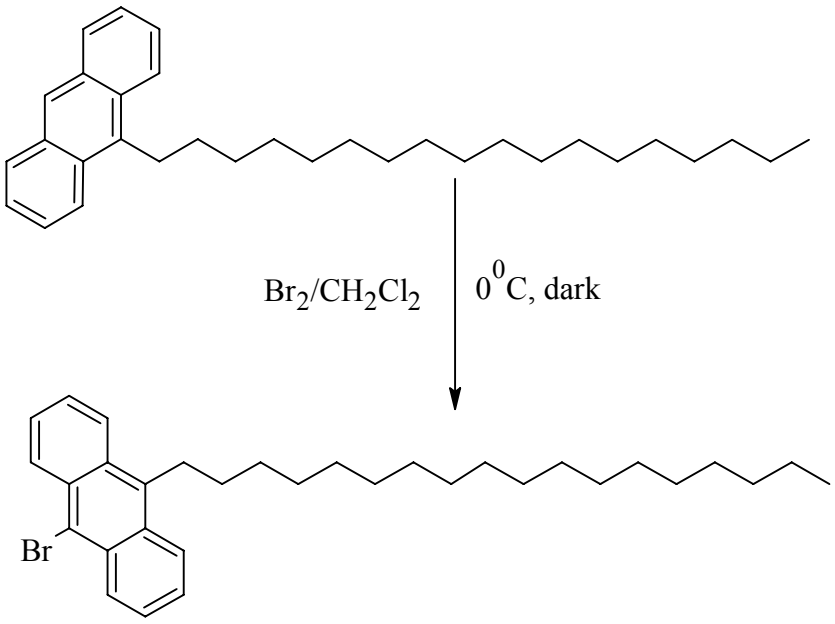

Figure 3.9. A schematic of the synthetic pathway used to create 9-octadecyl,10-bromoanthracene via the attachment of bromine to the *para* position of 9-octadecylanthracene.

The predicted ^{1}HNMR for 9-octadecyl,10-bromoanthracene is δ_H ($CDCl_3$), 0.99 (-CH_3, 3H), 1.31 (-CH_2-, 30 H), 1.73 (-CH_2-,1H), 2.93 (-CH_2-Aromatic, 1H) 7.51 (2H), 7.55 (1H), 8.12 (2H) and 8.33 (2H). Due to the difficulty of separating the desired product from the side products, no ^{1}HNMR was collected for 9-octadecyl,10-bromoanthracene.

3.3.3 Synthesis of 9-octadecyl,10-trichlorosilanthracene

The synthesis of 9-octadecyl,10-trichlorosilanthrance can be divided into two steps: 1) synthesis of a Grignard reagent from 9-octadecyl,10-bromoantracene; 2) replacement of the magnesium bromide with a trichlorosilane to synthesis 9-octadecyl,10-trichlorosilanthrance. This procedure was laid out by Martin Oestreich in "On the Mechanism of the Reductive Metallation of Asymmetrically Substituted Silyl Chlorides" [6].

3.3.3.1 Synthesis of Grignard reagent 9-octadecylanthracene magnesium bromide

This reaction was carried out on the Schlenk line to avoid exposure to air and water. The procedure to create the Grignard reagent started with cleaning a 250 mL three neck flask by purging with nitrogen gas and flame drying under vacuum. Then magnesium (0.0243 g, mmol) and two iodine crystals were placed in the three neck flask, which was then purged and dried under nitrogen. Next, 9-octadecyl,10-bromoanthracene (0.1935 g, mmol,) was dissolved in anhydrous diethyl ether (20 mL) in a round bottom flask. The solution was then transferred to a dropping funnel, which was also purged with nitrogen gas and flame dried under vacuum prior to use. Initially, only 5 mL of the solution was added to the three neck flask containing the magnesium and iodine. The mixture was slightly heated using a heating mantle to the just below the boiling point of anhydrous diethyl ether to help initiate the exothermic reaction. Once the reaction started, the remaining 9-octadecyl,10-bromoanthracene and diethyl ether solution was added dropwise over an hour. After the addition was complete, the mixture was refluxed with stirring for 4 hours and then cooled to room temperature. A schematic of the reaction can be seen in Figure 3.10.

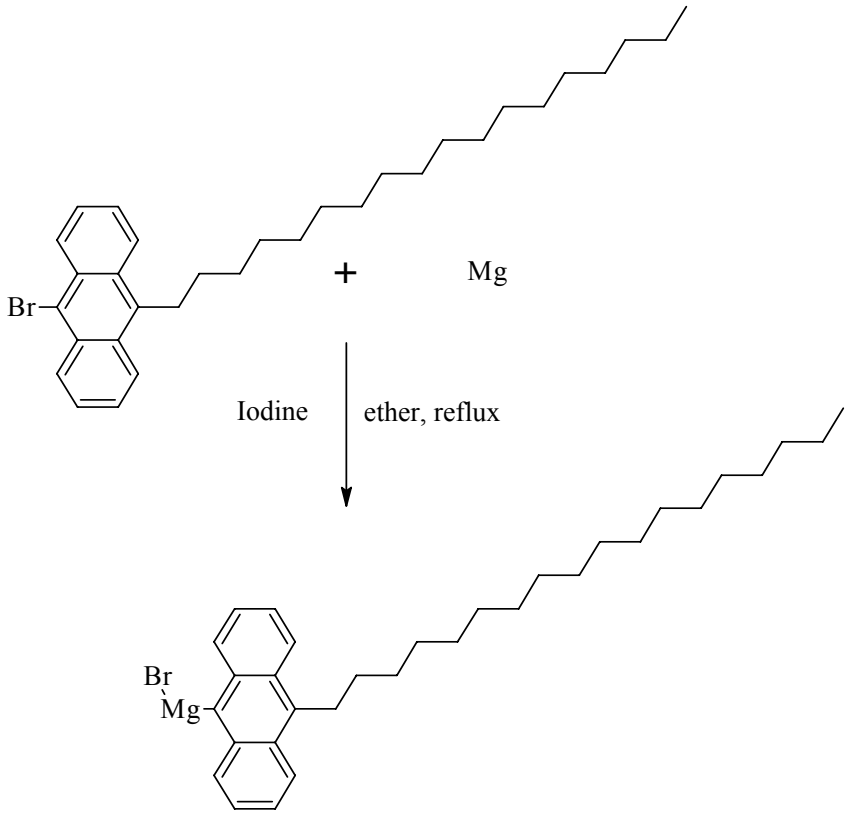

Figure 3.10. A schematic illustrate the synthesis of Grignard reagent 9-octadecylanthracene magnesium bromide from 9-octadecyl,10-bromoanthracene and magnesium. 9-Octadecylanthracene magnesium bromide was later reacted with tetrachlorosilane to complete the synthesis of 9-octadecyl,10-trichlorosilanthrance.

3.3.3.2 Synthesis of 9-octadecyl,10-trichlorosilanthrance

Once the Grignard reagent 9-octadecylanthracene magnesium bromide refluxed for 4 hours, it was allowed to cool to room temperature for use in the final reaction step. This step started with cleaning of another 250 mL three neck flask by purging with nitrogen gas and flame drying under vacuum. Tetrachlorosilane ($SiCl_4$, 65 μL, 395, 1.50 equiv to amount of 9-octadecyl,10-bromoanthracene) was added to the 3 neck flask with a magnetic stirrer and reflux condenser. Anhydrous ether (5 mL) was added to the flask to dissolve the tetrachlorosilane. The Grignard reagent 9-octadecylanthracene magnesium bromide was then transferred to a dropping funnel and

added dropwise over 10 minutes. The solution was slightly heated to help initiate the reaction, which was allowed to reflux over night at 40°C. A schematic of the reaction pathway is illustrated in Figure 3.11.

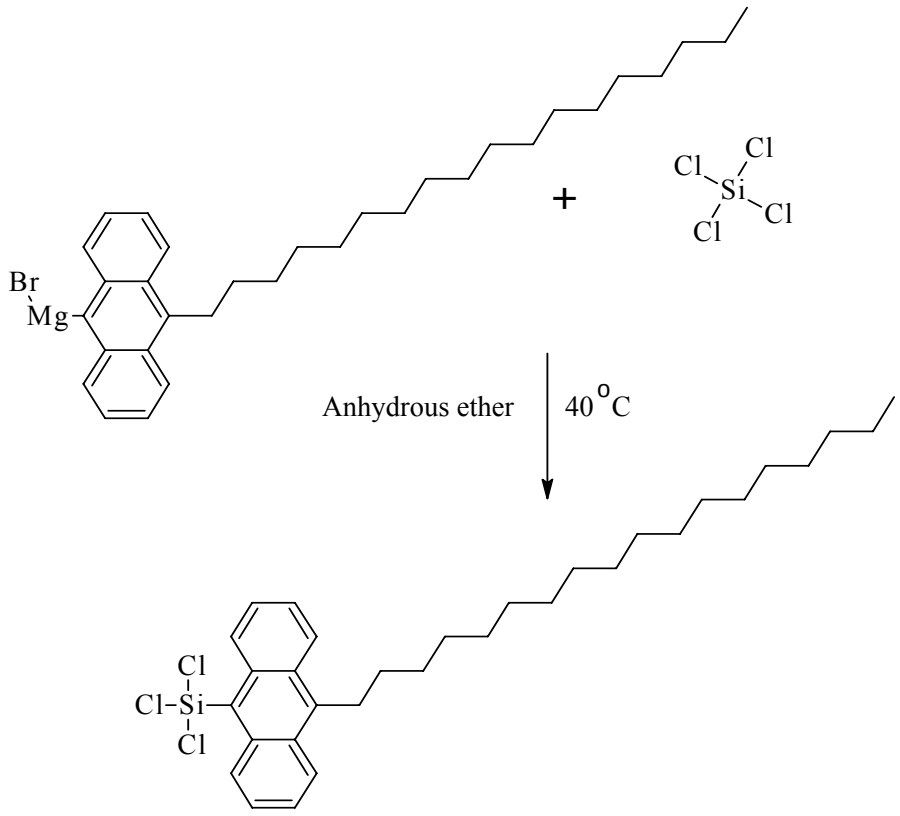

Figure 3.11. The final step in the synthesis of 9-octadecyl,10-trichlorosilanthrance was the reaction between tetrachlorosilane and 9-octadecylanthracene magnesium bromide.

After refluxing over night, the product was filtered through a gas-tight syringe with a filter attached to remove any unreacted solids from the product solution. The aqueous and organic phases were separated in a separatory funnel using three 40 mL portions of diethyl ether. The solvent was then evaporated off. ^{1}HNMR was then performed on all the products collected from the flash chromatography. The predicted ^{1}HNMR for 9-octadecyl,10-trichlorosilanthrance is δ_H ($CDCl_3$), 0.99 (-CH_3, 3H), 1.31 (-CH_2-, 30 H), 1.74 (-CH_2-,1H), 2.88 (-CH_2-Aromatic, 1H) 7.51 (2H), 7.51 (2H), 7.54 (2H), 8.13 (2H)

and 8.35 (2H). The actual ^{1}HNMR for 9-octadecyl,10-trichlorosilanthrance is δ_H (399 MHz, $CDCl_3$), 0.81 (-CH_3, 3H), 1.19 (-CH_2-, 30 H), 7.19 (2H), 7.49 (2H), 7.94 (2H) and 8.45 (2H). From the ^{1}HNMR analysis of the product and comparing the results to the predicted peaks, the absences of the higher order shifts (the 2.88ppm shift) in the alkyl chain suggests that the ring structure became detached from the alkyl chain during the synthesis process. Two possible reasons for the detachment are that the molecule immediately polymerized upon contact with air and separated during the removal of any aqueous components or there were containments present in the crude product from the bromination of 9-octadecylanthracene that interfered with the reaction and prevented the desired product from being formed.

3.4 References

1. *ACD/ChemSketch*. 2008, Advanced Chemistry Development, Inc (ACD/Labs). p. Chemical drawing program.

2. Depalma, V. and N. Tillman, *Friction and Wear on Self-Assembled Trichlorosilane Monolayer Films on Silicon.* Langmuir, 1989. **5**(3): p. 868-872.

3. *MestreNova*. 2008, MESTRELAB Research. p. Nuclear Magnetic Resonance data processing, visualization, simulation, prediction, presentation and analysis software package.

4. Wang, S., et al., *Amphiphilic Anthracyl Crown Ether. A Langmuir and Langmuir-Schaefer Films Study.* Langmuir, 2000. **16**: p. 4607-4612.

5. Cakmak, O., et al., *Synthesis of New Anthracene Derivatives.* The Journal of Organic Chemistry 2005. **71**: p. 1795 - 1801.

6. Oestreich, M., G. Auer, and M. Keller, *On the Mechanism of the Reductive Metallation of Asymmetrically Substituted Silyl Chlorides.* European Journal of Organic Chemistry, 2005: p. 184 - 195.

4. Results and Discussion

In this thesis chapter, the results of the grazing incident X-ray diffraction (GIXD), specular X-ray reflectivity (XRR) and stability tests for 'host-guest' Langmuir-Blodgett thin films are presented. Each guest molecule used in the Langmuir-Blodgett films has as separate result section, which includes surface pressure-area isotherms, GIXD patterns, unit cell parameters, XRR results and film thickness. The self-assembly results were divided by component used and includes contact angle measurements and synthetic pathways. Results of the Langmuir-Blodgett films at the air-water interface were reproduced with permission from "*Structure and properties of organic materials reinforced by hydrogen-bonding*, in *Chemical Engineering"* by Dr. Stephen M. Martin. The nonlinear least-squares fitting program, Stochfit, was used to determine the film thickness [1].

4.1 Langmuir-Blodgett Results

4.1.1 Guest-Free Octadecylsulfonate (C18S) Monolayers

The surface pressure-area (Π-A) isotherm of the sodium salt of octadecanesulfonic acid (NaC18S) Langmuir film on a 10^{-2} M aqueous guanidinium carbonate (**G**) subphase revealed a pressure liftoff – the area per sulfonate at which a noticeable pressure increase occurs – at $A_{lift\text{-}off}$ = 54 Å^2/sulfonate. The monolayer then collapsed at a surface pressure of Π ≈ 22 mN/m. Figure 4.1 shows the Π-A isotherm of NaC18S monolayer on an aqueous subphase containing 10^{-2} M G_2C0_3.

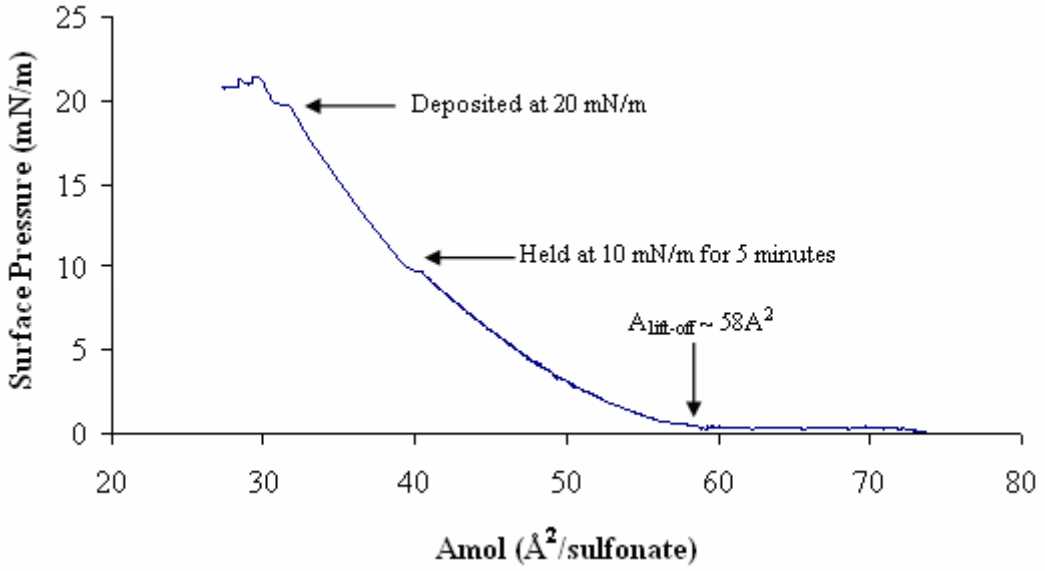

Figure 4.1. Langmuir isotherm of NaC18S monolayer deposited on an aqueous subphase containing 10^{-2} M **G** aqueous subphase. It exhibited a liftoff area of $A_{liftoff} \sim 58$ Å^2/sulfonate. The isotherm then rose rapidly as the monolayer was compressed. The monolayer collapsed at a surface pressure of $\Pi \approx 22$ mN/m. The monolayer was deposited on a silicon substrate at a surface pressure of $\Pi \approx 20$ mN/m.

It has been previously reported that Langmuir monolayers of octadecanesulfonic acid sodium salt on a pure water subphase collapsed at a low surface pressure ($\Pi \approx 5$ mN/m) and are thus unstable under compression [2]. Martin reported that for a (**G**)C18S monolayer at the air-subphase interface at an $A_{sulfonate}$ = 45 Å^2/sulfonate, the GIXD pattern exhibited weak monolayer peaks at q_{xy} = 0.97 Å^{-1}, 1.37 Å^{-1} and 1.41 Å^{-1} which were indexed to a rectangular unit cell with a = 4.83 Å, b = 12.84 Å and γ = 92.5° with a cell area of 62.0 Å^2. These parameters were substantially different that those determined for the NaC18S monolayer indicating that the **G** ion does play a structure directing role, probably via hydrogen bonding with the sulfonate groups at the air-water interface. GIXD patterns at an $A_{sulfonate}$ of 39 Å^2/sulfonate showed a poorly crystalline monolayer phase with Bragg roads at q_{xy} = 1.63 Å^{-1} and 1.66 Å^{-1} and a third Bragg rod at $q_{xy} \approx$ 1.45

$Å^{-1}$. The peaks were indexed to a unit cell with a = 4.34 Å, b = 7.71 Å and γ = 90 ° with an area of 33.5 $Å^2$ [2].

Based on the Π-A isotherm in Figure 4.1, it was determined that the ideal pressure range to deposit NaC18S monolayer onto a silicon slide was between 20 to 25 mN/m as this was the range that exhibited the highest slope. GIXD of the deposited (**G**)C18S films, formed from NaC18S on a 10^{-2} M G_2CO_3 aqueous subphase, did not reveal a stable crystalline monolayer. The majority of the (**G**)C18S films exhibited no diffraction. One weak Bragg rod was observed at q_{xy} = 1.51 $Å^{-1}$ for a single sample deposited at 20 mN/m. This single Bragg rod was indexed to a hexagonal unit cell with a = b = 8.32 Å, and γ = 120° and an A_{cell} = 59.9 $Å^2$. The lack of reproducible GIXD evidence for a crystalline (**G**)C18S LB film suggests that an amorphous film, in which the alkane tails are unable to achieve close-packing, is being produced.

Figure 4.2 exhibits XRR results for a (**G**)C18S film deposited at 20 mN/m on a silicon substrate compared to the XRR of a blank silicon slide. The reflected intensity was measured as a function of incidence angle, θ, normalized by dividing by the incidence intensity, and plotted as a function of $Q_Z = 4\pi \sin\theta/\lambda$. The shape of the XRR curve clearly indicates the presence of a monolayer at the silicon surface.

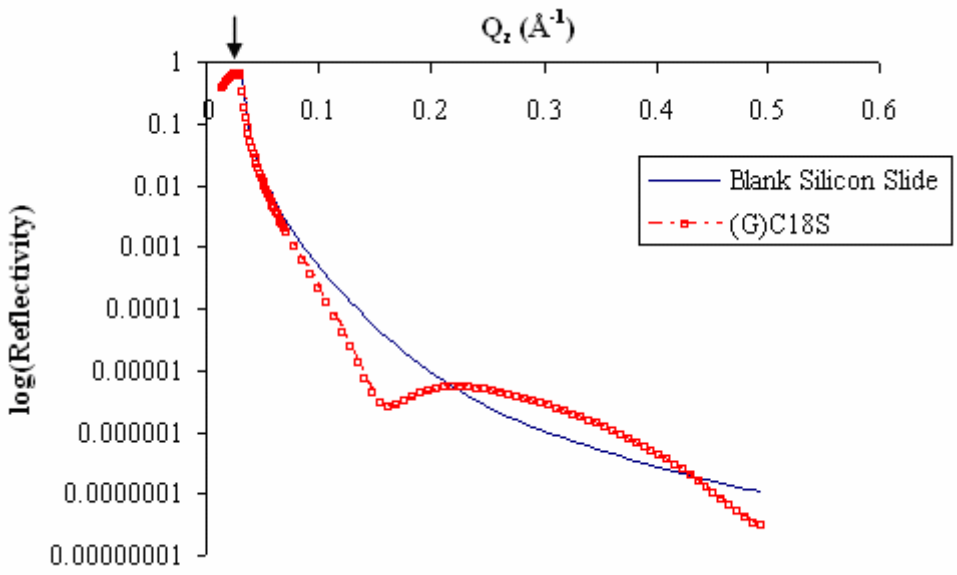

Figure 4.2. Comparison of the log of the normalized reflected intensity versus Q_z for X-rays reflected from the (**G**)C18S film (dashed line) and blank silicon slide (solid line). The (**G**)C18S film caused a change in the reflected intensity, thus indicating that it had been deposited. The arrow at the top of the plot marks Q_C.

For values less than Q_C (where $Q_C = 0.0311$ Å^{-1}), which is indicated by the arrow in Figure 4.2, total reflection occurs as a result of the comparable beam and sample widths, which prevents the sample intercepting the entire incoming beam [3]. For higher values of Q, the reflectivity drops as Q increases, and a broad oscillatory pattern, becomes apparent. Since a film has a top and bottom interface; interferences between X-rays reflected at these interfaces leads to an oscillatory pattern [3]. The oscillation period is inversely proportional to the film thickness; the broad pattern in Figure 4.2 indicates that the adsorbed film is thin. An incomplete oscillation was recorded due to the resolution of the XRR machine, preventing a calculation of the film thickness from the unfitted data.

The ultimate goal of the analysis of the XRR thin film data was to obtain a model of the electron density profile to determine the thickness of the film. The reflectivity data in Figure 4.2 were analyzed using a nonlinear least-squares fitting program, Stochfit. The

program produces a best-fit model for the XRR data, which is then used to calculate an electron density profile. The density profiles were modeled as a box fit model where each layer of a film is characterized by different chemical compositions, electron density and interfacial roughness. Using a two box model, StochFit found a best-fit model to the XRR data for the (**G**)C18S, as seen in Figure 4.3, and then calculated the electron density profile from the best-fit model, as illustrated in Figure 4.4.

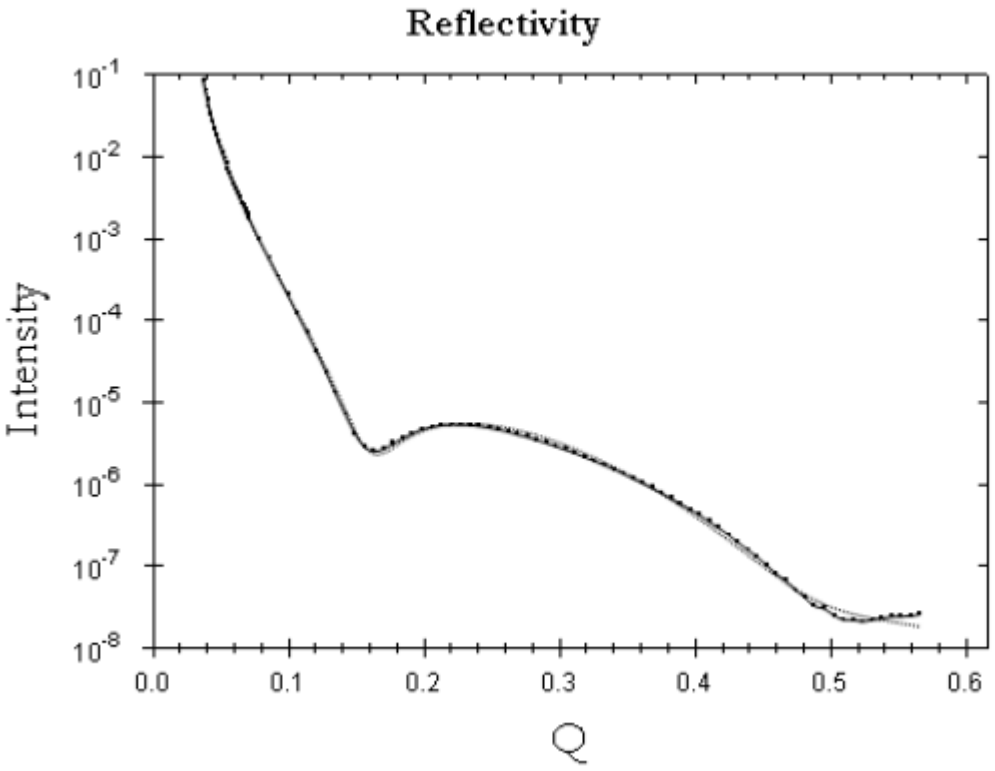

Figure 4.3. Reflectivity of (**G**)C18S LB film on Si(100) plotted against Q. The XRR data are represented by the heavy solid line and the best fit by the dashed line. The chi square, χ^2, for the reflectivity fit was 2.888 E^{-4}.

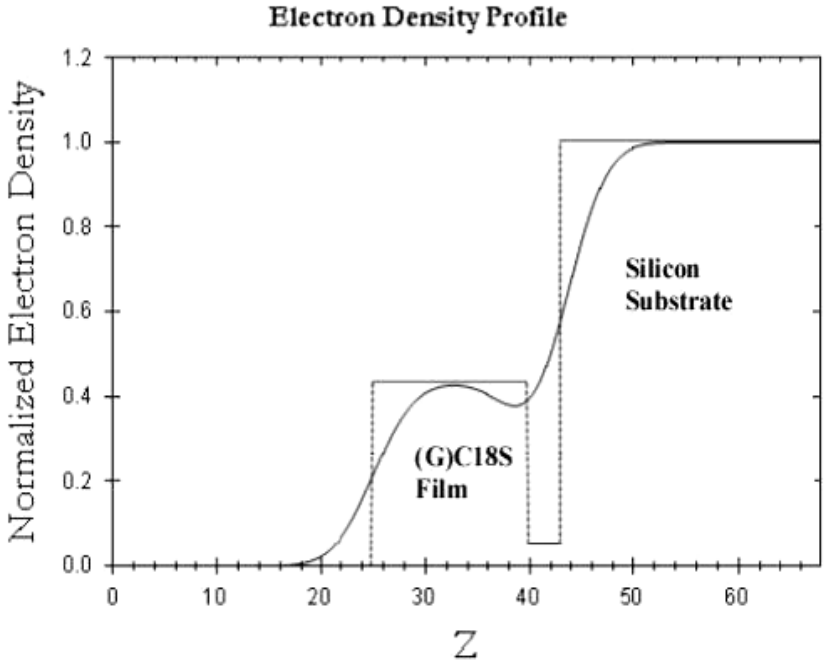

Figure 4.4. Two box model of the normalized electron density of (**G**)C18S film deposited on Si(001). The solid line curve is the data extracted from the XRR fitting while the dashed curve is the box model fitted to the electron density. From the fitting process, the overall film thickness was determined to be ~ 17.4 Å.

The density profile is the physically relevant quantity that XRR measures [3]. The density profile calculated that the average thickness of the (**G**)C18S film was ~ 17.4 Å. As seen in Figure 4.4, the electron density exhibited a noticeable dip at the interface between the silicon surface and the film. It is important to note that the density profile needed to have this dip to fit the XRR data. Since the dip corresponds to a lower electron density than the silicon substrate and increased over distance, it is attributed to the interface between the LB film and the surface of the silicon substrate.

4.2 Host-Guest C18S Monolayers

Mixed monolayers that consisted of a 1:1 mixture of NaC18S and non-amphiphilic guest molecules were spread over a 10^{-2} M guanidinium aqueous subphase.

The host-guest Langmuir films were then deposited on a silicon substrate at a rate of 5 mm/minute. These Langmuir-Blodgett films were studied by GIXD and XRR. The non-amphiphilic guest molecules included in this study were octadecane (C18), octadecanol (C18OH), cholestearyl stearate (C18chol), naphthyl stearate (C18naph) and 2-hydroxystearic acid (2HSA).

4.2.1 1:1 C18S:C18 Monolayers

The Langmuir isotherm formed using a 1:1 solution of NaC18S and C18 over a 10^{-2} M aqueous guanidinium carbonate subphase [(**G**)C18S:C18] showed a liftoff at $A_{lift\text{-}off}$ = 52 Å^2/sulfonate. This was followed by a gradual increase in surface pressure before approaching a condensed phase at $A_{lift\text{-}off}$ = 22 Å^2/sulfonate. The film experienced collapse at a surface pressure of $\Pi \approx 40$ mN/m. Figure 4.5 shows the Π-A isotherm of the 1:1 NaC18S:C18 mixed monolayer over 10^{-2} M **G** aqueous subphase and the subsequent deposition at a surface pressure of 25 mN/m.

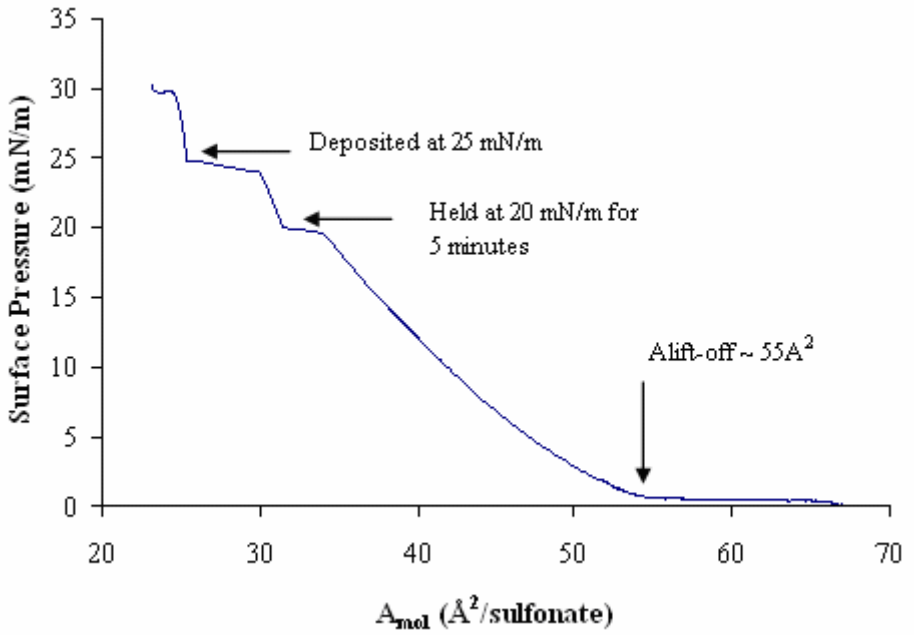

Figure 4.5. Langmuir isotherm of 1:1 NaC18S:C18 mixed monolayer over 10^{-2}M **G** aqueous subphase. Compression was halted at surface pressure of 20 mN/m for 5 minutes to allow the formation of a more uniform monolayer. After the allotted 5 minutes were over, the compression was allowed to resume till a surface pressure of 25 mN/m was reached. Once again compression was stopped and the monolayer was allowed to sit for 5 minutes prior to deposition. Deposition of the monolayer occurred at a surface pressure of 25 mN/m and an area of 27 $Å^2$/sulfonate.

Martin et al reported that the 1:1 (**G**)C18S:C18 monolayer isotherm exhibited three distinct crystalline monolayer phases [2]. At molecular areas less than 55 $Å^2$/sulfonate, which was prior to the surface pressure liftoff, GIXD patterns exhibited a single large peak at q_{xy} = 1.46 Å-1. This single peak was indexed to a hexagonal unit cell with a = b = 4.97Å and $\gamma = 120°$ where the molecules are tilted at an angle of 26° from the normal. At molecular area of 45 $Å^2$/sulfonate, the GIXD pattern exhibited peaks at q_{xy} = 1.46 $Å^{-1}$ and q_{xy} = 1.52 $Å^{-1}$, which were indexed to a rectangular unit cell with a = 4.95 Å, b = 8.27Å and $\gamma = 90°$ with a tilt of 22.4°. As the monolayer is further compressed to a molecular area of 20 $Å^2$/sulfonate, it was found that the system changed back to a hexagonal unit cell that was characterized by one peak at q_{xy} = 1.52 $Å^{-1}$, which was

indexed to a unit cell with a = b = 8.26 Å with γ = 120° where the components are oriented vertically with respect to the air-subphase interface [2].

From Dr. Martin's previous GIXD results at the air-subphase interface and the Langmuir isotherm of a 1:1 NaC18S:C18 mixed monolayer, it was determined that the ideal pressure range to deposit the host-guest monolayer onto a silicon slide was between 25 to 30 mN/m. As seen from Figure 4.5, deposition occurred at a surface pressure of 25 mN/m. Only a few of the (G)C18SC18 films displayed GIXD patterns, which exhibited a single broad, weak peak at q_{xy} = 1.51 $Å^{-1}$, which was indexed to a hexagonal unit cell with a = b = 8.32 Å, γ = 120° and A_{cell} = 59.96 $Å^2$.

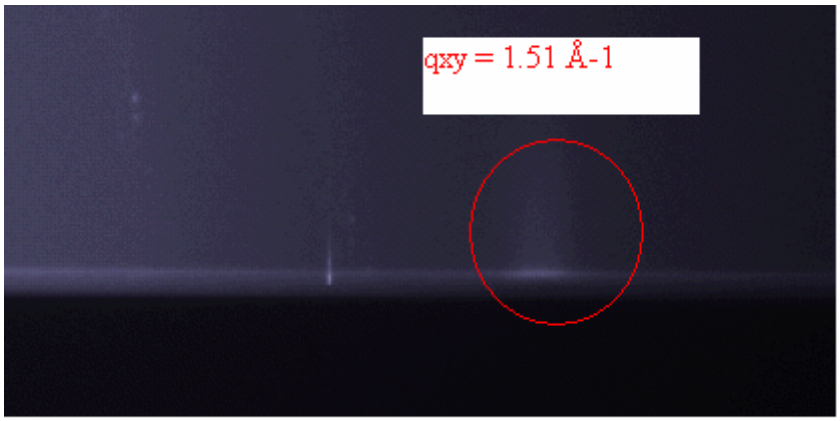

Figure 4.6. GIXD image of (G)C18S:C18 film deposited on a silicon substrate. The peak was at q_{xy} = 1.51 $Å^{-1}$, which was indexed to a hexagonal unit cell with a = b = 8.32 Å, γ = 120° and A_{cell} = 59.96 $Å^2$.

The unit cell parameters were consistent with Martin et al's previous results at the air-subphase interface for a (**G**)C18S:C18 monolayer compressed past a molecular area of 20 $Å^2$/sulfonate [2]. Since the majority of the (G)C18S:C18 films did not diffract, this suggests that an amorphous film was created where the close-packing of the alkyl chains was not achieved.

XRR data for the (**G**)C18S:C18 LB film, as seen in Figure 4.7, indicated a thin film was deposited on the silicon substrate from the oscillations present. Figure 4.7 compares

the XRR of a blank silicon slide (solid line) to a deposited (**G**)C18S LB:C18 film (squares).

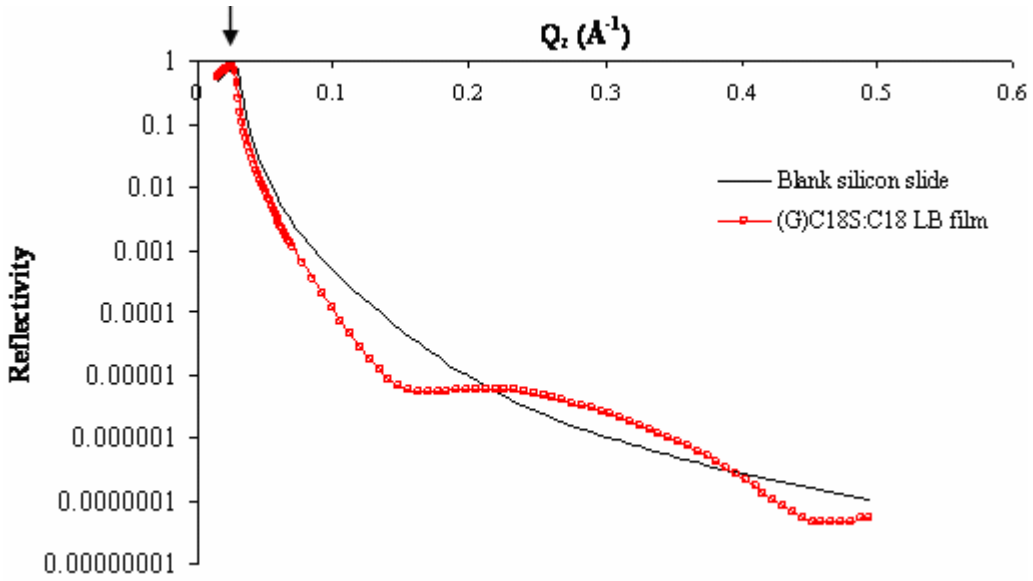

Figure 4.7. Comparison of the specular X-ray reflectivity results for a deposited (**G**)C18S:C18 'host-guest' LB film on a silicon substrate and a blank silicon substrate. The arrow at the top of the plot marks Q_C.

For higher values of Q, the reflectivity drops as Q increases, and a complete oscillatory pattern, becomes apparent, unlike the incomplete pattern seen for the (**G**)C18S film. The peaks of the complete pattern are at 0.155 Å^{-1} and 0.452 Å^{-1}, giving a periodicity of 0.297 Å^{-1}. Using the relationship between periodicity and thickness, $\text{periodicity} = 2\pi/\text{thickness}$, the predicted film thickness was ~ 21 Å. StochFit was used to fit the XRR data and to model the electron density profile for (**G**)C18S:C18. Figure 4.8 illustrates the best-fit model of the XRR data while Figure 4.9 shows the electron density profile calculated from the fit in Figure 4.8.

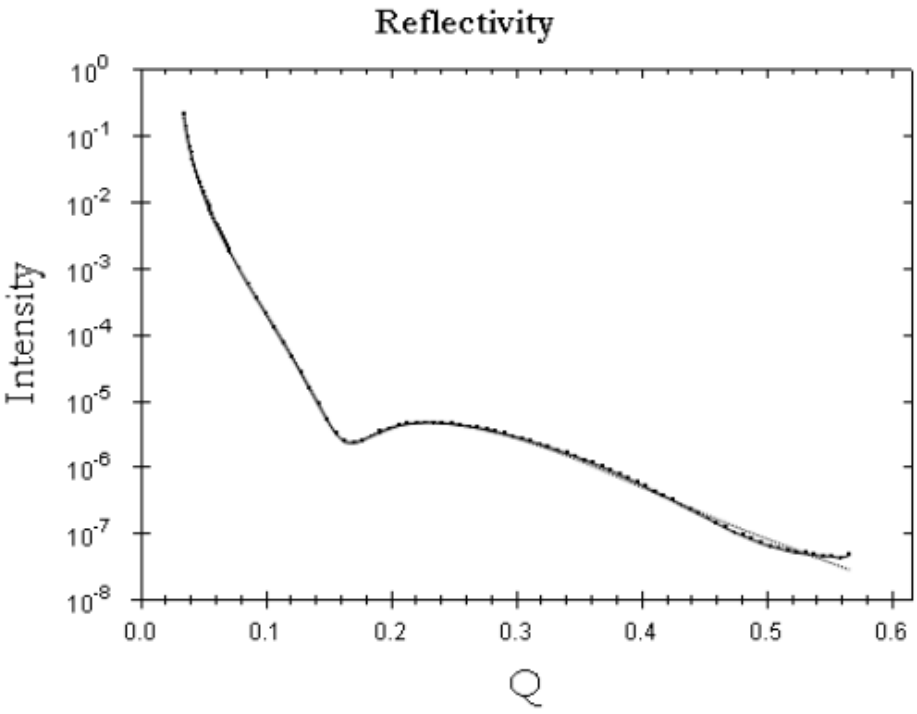

Figure 4.8. XRR of a monolayer film of (**G**)C18S:C18 deposited on Si(100) at a surface pressure of 25 mN/m and the model fit curve produced by StochFit using a non-linear regression. The heavy solid line is the XRR data and the dashed line is the fit. χ^2 for the reflectivity fit was 1.542 E^{-3}.

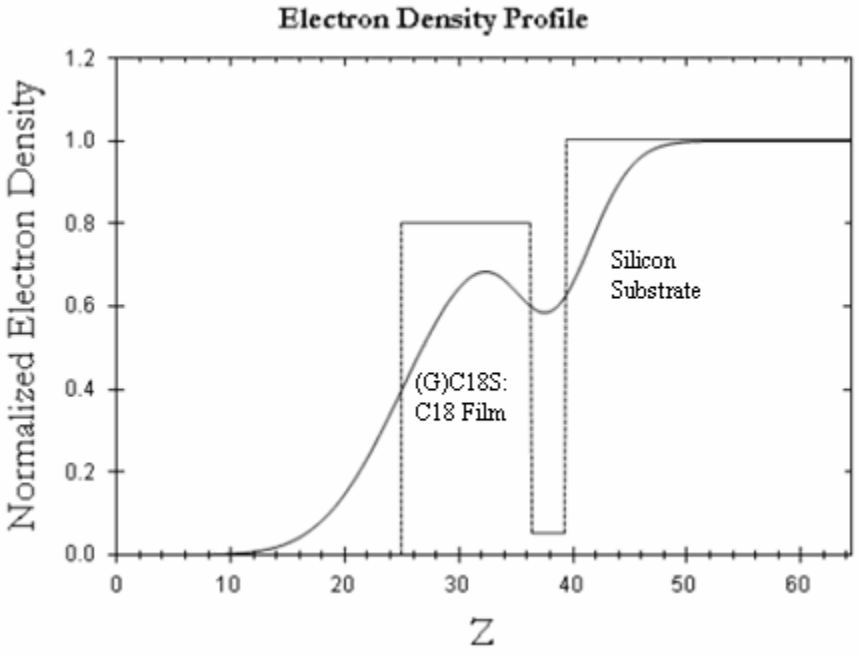

Figure 4.9. Electron density profile calculated for of (**G**)C18S:C18 film deposited on Si(001) from the best- model fit shown in Figure 4.8**Error! Reference source not found.**. The solid line

is the electron density and the dotted line is the two box model fit. The overall film thickness was determined to be ~ 19.5 Å.

The profile for (**G**)C18S:C18 also shows a noticeable dip in electron density at the silicon substrate/thin film interface that is similar to the electron density profile for (**G**)C18S. This is attributed to the interface between the (**G**)C18S:C18 film and the surface of the silicon substrate due to the mismatching of the packing of the LB molecules and the surface silicon molecules. The density profile shows that the average overall thickness of the (**G**)C18S:C18 film was ~ 19.5 Å, which was ~ 1.5 Å decrease from the thickness predicted from the oscillations in the XRR data. This difference could be the result of an error in picking the period of the oscillations from the raw XRR data.

4.2.2 1:1 C18S:C18OH

The Π-A isotherm of the monolayer formed by spreading a 1:1 solution of NaC18S and C18OH over a 10^{-2} M G_2CO_3 aqueous subphase showed a liftoff at $A_{liftoff} \approx 64.4$ $Å^2$/sulfonate, as seen in Figure 4.10, followed by a gradual increase in the surface area as A decreases. The slope of the isotherm increased sharply at ~ 40 $Å^2$/sulfonate, which indicated the formation of a close-packed monolayer phase. The monolayer collapsed at a surface pressure of Π = 47.7 mN/m.

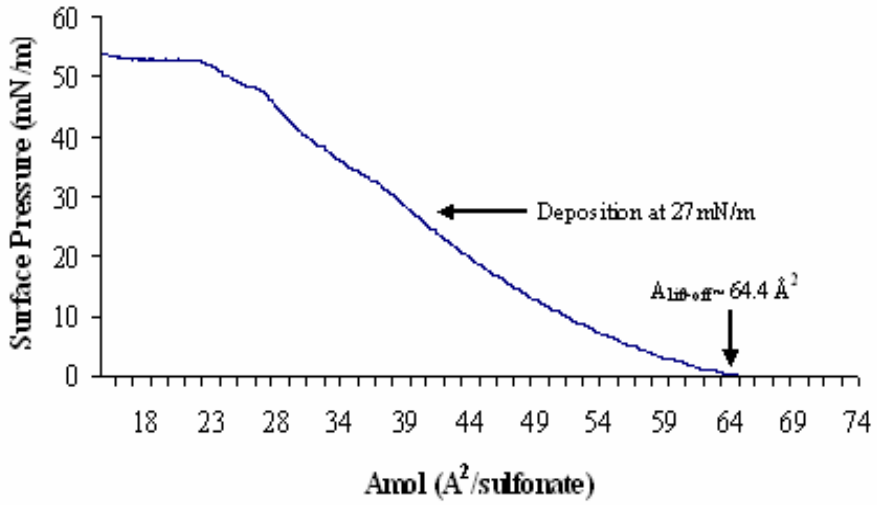

Figure 4.10. Langmuir isotherm of 1:1 NaC18S:C18OH mixed monolayer over 10^{-2} M **G** aqueous subphase. Compression was halted at surface pressure of 20 mN/m for 5 minutes to allow the formation of a more uniform monolayer. After the allotted 5 minutes were over, the compression was allowed to resume till a surface pressure of 25 mN/m was reached. Once again compression was stopped and the monolayer was allowed to sit for 5 minutes prior to deposition. Deposition of the monolayer occurred at a surface pressure of 25 mN/m and an area of 27 $Å^2$/sulfonate.

As seen from Figure 4.10, deposition occurred at a surface pressure of 27 mN/m. All of the (**G**)C18S:C18OH films exhibited GIXD patterns with a single Bragg rod at q_{xy} = 1.51 $Å^{-1}$, which was the same as that produced by the (**G**)C18S:C18 film. The Bragg rod was indexed to a hexagonal unit cell with a = b = 8.32 Å, $\gamma = 120°$ and A_{cell} = 59.96 $Å^2$. The increased crystallinity of the (G)C18S:C18OH is attributed to additional hydrogen bonding occurring at either the top of the film between the –OH function groups or if the between the –OH group and the sulfonate group.

XRR data for the (**G**)C18S:C18OH LB film, as seen in Figure 4.11, indicated a that a thin film was present on the silicon substrate. Figure 4.11 compares the XRR of a blank silicon slide (solid line) to a deposited (**G**)C18S LB:C18OH film (squares).

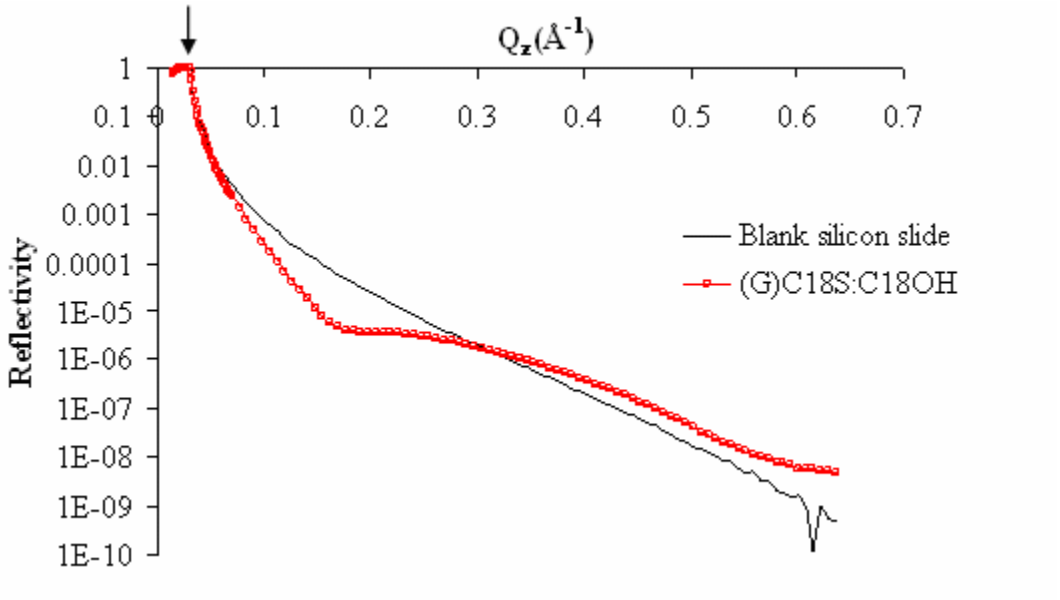

Figure 4.11. Comparison of the XRR data (**G**)C18S:C18OH 'host-guest' LB film on a silicon substrate (squares) and a blank silicon substrate (solid line). The arrow at the top of the plot marks Q_C.

Total reflection occurs for (**G**)C18S:C18OH for values less than Qc and for higher values of Q, a broad incomplete oscillatory pattern becomes apparent in. Unlike the (**G**)C18S:C18 film, a full oscillation was not recorded because of the resolution of the machine, preventing an accurate calculation of the film thickness from the unfitted XRR data. To calculated the film thickness, the XRR data were inputted into StochFit to acquire the electron density profile for (**G**)C18S:C18OH from the best-model of the XRR data. The best-fit model for the XRR data is displayed in Figure 4.12 and the electron density profile calculated from the fit is displayed in Figure 4.13 for (**G**)C18S:C18OH film deposited at 25 mN/m.

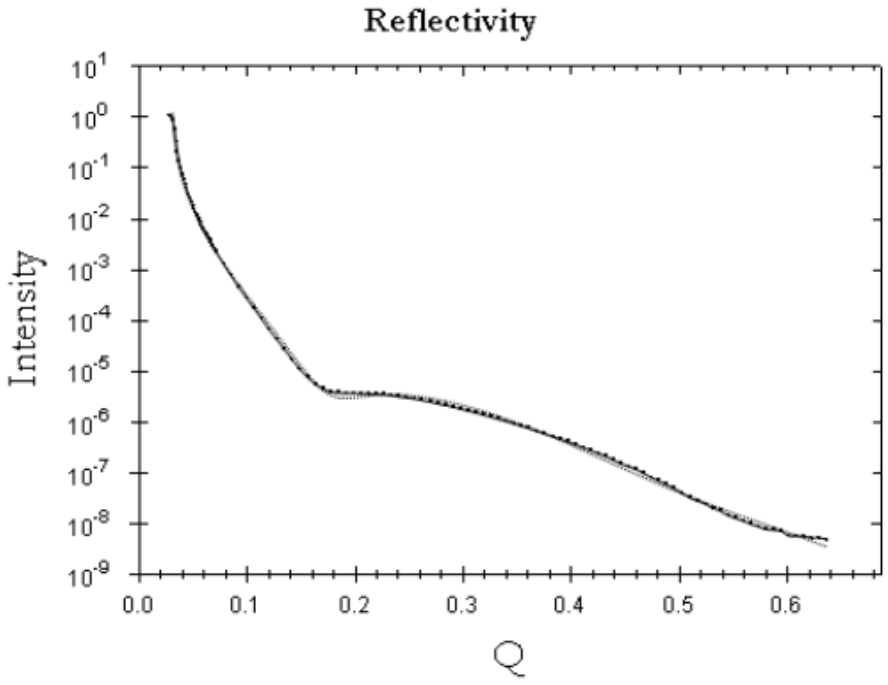

Figure 4.12. XRR from (**G**)C18S:C18OH on silicon deposited at a pressure 25 mN/m. The data are shown with heavy dotted lines and the best nonlinear least-squares regression fit by the dashed lines. χ^2 for the reflectivity fit was $1.196E^{-1}$.

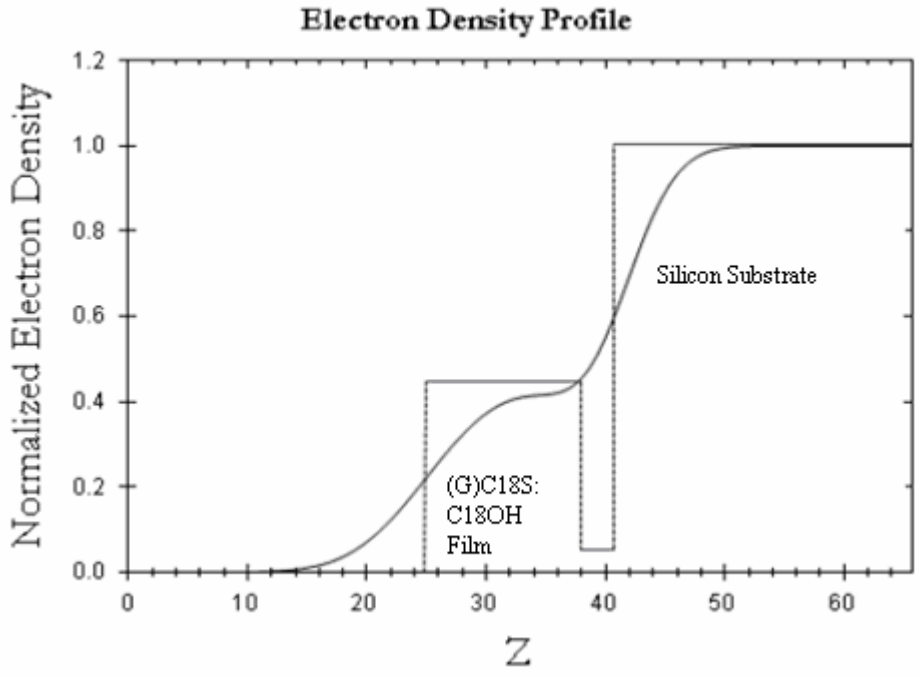

Figure 4.13. Electron density profile calculated from the best-fit XRR model shown in Figure 4.12. The total layer thickness for (**G**)C18S:C18OH was determined to be ~ 15.8 Å.

The electron density profile in Figure 4.13 shows that the average overall thickness of the (**G**)C18S:C18OH film was ~ 15.8 Å. Unlike the electron density profile for (**G**)C18S:C18, the profile for (**G**)C18S:C18OH did not exhibit as noticeable a dip in electron density at the silicon substrate/thin film interface, which indicates that the difference in density between the thin film and silicon substrate is not distinguishable. This could be the result of the OH group of the C18OH guest molecule disrupting part of the film by interfering with the hydrogen bonds between the host film and the spacer molecule and removes the film from the silicon substrate.

4.2.3 1:1 C18S:C18chol

The Π-A isotherm of the monolayer formed by spreading a 1:1 solution of NaC18S and C18chol over a 10^{-2} M G_2CO_3 aqueous subphase showed a liftoff at $A_{liftoff} \approx$ 51 $Å^2$/sulfonate, as seen in Figure 4.14 The monolayer collapsed at A_{mol} = 20 $Å^2$/sulfonate and Π = 42 mN/m.

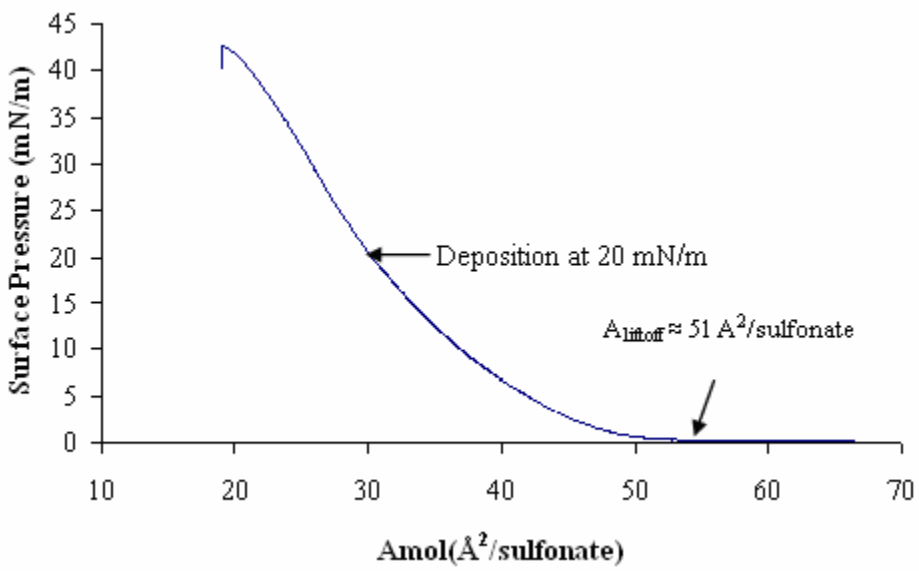

Figure 4.14. Langmuir isotherm of 1:1 NaC18S:C18chol mixed monolayer over 10^{-2} M **G** aqueous subphase. Compression was halted at surface pressure of 20 mN/m for 5 minutes to allow the formation of a more uniform monolayer. After the allotted 5 minutes were over, the film was deposited onto a silicon substrate at the rate of 5 mm/min at 20 mN/m.

Martin et al reported that the 1:1 (**G**)C18S:C18chol Langmuir monolayer GIXD patterns for $A_{mol} \geq 70$ Å^2/sulfonate exhibited a number of Bragg rods [2]. The Bragg rods were indexed to a unit cell with a = 10.0 Å, b = 7.5 Å, and $\gamma = 90$ ° in which the molecules were not tilted with respect to the interface [2]. Dr. Martin stated that this suggested that the cholesterol dominated the packing of the monolayer regardless of the presence of **G** [2].

From Dr. Martin's previous GIXD results at the air-subphase interface and the Langmuir isotherm of a 1:1 (**G**)C18S:C18chol host-guest monolayer, it was determined that the best range of area per sulfonate at which to deposit the monolayer onto a silicon substrate was around 30 Å^2/sulfonate. As seen from Figure 4.14, deposition occurred at a surface pressure of 20 mN/m. The resulting GIXD patterns exhibited a peaks at q_{xy} = 0.83, 1.24, 1.51 and 1.65 Å^{-1}, which was indexed to a unit cell with a = 10.13 Å, b = 7.61

Å, $\gamma = 90°$ and $A_{cell} = 77.16$ Å^2. These results were consistent with the peaks seen at the air/subphase interface.

The XRR data for (**G**)C18S:C18chol film indicated that a film had been deposited on the silicon substrate, illustrated by Figure 4.15, which compares the log of the XRR data of a blank silicon slide to a deposited (**G**)C18S LB:C18chol film.

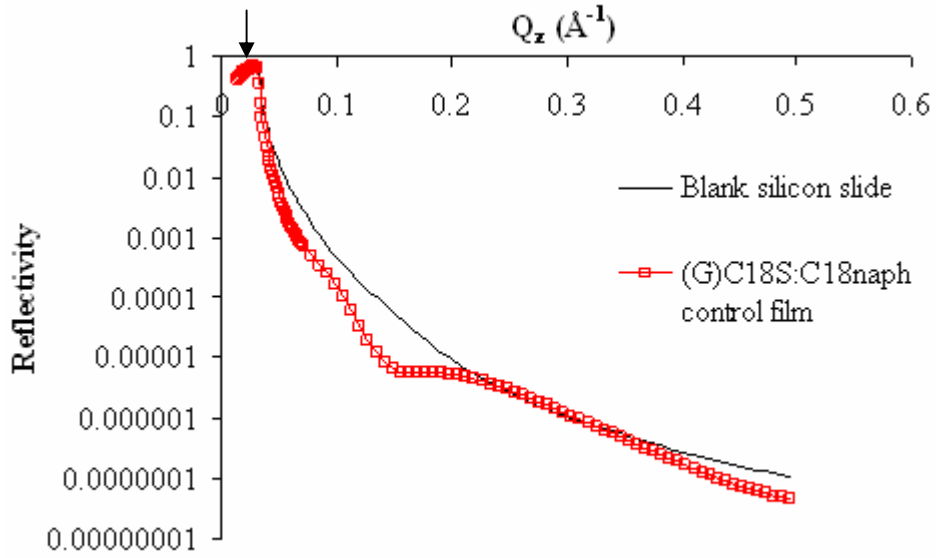

Figure 4.15. XRR data for (**G**)C18S:C18chol LB film on silicon substrate. The solid line is the XRR data for a blank silicon slide while the squares represent the XRR data for the (**G**)C18S:C18chol film. The arrow at the top of the plot marks Q_C.

At values of Q greater than Qc, a broad incomplete oscillatory pattern becomes apparent. A full oscillation was not recorded because of the resolution of the machine, which prevents an accurate calculation of the film thickness from the unfitted XRR data. To calculated the film thickness, the XRR data were inputted into StochFit to acquire the electron density profile for (**G**)C18S:C18chol from the best-model of the XRR data. . Figure 4.16 illustrates the best-fit model of the XRR data for the (**G**)C18S:C18chol film

deposited at 20 mN/m and Figure 4.17 shows the electron density profile calculated from the fit.

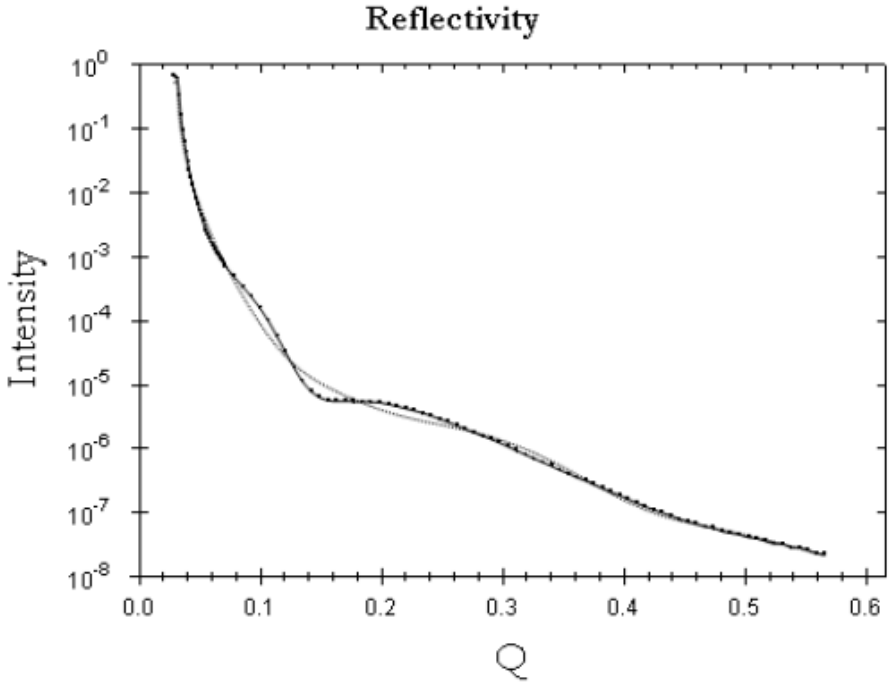

Figure 4.16. XRR from (**G**)C18S:C18chol on silicon deposited at a pressure 20 mN/m. The data are shown with heavy dotted lines and the best nonlinear least-squares regression fit by the dashed lines. χ^2 for the reflectivity fit was $9.36E^{-2}$.

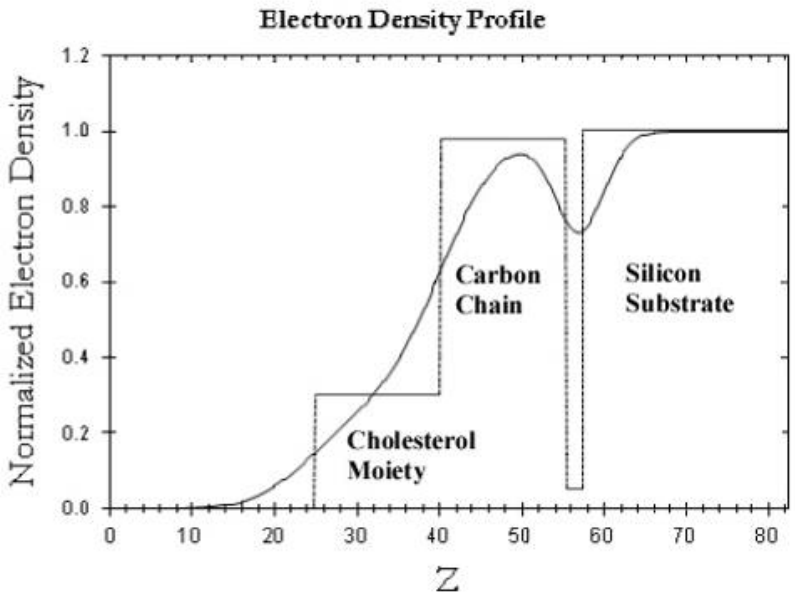

Figure 4.17. Electron density profile calculated from the best-fit XRR model shown in Figure 4.16. A three box model was used to determine the overall film thickness due to the size of the cholesterol moiety. The total layer thickness for (**G**)C18S:C18chol was determined to be ~ 33 Å.

The overall thickness calculated for a (**G**)C18S:C18chol film was ~ 33 Å using a three box model fit to the electron density profile, as illustrated in Figure 4.17. A two box model fit of the electron data did not produce an adequate fit because the cholesterol moiety is large enough to have a different electron density than the carbon chain of the film and possibly dominate the packing of the monolayer.

4.2.4 1:1 C18S:C18naph

The Π-A isotherm of the monolayer formed by spreading a 1:1 solution of NaC18S and C18naph over a 10^{-2} M G_2CO_3 aqueous subphase – (**G**)GC18S:C18naph – exhibited a liftoff at $A_{lift\text{-}off} \approx 81$ Å^2/sulfonate followed by a steady increase in surface pressure. This was followed by a significant change in slope, which may indicate a

possible phase change at 50 $Å^2$/sulfonate and $\Pi \approx 10$ mN/m. Deposition onto a silicon substrate occurred at a surface pressure of 20 mN/m, as illustrated in Figure 4.18.

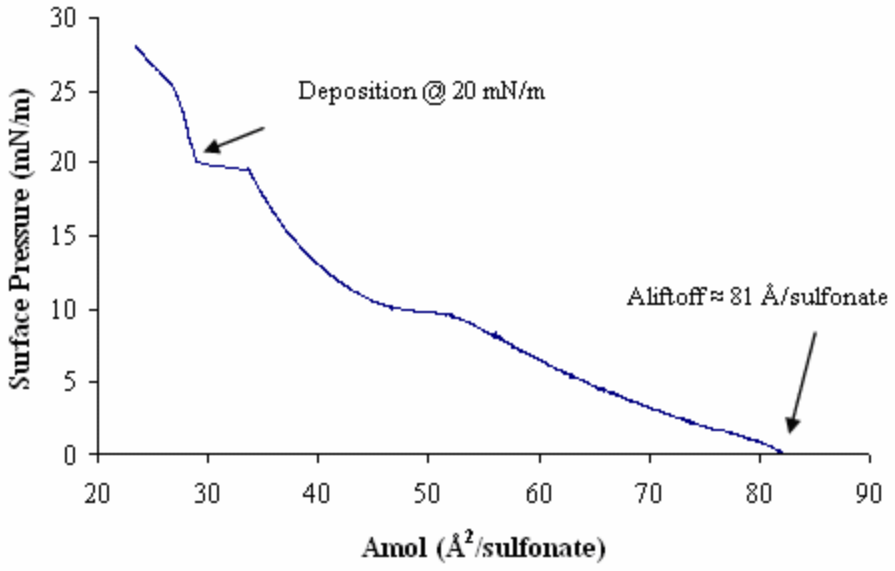

Figure 4.18. Langmuir isotherm of 1:1 NaC18S:C18naph mixed monolayer over 10^{-2} M **G** aqueous subphase. The film was deposited onto a silicon substrate at the rate of 5 mm/min at 20 mN/m.

The resulting GIXD patterns exhibited a Bragg rods at $q_{xy} = 0.83$, 1.24, 1.51 and 1.65 $Å^{-1}$, which were indexed to a unit cell with a = 9.26 Å, b = 7.68 Å, and $\gamma = 90$ ° with $A_{cell} = 71.16$ $Å^2$, which are illustrated in Figure 4.19.

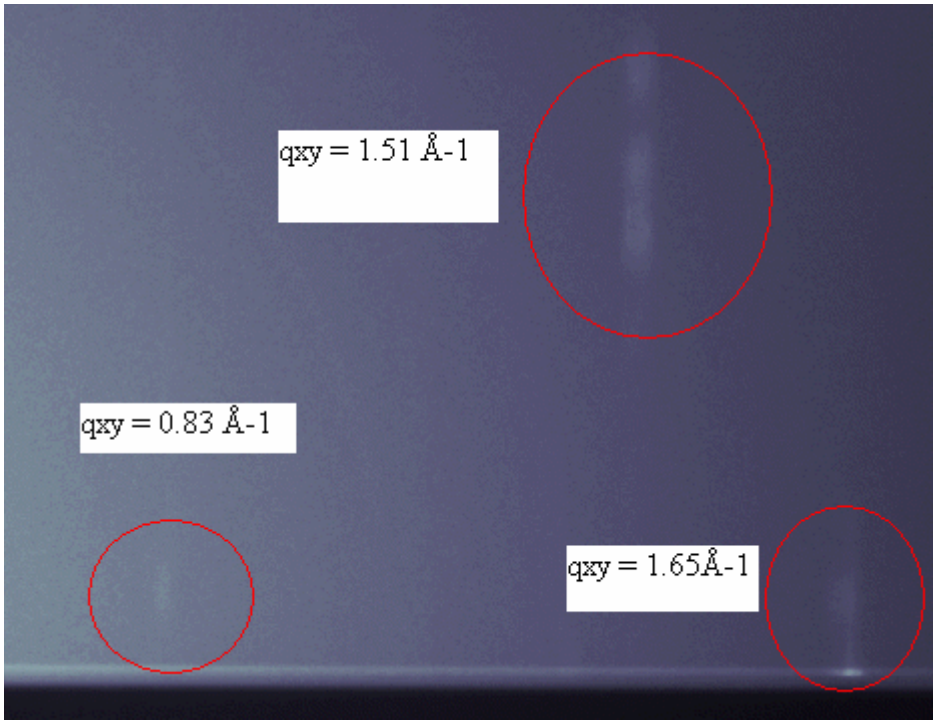

Figure 4.19. The resulting GIXD patterns for (**G**)C18S:C18naph exhibited Bragg rods at q_{xy} = 0.83, 1.24, 1.51 and 1.65 $Å^{-1}$, which were indexed to a unit cell with a = 9.26 Å, b = 7.68 Å, and γ = 90 ° with A_{cell} = 71.16 $Å^2$.

Figure 4.20 exhibits XRR results for a (**G**)C18S:C18naph film deposited at 20 mN/m on a silicon substrate compared to the XRR of a blank silicon slide. The reflected intensity was measured as a function of the incidence angle, normalized by dividing by the incidence intensity and plotted. The shape of the XRR curve indicates the presence of a monolayer at the silicon surface.

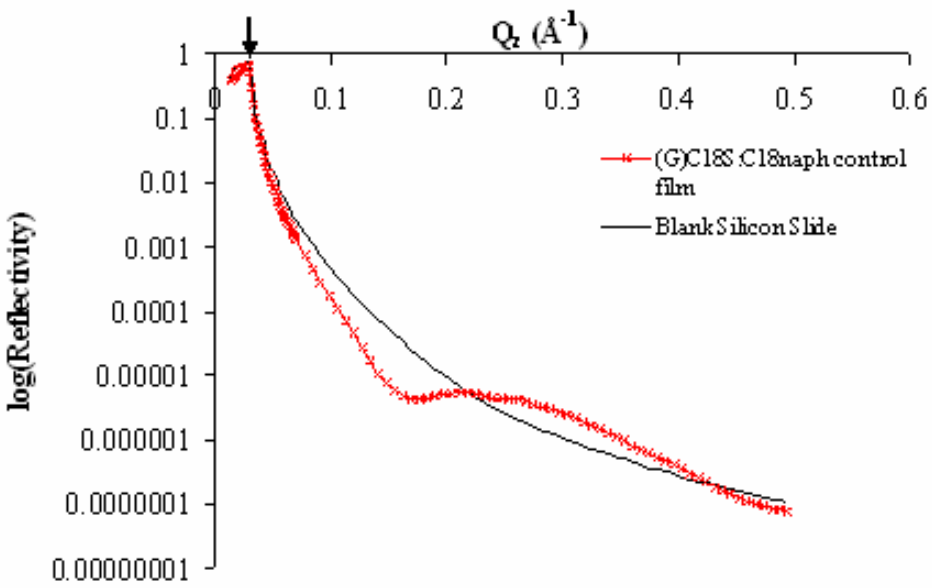

Figure 4.20. XRR data for (**G**)C18S:C18naph LB film on silicon substrate. The solid line is the XRR data for a blank silicon slide while the crosses represent the XRR data for the (**G**)C18S:C18naph film. The arrow at the top of the plot marks Q_C.

Figure 4.20 displays the XRR data for (**G**)C18S:C18naph and a incomplete broad oscillatory pattern was produced as Q increased. To calculated the film thickness for (**G**)C18S:C18naph, the normalized XRR data was inputted into StochFit to extract the electron density profile from the best-fit model of the XRR data. Figure 4.21 illustrates the best-fit model of the XRR data for a (**G**)C18S:C18naph film deposited at 20 mN/m and Figure 4.22 displays the electron density profile. A three box model was used because the naphthyl moiety is large enough to have a significantly different electron density than the carbon chain.

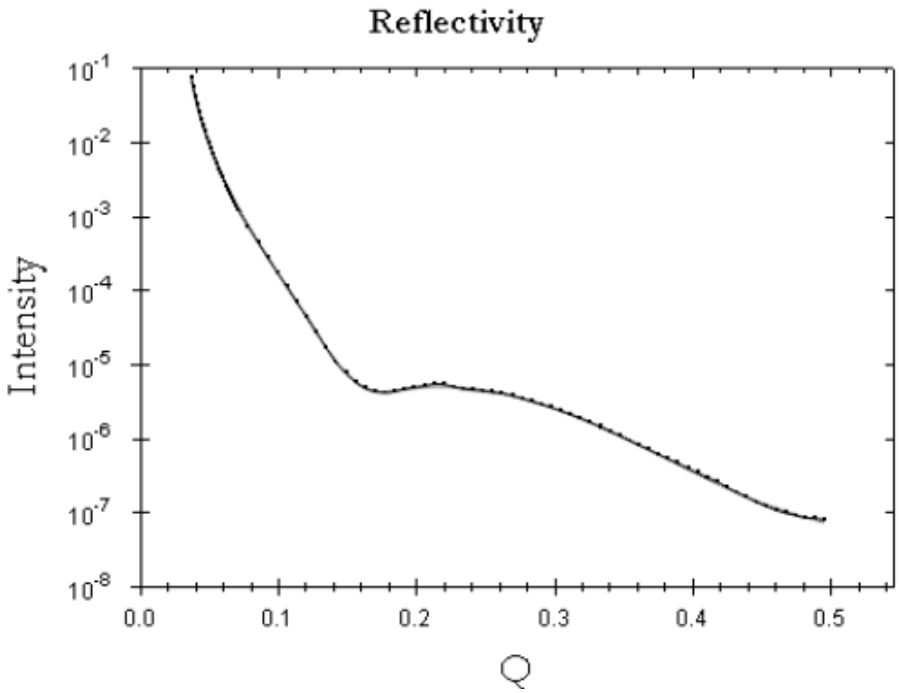

Figure 4.21. XRR data from a (G)C18S:C18naph film deposited on a silicon substrate at a surface pressure of 20mN/m. The heavy dotted line is the actually XRR data and the best nonlinear regression least-squares fit is the dashed line. χ^2 of the reflectivity fit was $1.5E^{-3}$.

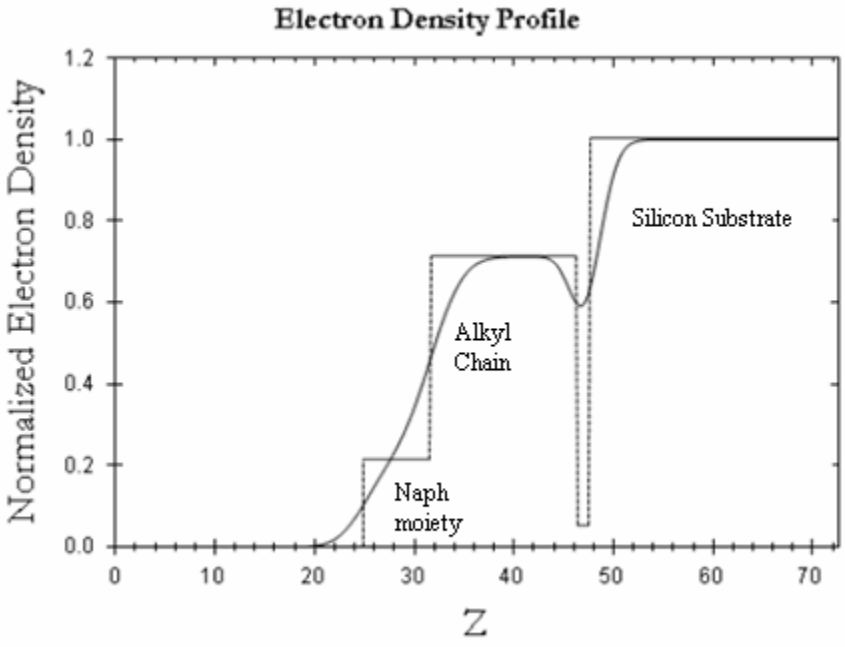

Figure 4.22. The electron density profile calculated from the best fit shown in Figure 4.21 for (G)C18S:C18naph on silicon. The solid line is the electron density and the dashed line is the box model fitted using 3 boxes. The overall thickness calculated from the box model was ~22.7 Å.

Using a three box model fit to the electron density profile, the overall thickness calculated for a (**G**)C18S:C18naph film was ~ 22.7 Å.

4.2.5 1:1 (G)C18S:2HSA

The Π-A isotherm of the monolayer formed by spreading a 1:1 solution of NaC18S and 2HSA over a 10^{-2} M G_2CO_3 aqueous subphase – (**G**)GC18S:2HSA – exhibited a liftoff at $A_{lift\text{-}off} \approx 88$ Å^2/sulfonate followed by a steady increase in surface pressure. This was followed by a significant change in slope. Deposition onto a silicon substrate occurred at a surface pressure of 20.4 mN/m, as illustrated in Figure 4.23.

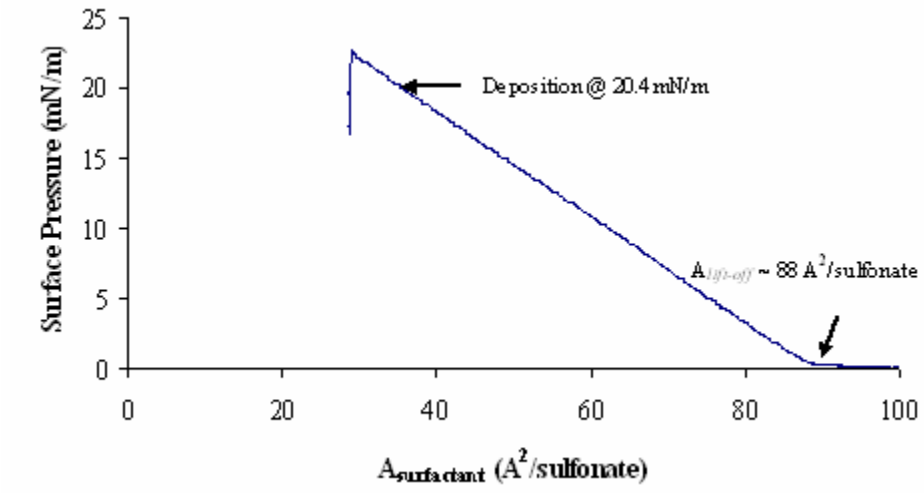

Figure 4.23. Langmuir isotherm of 1:1 NaC18S:2HSA host-guest monolayer over 10^{-2} M **G** aqueous subphase. The film was deposited onto a silicon substrate at the rate of 5 mm/min at 20.4 mN/m.

No diffraction peaks were observed from the deposited (**G**)C18S:2HSA film suggesting that the hydrogen bonds were disrupted preventing a crystalline structure from forming.

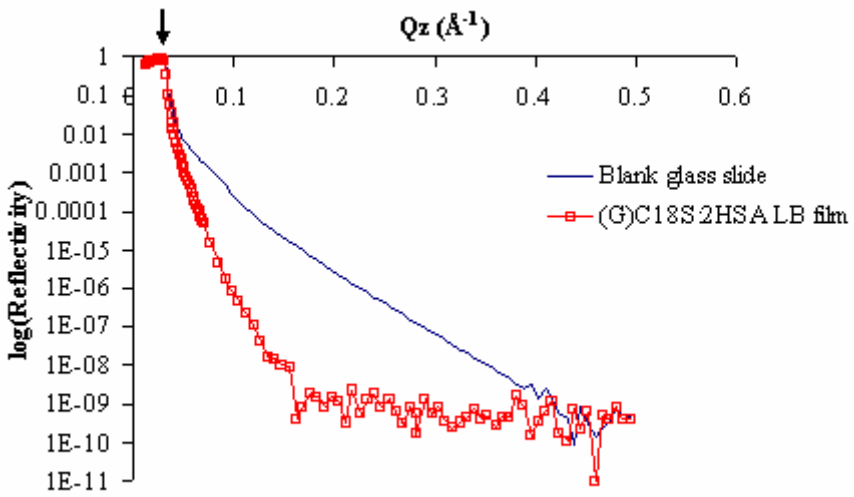

Figure 4.24. XRR data for (**G**)C18S:2HSA LB film on silicon substrate. The solid line is the XRR data for a blank glass slide while the crosses represent the XRR data for the (**G**)C18S:2HSA film. The arrow at the top of the plot marks Q_C.

Figure 4.24 exhibits XRR results for a (**G**)C18S:2HSA film deposited at 20.4 mN/m on a glass substrate compared to the XRR of a blank glass slide. The shape of the XRR curve indicates the presence of a monolayer at the silicon surface. However, as Q increased, the count rate was so low that the specularly reflected beam was not distinguished from the background. This prevented StochFit from computing a best-fit model of the raw XRR data; therefore, the film thickness was not determined from the electron density profile.

4.3 LB Stability Test Results

4.3.1 (G)C18S LB film stability test results from immersion in hexane

The LB films used in the stability tests were fabricated at the same time as the slides for the GIXD and XRR studies. This was accomplished by submerging four silicon slides of the same dimension into the **G** subphase. As previously stated, two of

the four slides were used immediately used for GIXD and XRR studies and functioned as the control slides to which the stability tests were compared. The other two slides were subjected to various stability tests. The effects of immersion in a nonpolar solvent, hexane, for 30 minutes on the (**G**)C18S film was the first stability test conducted. The second stability test was the immersion of the (G)C18S film into a polar solvent, either a 20% THF:hexane mixture or DI water. These results are discussed in the next section. Upon removal from hexane, specular X-ray reflectivity was taken of the slide to determine the changes in the molecular structure of the film. The reflectivity intensity of the (**G**)C18S film was altered by the hexane, as seen in Figure 4.25.

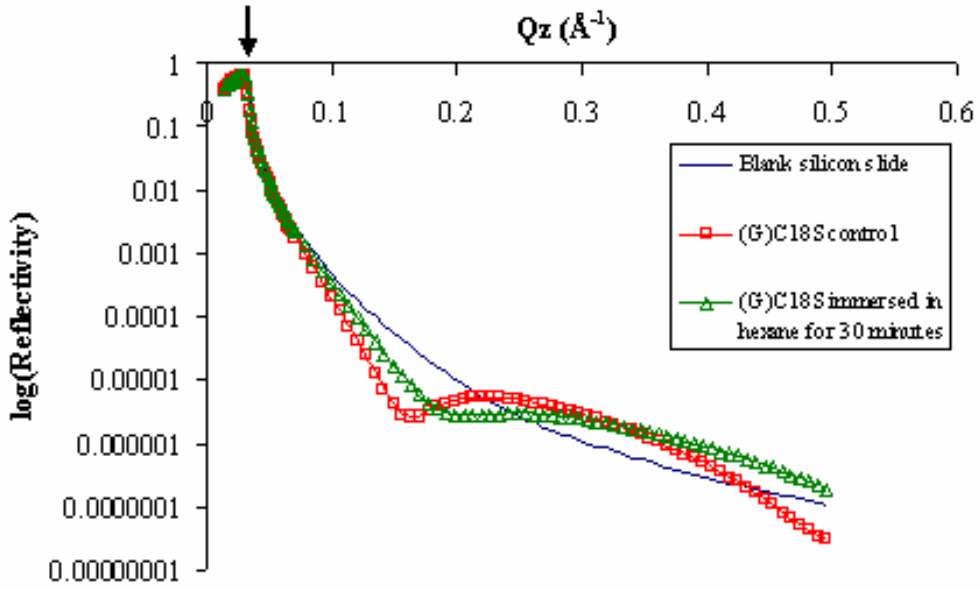

Figure 4.25. Comparison of the reflected intensity versus q_z for X-rays reflected from the blank silicon slide (solid line), (**G**)C18S control film (squares) and (**G**)C18S film immersed in hexane for 30 minutes (triangles). The arrow at the top of the plot marks Q_C.

The solid line in Figure 4.25 represents the XRR from a blank silicon slide, the squares represent the XRR data for the (**G**)C18S control film while the triangles are the XRR data after immersing the (**G**)C18S film in hexane for 30 minutes. The oscillations

within the XRR data in Figure 4.25 can be seem more clearly in Figure 4.26, where the XRR data for the (**G**)C18S films were normalized by the XRR data of the blank silicon slide.

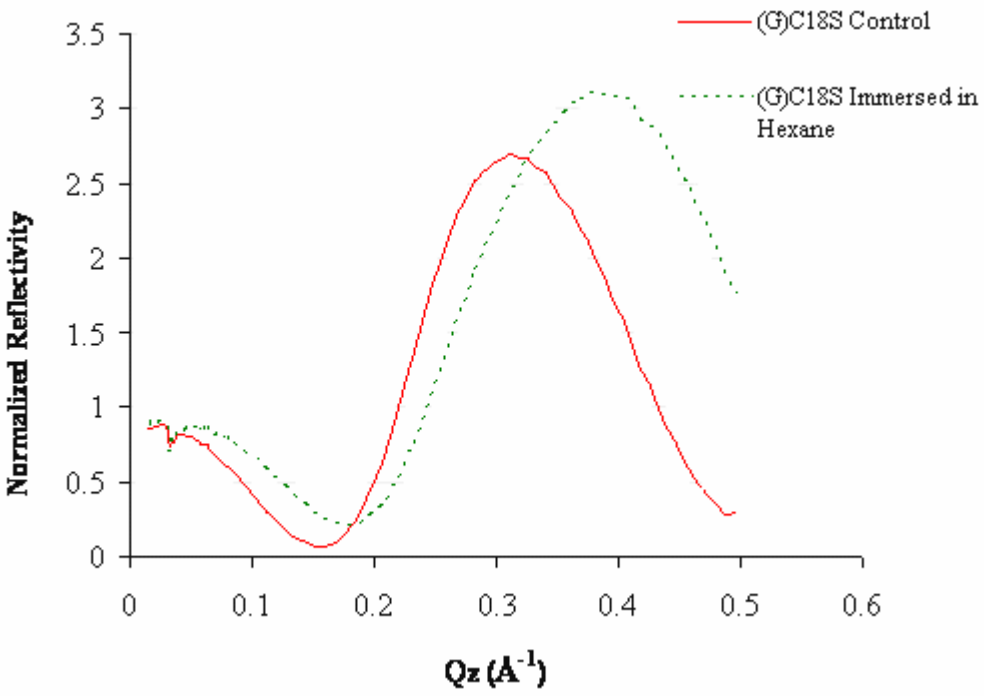

Figure 4.26. Normalized to the intensity of the blank silicon slide, shifts in the XRR data in Figure 4.25 for the (**G**)C18S control film and the (**G**)C18S film immersed in hexane for 30 minutes become more apparent in this figure.

From both Figure 4.25 and Figure 4.26, an increase in the oscillation period resulting from the immersion of the (**G**)C18S film into hexane suggests that the total film thickness is decreasing. This decrease could be due to the hexane altering the crystal structure of the (**G**)C18S film or removing the film from the silicon surface by disrupting the hydrogen bonds. GIXD results would be needed to fully understand the mechanism.

To quantify the decrease in total film thickness, the electron density for both (**G**)C18S films was extracted from the best-fit XRR data and modeled using a two box model fit.

Figure 4.27 shows the best-fit density profiles for the (**G**)C18S control film (the solid line) and the (**G**)C18S film immersed in hexane for 30 minutes (the dashed line).

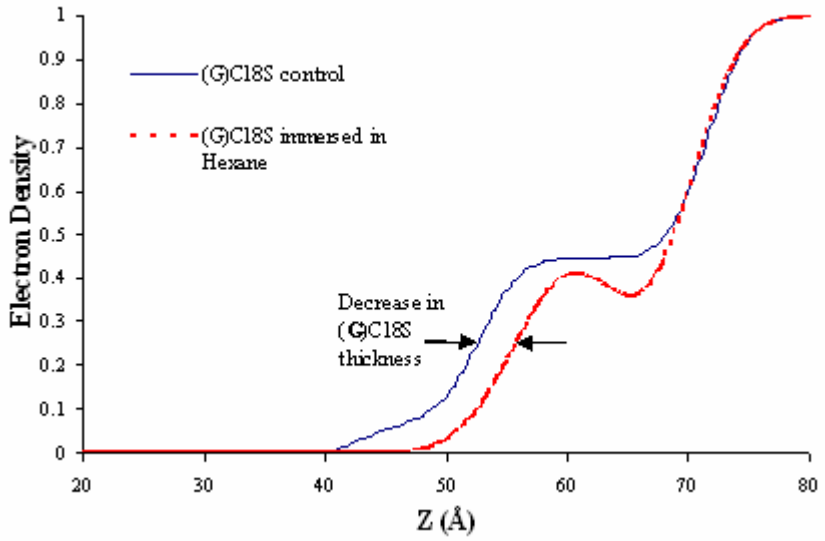

Figure 4.27. Electron density profile calculated from the best fits for (**G**)C18S control and (**G**)C18S immersed in hexane. The solid line is the initial profile and the dashed line is after immersion in hexane after 30 minutes. The total layer thickness shifted from ~17.4 Å to ~10.3 Å.

It is important to note that a dip in the electron density appears at the substrate/film interface and the film thickness decreases from ~ 17.4 Å to ~ 10.3 Å for the film that has been immersed in hexane for 30 minutes. The dip in the electron density is still attributed to the adsorption of the hydrocarbon film on the silicon surface; however, it is better defined in the (**G**)C18S immersed in hexane. The significant decrease in film thickness is attributed to the hexane molecules inserting themselves into the film causing changes in the overall film height.

4.3.2 (G)C18S LB Film stability test results from immersion in a 20% THF: Hexane mixture

The second stability test conducted on (**G**)C18S film was to see the effects of polar solvents on the film. The slide was immersed in a mixture of 20% THF to 80% hexane for a 30 minute time period. Upon removal from the mixture, the slide was immediately subjected to XRR. The changes in the XRR data from the (**G**)C18S control slide and the slide immersed in 20% THF:hexane for 30 minutes are illustrated in Figure 4.28.

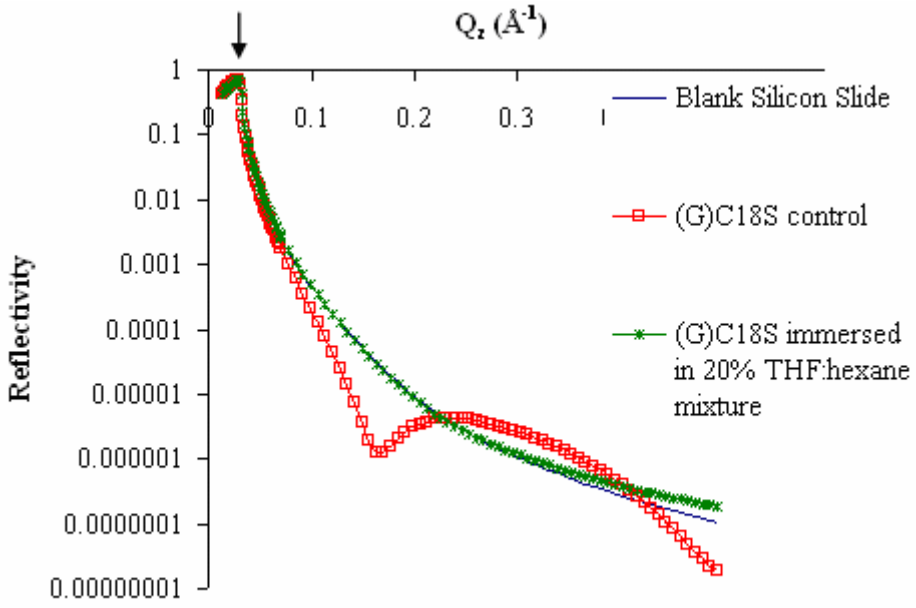

Figure 4.28. XRR from a blank silicon slide (solid line), (**G**)C18S control film (squares line) and (**G**)C18S film immersed for 30 minutes in 20 % THF:hexane mixture (crosses line). The arrow at the top of the plot marks Q_C.

The absence of oscillations in the XRR data for (**G**)C18S immersed in 20% THF:hexane mixture, as seen in Figure 4.28, can be seen more clearly in Figure 4.29, where the XRR data for the (**G**)C18S films were normalized by the XRR data of the blank silicon slide.

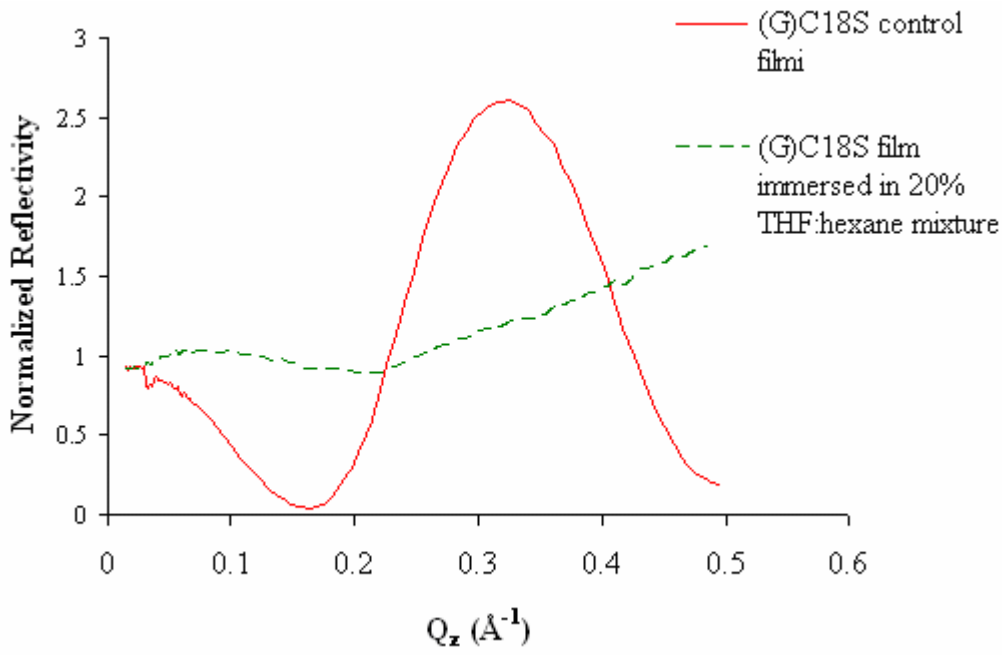

Figure 4.29. Normalized to the intensity of the blank silicon slide, shifts in the XRR data in Figure 4.28 for the (**G**)C18S control film (solid line) and the (**G**)C18S film immersed in 20% THF:hexane for 30 minutes (dashed line) become more apparent in this figure. The absence of any oscillations indicated that the film was completely removed by the 20% THF:hexane mixture.

The absence of oscillations in the XRR data for the (**G**)C18S film immersed in the 20% THF:hexane mixture suggests that the THF completely removed the (**G**)C18S film from the silicon. This could be the result of the THF disrupting the physisorption between the LB molecules and the silicon substrate by interacting with the polar head group of the LB molecules.

4.3.3 (G)C18S:C18 LB film stability results from immersion in Hexane

As with the (**G**)C18S films, the (**G**)C18S:C18 films used in the stability tests were fabricated at the same time as the slides for the GIXD and XRR studies. As previously stated, two of the four slides were used immediately used for GIXD and XXR studies as the control slides to which the stability tests results would be compared too. Hexane was again used to observe the effects of immersing the (**G**)C18S:C18 films in a nonpolar

solvent. The films were immersed for 30 minutes and on removal, XRR was performed to determine the changes in the overall molecular structure of the film. The reflectivity intensity of the (**G**)C18S:C18 film was altered by the hexane, as seen in Figure 4.30.

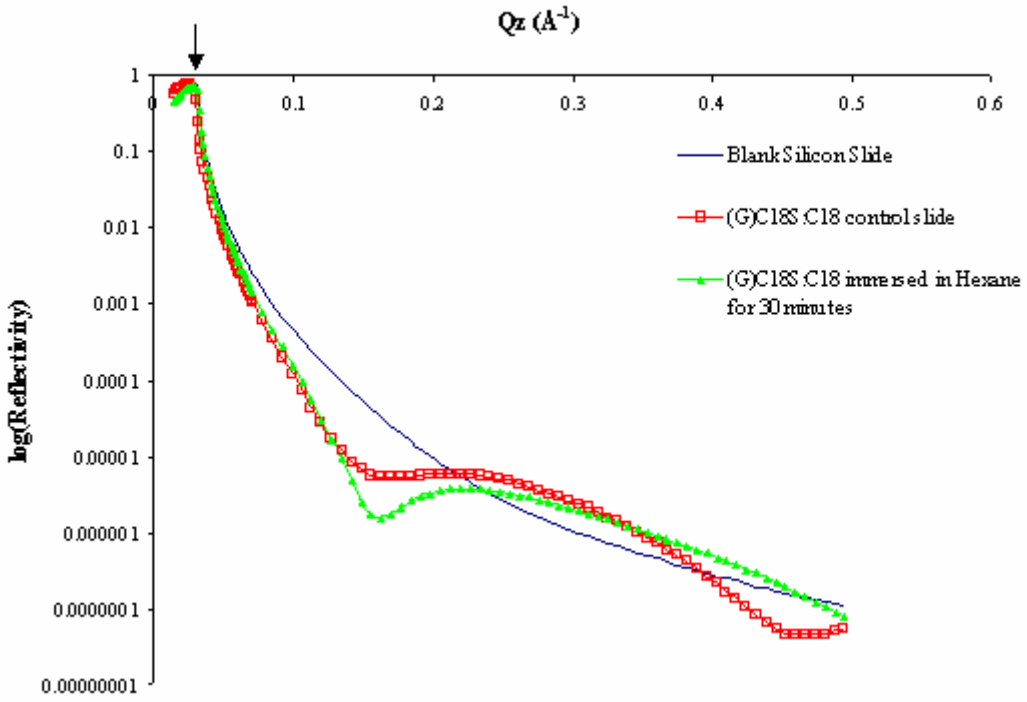

Figure 4.30. XRR from a blank silicon slide (solid line), (**G**)C18S:C18 control film (squares) and (**G**)C18S:C18 film immersed for 30 minutes in hexane (triangles).

The solid line in Figure 4.30 represents the XRR data from a blank silicon slide (no film deposited), the square are the XRR data for the (**G**)C18S:C18 control film (no stability test performed) while the triangle are the XRR data for the (**G**)C18S:C18 film immersed in hexane for 30 minutes. From this figure, it can be seen that the immersion of the (**G**)C18S:C18 film in hexane resulted in an increase in the oscillation period of the reflectivity data, implying that the total film thickness decreased. The oscillations in the XRR data are better illustrated in Figure 4.31 where the data were normalized to the intensity of the blank silicon slide.

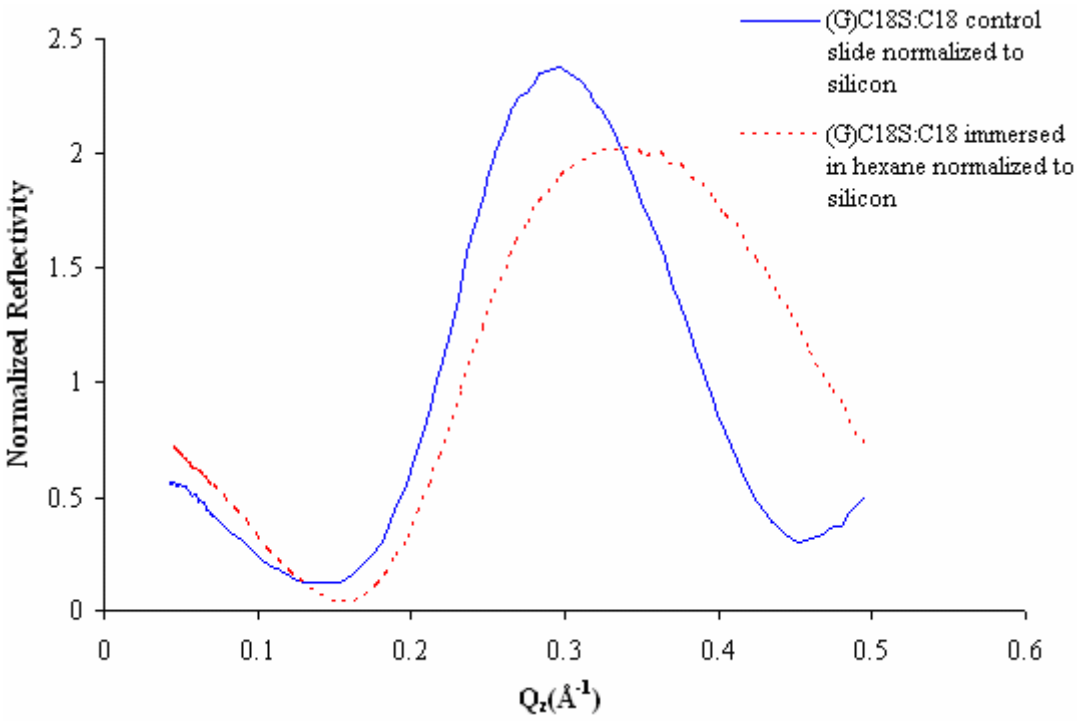

Figure 4.31. Normalized to the intensity of the blank silicon slide, shifts in the XRR data in Figure 4.30 for the (**G**)C18S:C18 control film (solid line) and the (**G**)C18S:C18 film immersed in hexane for 30 minutes (dashed line) become more apparent in this figure. The increase in the oscillation period of (**G**)C18S:C18 from immersion implies that the overall thickness of the film decreased, since the oscillation period has an inverse relation with film thickness.

From both Figure 4.30 and Figure 4.31, a significant increase in oscillation of the XRR data from the immersion of the (**G**)C18S:C18 film in hexane. In order to quantify the corresponding decrease in film thickness, the electron density for both (**G**)C18S:C18 films was extracted from their respective best fit model of the XRR data. The best-fit model for XRR data for the control slide was illustrated earlier in this chapter in Figure 4.8 and the calculated electron density was shown in Figure 4.9. Figure 4.32 illustrates the best-fit nonlinear least square regression model for the reflectivity data from (**G**)C18S:C18 film immersed in hexane for 30 minutes, which was then used to extract the electron density profile for the film, as seen in Figure 4.33.

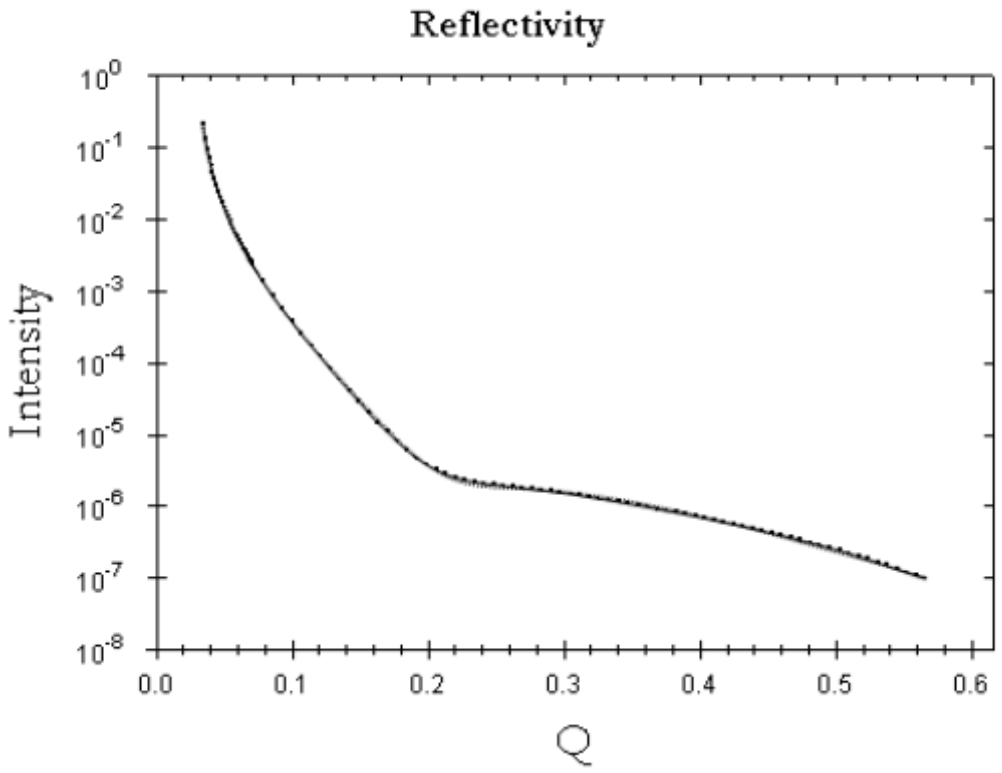

Figure 4.32. XRR of a monolayer film of (**G**)C18S:C18 deposited on Si(100) at a surface pressure of 25 mN/m and immersed in hexane for 30 minutes. The dotted line is the XRR data and the dashed line is the fit. The chi square for the reflectivity fit was 7.889 E^{-4}.

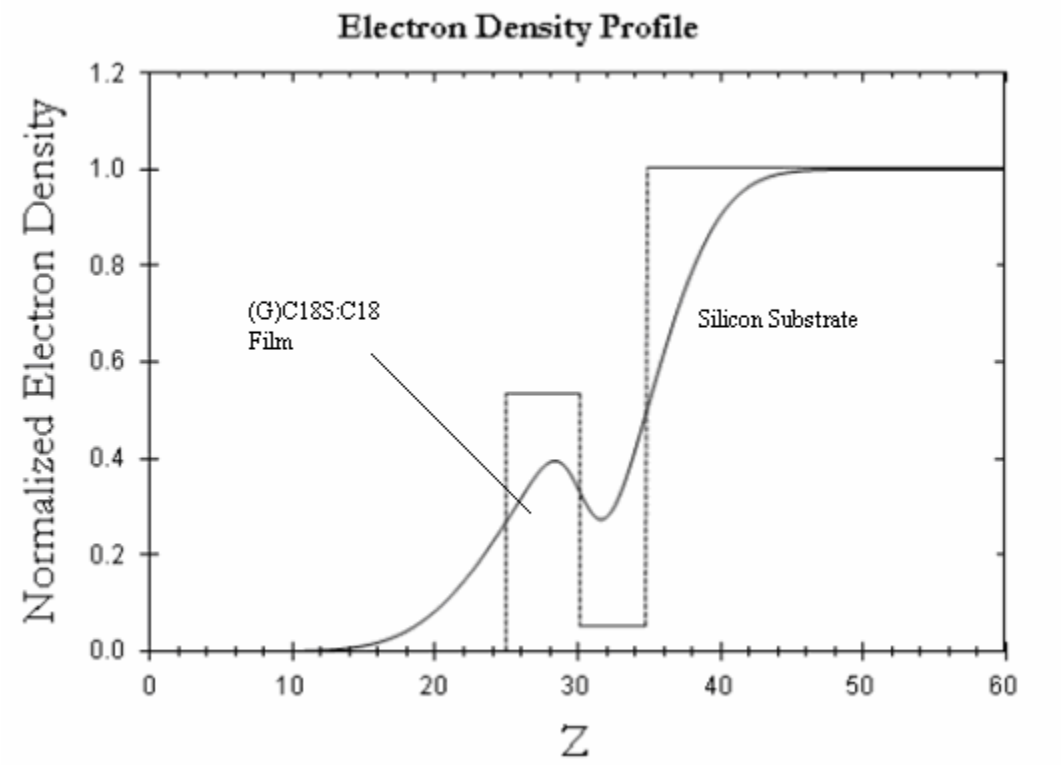

Figure 4.33. Electron density profile calculated from the best fit shown in Figure 4.32. The solid line electron density profile and the dashed line the box model fit. The total layer thickness was determined to be ~ 13 Å.

Figure 4.33 illustrates the best-fit density profile for the (**G**)C18S:C18 film immersed in hexane for 30 minutes (solid line) and the box model (dotted line) fitted to the data. From the density profile, the overall film thickness was calculated ~ 13 Å.

The electron density profiles for the (**G**)C18S:C18 control film and the (**G**)C18S:C18 film immersed in hexane were overlaid, as seen in Figure 4.34, to observe the shift in electron density caused by the hexane and to calculate the corresponding change in overall film thickness.

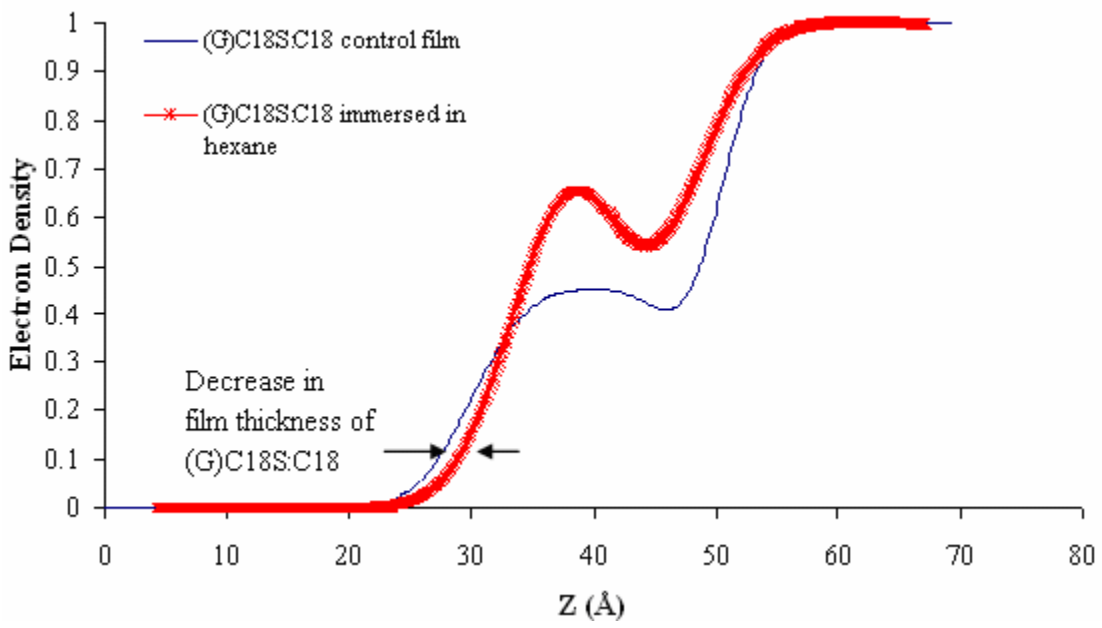

Figure 4.34. Electron density profile calculated from the best fits shown in Figure 4.9 and Figure 4.33. The solid line is the initial profile and the crosses are after immersion in hexane after 30 minutes. The total layer thickness shifted from ~19 Å to ~ 13 Å.

Figure 4.34 illustrates the shift in electron density from immersing the (**G**)C18S:C18 film in hexane for 30 minutes, which resulted in a decrease from ~ 19 Å to ~ 13 Å in overall film thickness. This significant decrease in film thickness suggested that the C18 guest molecules were replaced by hexane, thus reducing the average thickness of the film. This could be confirmed by GIXD data by observing the changes in crystal structure from the possible hexane substitution.

4.3.4 (G)C18S:C18 LB Film stability results from immersion in a 20% THF: Hexane mixture and 40% THF:Hexane mixture

Immersion in polar solvents was the second stability test conducted on (**G**)C18S:C18 films. A 20% THF:hexane mixture and a 40% THF:hexane mixture were used to observe the effects of a polar solvent on the film. The slides were immersed in

each mixture for 30 minutes. Upon removal from the mixture, the slides were immediately subjected to XRR.

Figure 4.35 shows the XRR data for the blank silicon slide (solid line), the (**G**)C18S:C18 control slide (squares) and the (**G**)C18S:C18 slide immersed in the 20% THF:hexane mixture (crosses). The film immersed in the 40% THF:hexane mixture did not exhibit any reflectivity, which suggests that the film had been completely removed from the silicon substrate. The removal of the film could be from the THF interacting with the polar head group of the molecules, thus disrupting physisorption and the hydrogen-bonding network between the polar head and **G** spacer molecules.

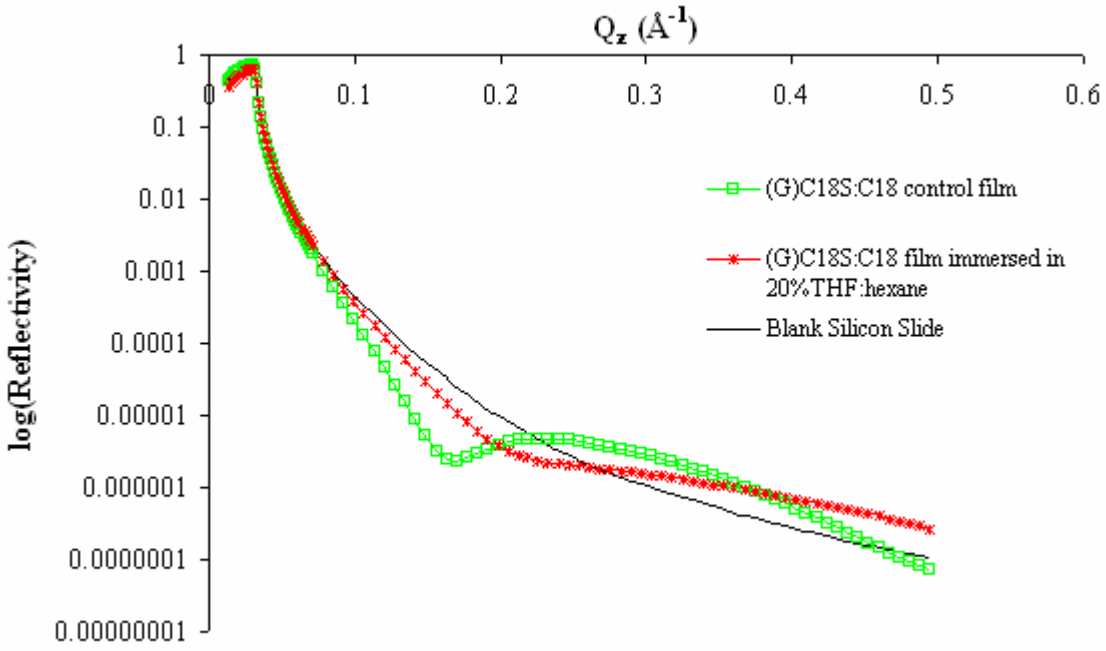

Figure 4.35. XRR data from a blank silicon slide (thin solid line), the (**G**)C18S:C18 control film (squares) and the (**G**)C18S:C18 film immersed in the 20% THF:hexane mixture (crosses). No XRR data was collected for the film immersed in the 40% THF:hexane mixture, suggesting the film had been completely removed. An increase in the oscillation period resulting from the immersion in 20% THF:hexane mixture suggests a decrease in the film thickness.

From Figure 4.35, it can be seen that the immersion of the (**G**)C18S:C18 film in the 20% THF:hexane mixture resulted in a significant increase in the oscillation period, implying that the total film thickness significantly decreased. The oscillations in the XRR data become more apparent in Figure 4.36 where the XRR for the films are normalized by the blank silicon XRR data.

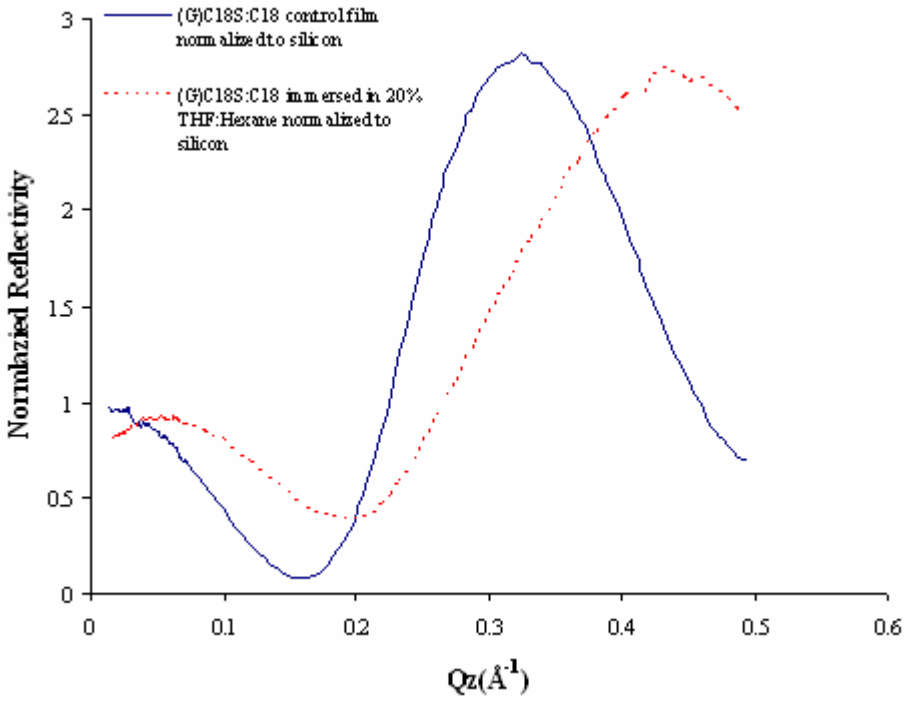

Figure 4.36. Normalized to the intensity of the blank silicon slide, shifts in the XRR data in Figure 4.35 for the (**G**)C18S:C18 control film (solid line) and the (**G**)C18S:C18 film immersed in the 20% THF:hexane mixture for 30 minutes (dashed line) become more apparent.

Both Figure 4.35 and Figure 4.36 exhibited a significant increase in oscillation of the XRR data resulting from the immersion of the (**G**)C18S:C18 film in the 20% THF:Hexane mixture. In order to calculated the total decrease in film thickness, the electron densities for both (**G**)C18S:C18 films were determined from the best-fit nonlinear least-squares regression model for their respective XRR data. The best-fit model for XRR data for the control slide was illustrated earlier in this chapter in Figure

4.8 and the calculated electron density was shown in Figure 4.9. The following plots are for the (**G**)C18S:C18 film immersed in 20% THF:hexane.

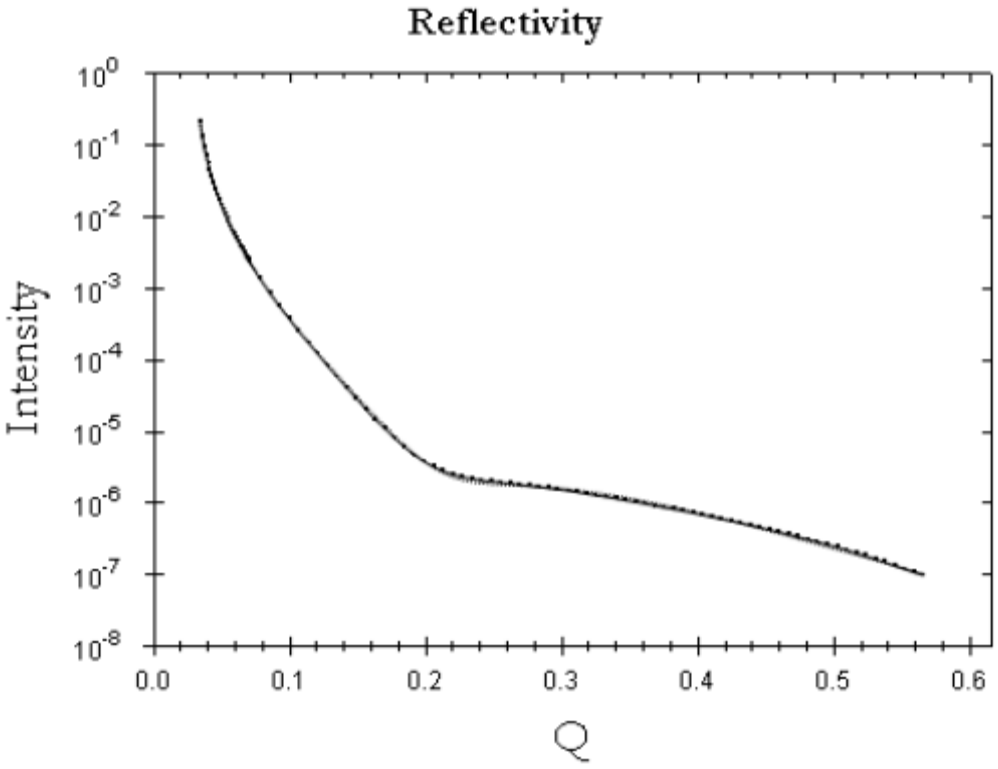

Figure 4.37. Best nonlinear least-squares fit of the XRR from (G)C18S:C818 film deposited on silicon immersed in 20% THF:hexane. The original data is the heavy dotted line and the best-fit is the dashed line. χ^2 for the reflectivity fit was 7.889 E^{-4}.

The heavy dotted line in Figure 4.37 represents the XRR data from the (**G**)C18S:C18 film, on a silicon substrate, after 30 minutes in a 20% THF:hexane mixture. The electron density profile calculated from the best-fit shown in Figure 4.38.

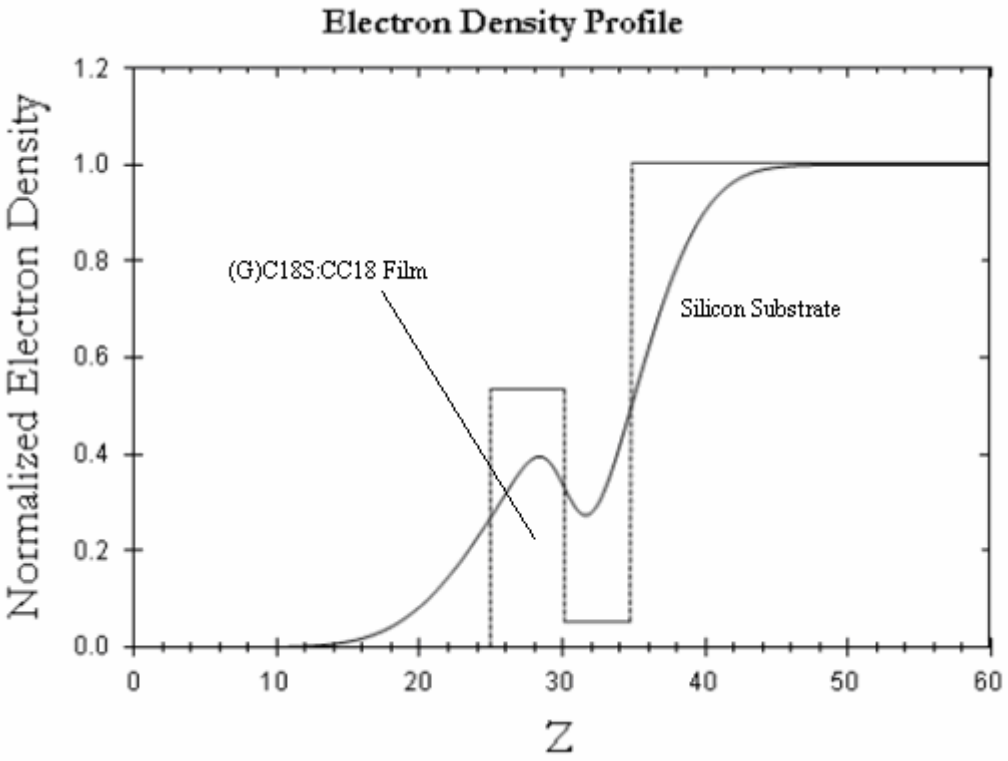

Figure 4.38. The electron density profile calculated from the best-fit shown in Figure 4.37. The solid line is the electron density and the dashed line is the boxes from the 2 box model fit. The overall thickness was determined to be ~ 9.8 Å.

The electron density profiles calculated from both best-fit models were then overlaid, as seen Figure 4.39, to observe the shift caused by the immersion in the 20% THF:hexane mixture and to quantify the reduction in the overall film thickness.

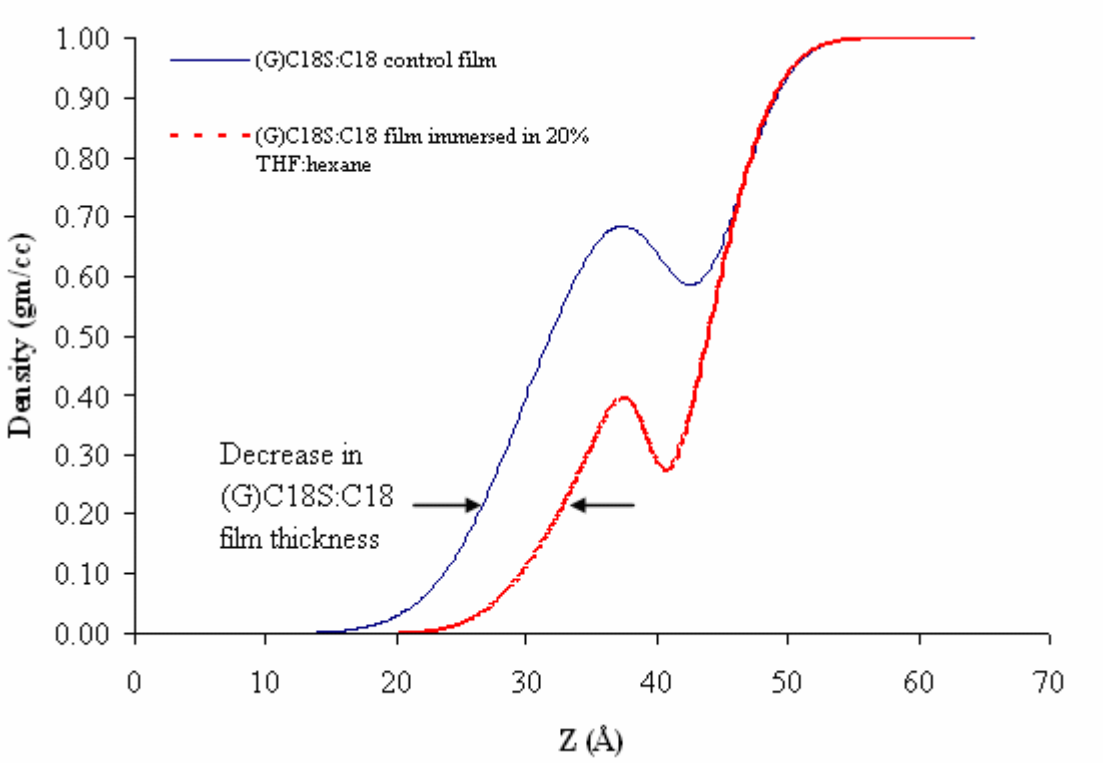

Figure 4.39. Electron density profilers calculated from the best fits for (**G**)C18S:C18 control and (**G**)C18S:C18 after immersion in 20% THF:hexane show in Figure 4.9 and Figure 4.38 respectively. The solid line is for the profile from the (**G**)C18S:C18 control slide and the heavy dashed line is for the (**G**)C18S:C18 immersed in the solvent. The decrease in the film thickness is indicated by arrows and is ~ 4.6 Å.

Figure 4.39 shows the best-fit electron density profiles for the (**G**)C18S:C18 control film (solid line) and for the (**G**)C18S:C18 immersed in the 20% THF:hexane (heavy dashed line). Important things to note about these profiles are: a smaller dip in density still occurs at the silicon substrate/film interface, which is attributed to fewer film molecules being physisorbed onto the silicon surface, and the film thickness is significantly decreased from 14.4 Å to 9.8 Å. The reduction in the dip size and the large decrease in film thickness both suggest that THF disrupted the hydrogen bonding between both the **G** and C18S head group. The more likely reason for the decrease in film thickness is the disruption of the physisorption between the film and silicon substrate, which would result in the film being dissolved and a smaller dip in the electron

density profile. One other cause for the thickness decrease can be hexane replacing the C18 guest molecules.

4.3.5 (G)C18S:C18naph immersed in hexane for 30 minutes, 1 hour and 5 hours

(**G**)C18S:C18naph films were immersed in hexane for periods of 30 minutes, 1 hour and 5 hours. These films were created using the same spreading solution, a 1:1 solution of NaC18S and C18naph over a 10^{-2} M G_2CO_3 aqueous subphase, as the control (**G**)C18S:C18naph film. The Π-A isotherm of these monolayer also exhibited a liftoff at $A_{lift\text{-}off} \approx 81$ Å^2/sulfonate followed by a steady increase in surface pressure. Deposition onto a silicon substrate occurred at a surface pressure of 20 mN/m. The films were then immediately immersed in hexane for their respective times. Upon removal, the films were subjected to XRR to observe any changes in film thickness as a result of the hexane. The XRR data for the immersed slides were then compared to the data for the control (**G**)C18S:C18naph film, as illustrated in Figure 4.40.

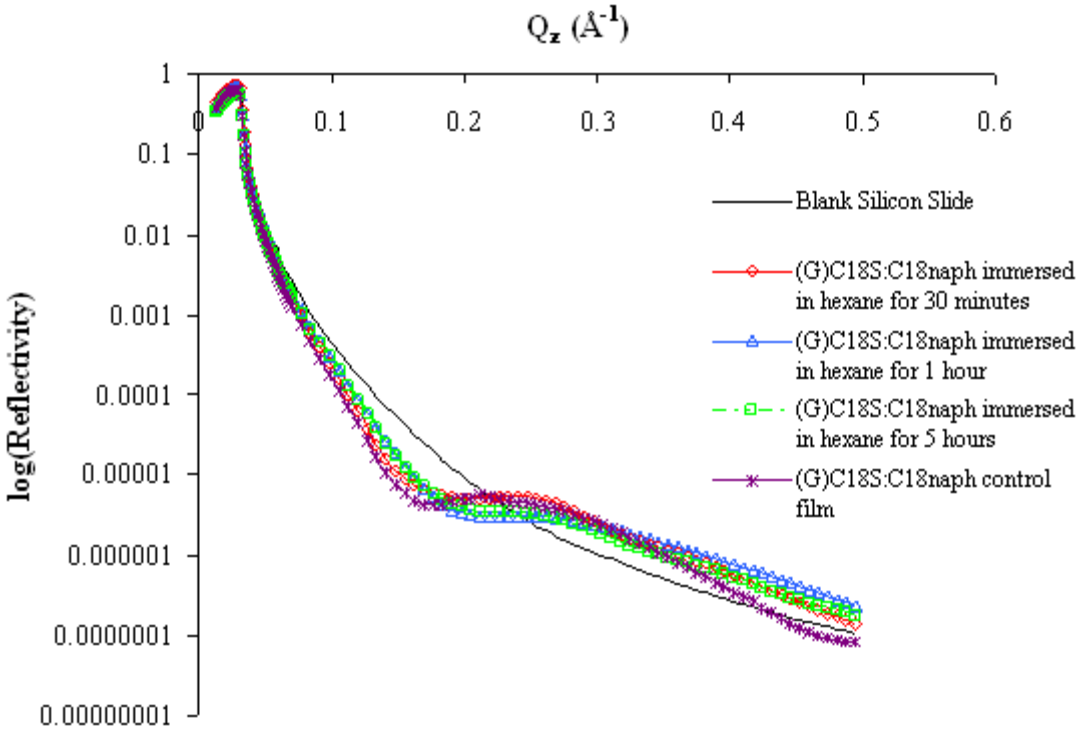

Figure 4.40. XRR data from a blank silicon slide (thin solid line), the (**G**)C18S:C18naph control film (asterisk), the (**G**)C18S:C18naph films immersed in hexane for 30 minutes (circles), 1 hour (triangles) and 5 hours (squares). A slight increase in the oscillation in the XRR data for the 1 hour and 5 hour samples suggests that thickness of the (**G**)C18S:C18naph did decreased as a result of immersion in hexane.

From Figure 4.40, it can be seen that the immersion of the (**G**)C18S:C18naph film in the hexane for increasing time periods resulted in an increase in the oscillation period, implying that the total film thickness decreased. The oscillations in the XRR data become more apparent in Figure 4.41 where the XRR for the films are normalized by the blank silicon XRR data.

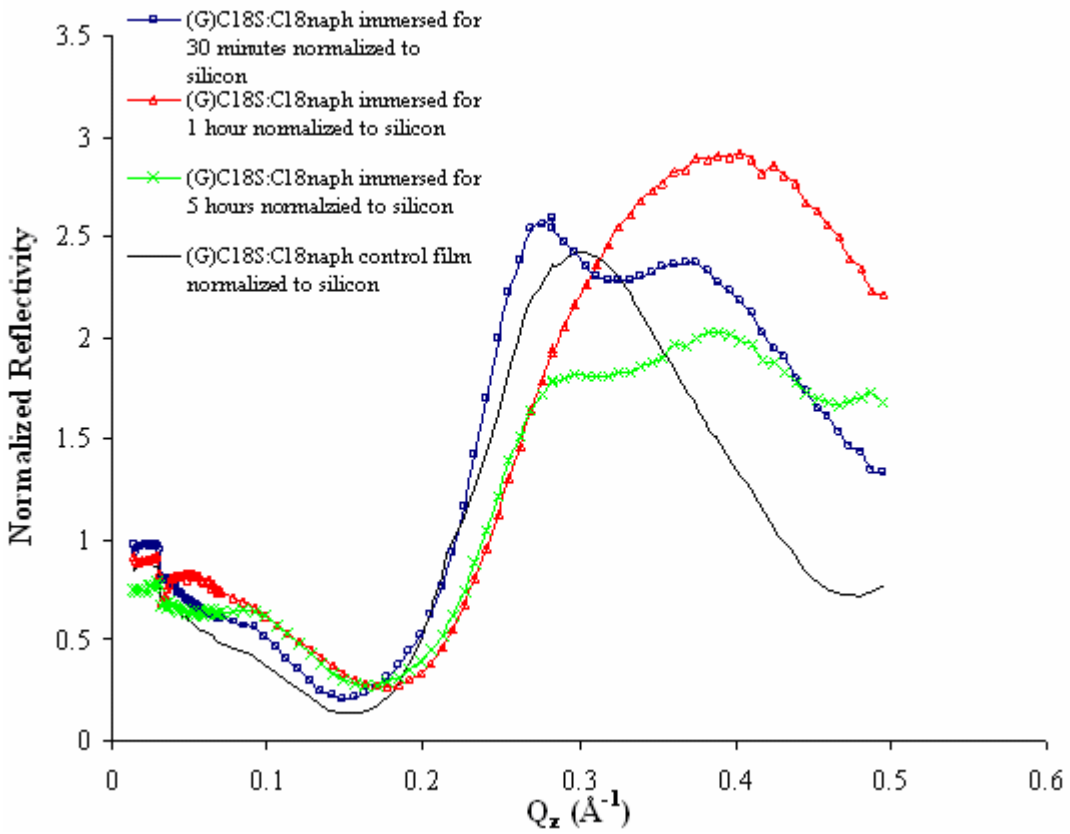

Figure 4.41. Normalized to the intensity of the blank silicon slide, shifts in the XRR data in Figure 4.40 for the (**G**)C18S:C18naph control film (solid line) and the (**G**)C18S:C18naph films immersed in hexane 30 minutes (squares), 1 hour (triangles) and 5 hours (crosses) become more apparent. The size of the oscillations increases with increasing immersion time, suggesting that the film thickness decreases over time.

Both Figure 4.40 and Figure 4.41 exhibited a gradual increase in the oscillation of the XRR data resulting from the increase immersion time of the (**G**)C18S:C18naph films in hexane. The bimodal peaks seen for the (**G**)C18S:C18naph film immersed for 30 minutes may be indicating the mechanism of the hexane molecules replacing the C18naph guest molecules. Nucleation is believed to be the substitution mechanism where bubbles of hexane aggregate at the edges of the film and grow with time, covering the entire film and replacing the guest molecules. Further studies using more sensitive surface measurements, such as X-ray photoelectron spectroscopy and infrared spectroscopy, are needed to fully understand the mechanism. The absence of a well-

defined oscillation pattern in the data for the (**G**)C18S:C18naph film immersed for 5 hours suggests that the film is starting to degrade.

In order to quantify the decrease in film thickness, the electron densities for all (**G**)C18S:C18naph films were determined from the best-fit nonlinear least-squares regression model for their respective XRR data. The best-fit model for XRR data for the control slide was illustrated earlier in this chapter in Figure 4.21 and the calculated electron density was shown in Figure 4.22. The following plots are for the (**G**)C18S:C18naph films immersed in hexane for 30 minutes.

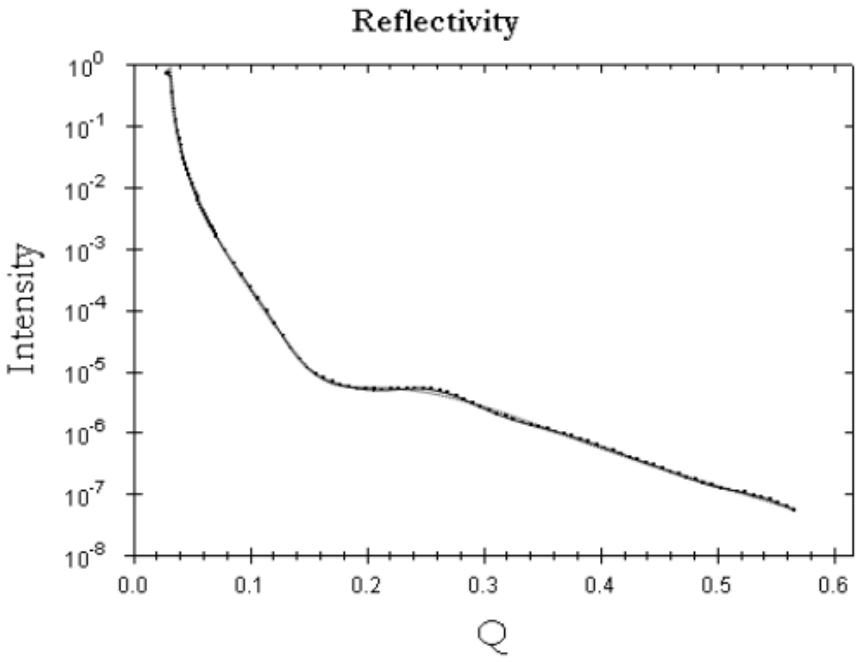

Figure 4.42. XRR from a (**G**)C18S:C18naph film on silicon immersed in hexane for 30 minutes. The data are shown with the heavy dotted line and the best nonlinear least-squares fit by the dashed lines. χ^2 for the fit was $6.45E^{-2}$.

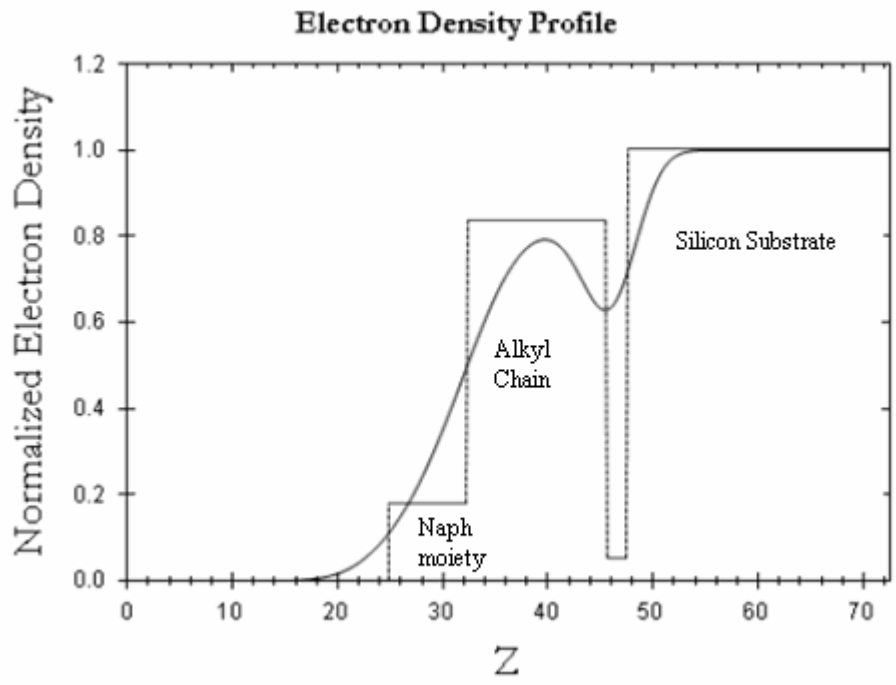

Figure 4.43. Electron density profile calculated from the best fit shown in Figure 4.42 for (**G**)C18S:C18naph immersed in hexane for 30 minutes. The dashed line is the 3 box fit model fitted to the data and the solid line is the electron density extracted from the best fit. The overall calculated film thickness was ~ 22 Å.

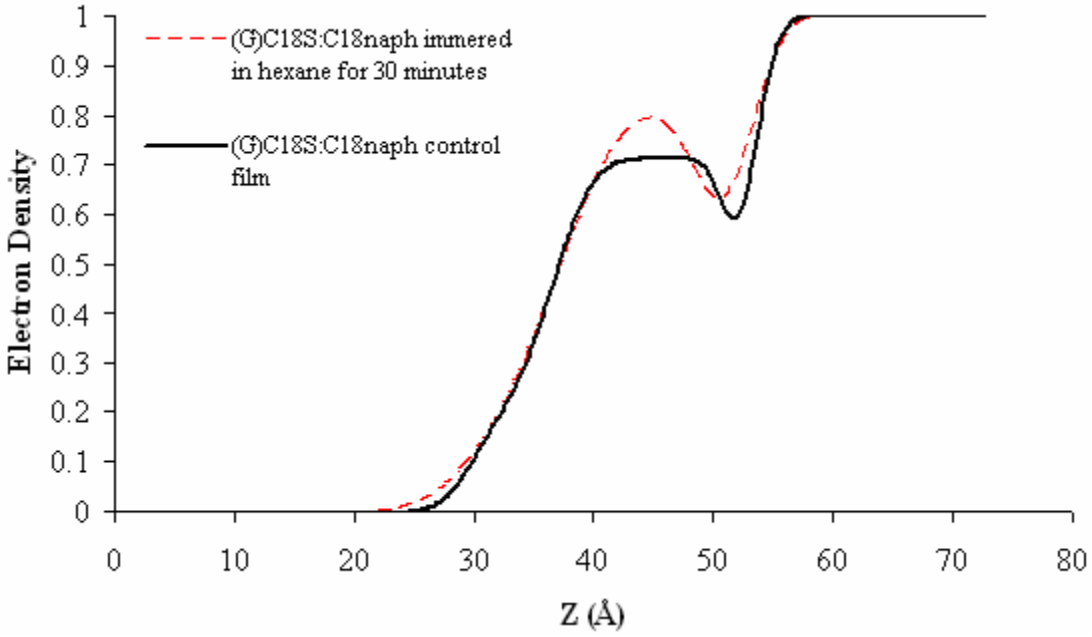

Figure 4.44. Electron density profilers calculated from the best fits for (**G**)C18S:C18naph control (solid line) and (**G**)C18S:C18naph after immersion in hexane for 30 minutes (dashed line). From the best fits, there was no decrease in the film thickness from immersion in hexane for 30 minutes.

Figure 4.44 shows the best-fit electron density profiles for the (**G**)C18S:C18naph control film (solid line) and for the (**G**)C18S:C18naph immersed in hexane for 30 minutes (dashed line). Important things to note about these profiles are: a similar dip in density occurs at the silicon substrate/film interface and the film thickness did not significantly decreased, 22.7 Å for the control film and 22 Å for the film immersed in hexane. This suggests that the aromatic groups stabilize the film through π interaction and the functional group dominates the packing of the film.

The next three plots are for the (**G**)C18S:C18naph films immersed in hexane for 1 hour.

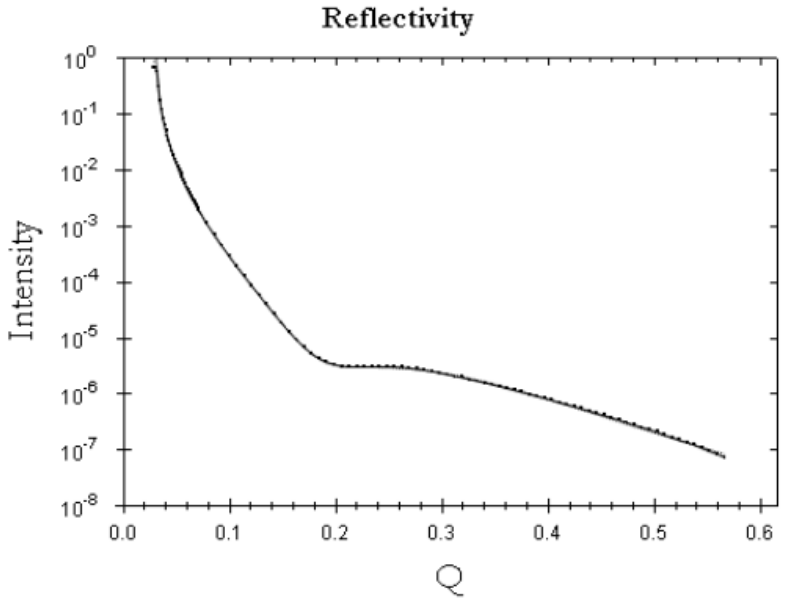

Figure 4.45. XRR from a (**G**)C18S:C18naph film on silicon immersed in hexane for 1 hour. The data are shown with the heavy dotted line and the best nonlinear least-squares fit by the dashed lines. χ^2 for the fit was $1.534E^{-1}$.

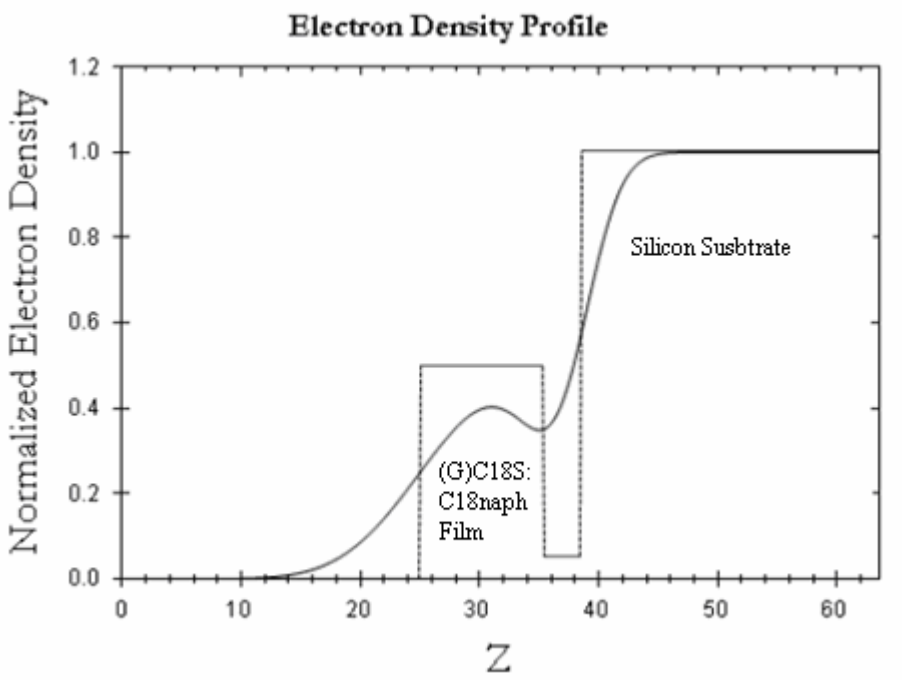

Figure 4.46. Electron density profile calculated from the best fit shown in Figure 4.45 for (**G**)C18S:C18naph immersed in hexane for 1 hour. The dashed line is the 2 box fit model fitted to the data and the solid line is the electron density extracted from the best fit. The overall calculated film thickness was ~ 13.5 Å.

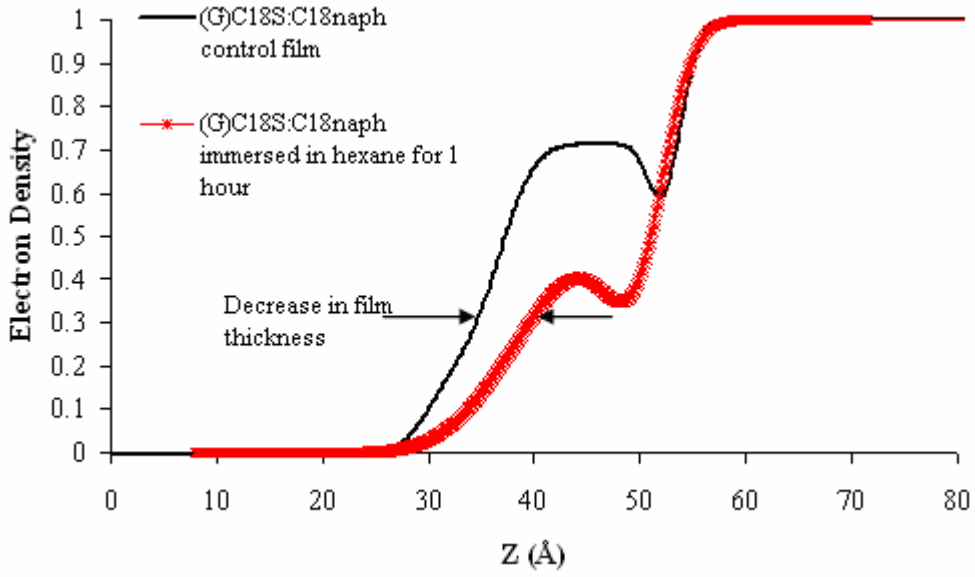

Figure 4.47. Electron density profilers calculated from the best fits for (**G**)C18S:C18naph control (solid line) and (**G**)C18S:C18naph after immersion in hexane for 1 hour (dashed line). From the best fits, the decrease in film thickness from immersion in hexane for 1 hour was determined to be ~ 9 Å.

Figure 4.47 shows the best-fit electron density profiles for the (**G**)C18S:C18naph control film (solid line) and for the (**G**)C18S:C18naph immersed in hexane for 1 hour (dashed line). Two important things to note about these profiles are: the dip in density is still present after immersion in hexane for 1 hour and the film thickness significantly decreased, 22.7 Å for the control film and ~13.5 Å for the film immersed in hexane. The thickness of the immersed (**G**)C18S:C18naph film is very similar to the thickness determined for the (**G**)C18S:C18 film immersed in hexane after 30 minutes, suggesting that the majority of the C18naph guest molecules were replaced by hexane molecules after 1 hour and that the functional group of C18naph did stabilize the film for at least 30 minutes.

The next three plots are for the (**G**)C18S:C18naph films immersed in hexane for 5 hours.

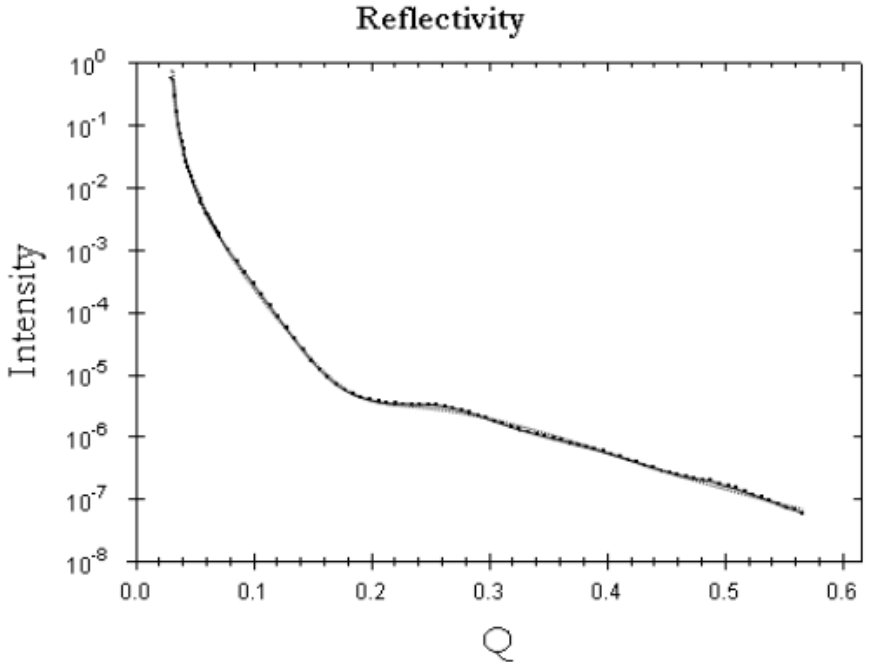

Figure 4.48. XRR from a (**G**)C18S:C18naph film on silicon immersed in hexane for 5 hours. The data are shown with the heavy dotted line and the best nonlinear least-squares fit by the dashed lines. χ^2 for the fit was 7.545 E^{-2}.

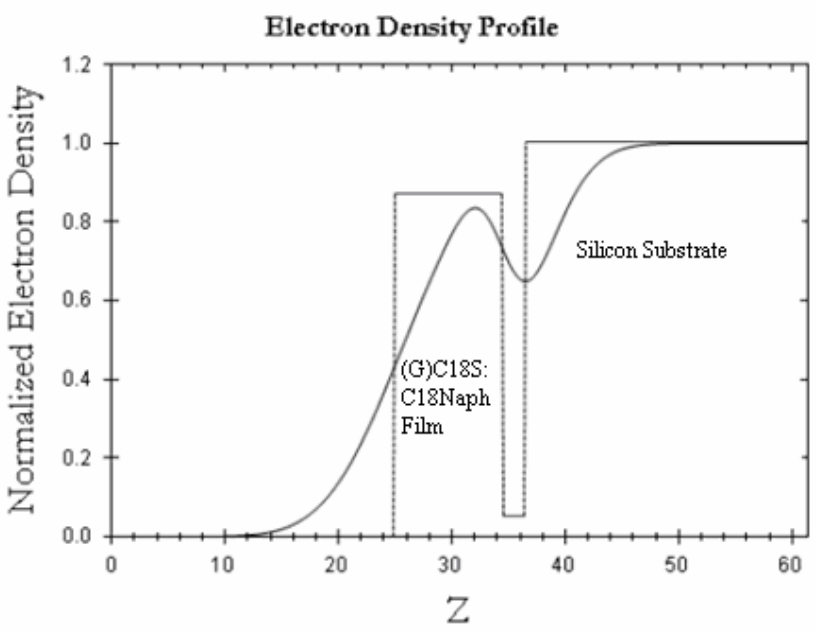

Figure 4.49. Electron density profile calculated from the best fit shown in Figure 4.48 for (**G**)C18S:C18naph immersed in hexane for 5 hours. The dashed line is the 2 box fit model fitted to the data and the solid line is the electron density extracted from the best fit. The overall calculated film thickness was ~ 11.5 Å.

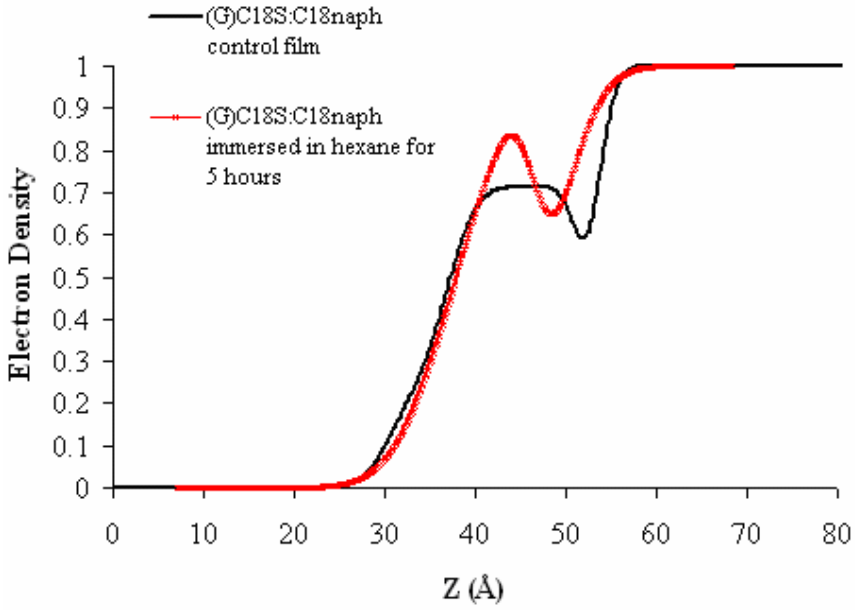

Figure 4.50. Electron density profilers calculated from the best fits for (**G**)C18S:C18naph control (solid line) and (**G**)C18S:C18naph after immersion in hexane for 5 hours (dashed line). From the best fits, the decrease in film thickness from immersion in hexane for 5 hours was determined to be ~ 10 Å

Figure 4.50 shows the best-fit electron density profiles for the (**G**)C18S:C18naph control film (solid line) and for the (**G**)C18S:C18naph immersed in hexane for 5 hours (dashed line). The profile is very similar to the one for (**G**)C18S:C18naph immersed in hexane for 1 hour. The dip in electron density is still present after 5 hours in hexane, thus indicating a film is still attached to the substrate surface. Also, the film thickness continued to decrease from 22.7 Å for the control film to ~ 11.5 Å for the film immersed in hexane. This suggests that the all of the C18naph guest molecules were replaced by hexane molecules and the film may be slowly removed from the surface since this thickness is less than that after immersion for 1 hour in hexane.

4.3.6 (G)C18S:C18naph immersed in 20%THF:hexane mixture for 30 minutes

The second stability test performed on (G)C18S:C18naph films was the immersion in 20%THF:hexane for 30 minutes. These films were created using the same spreading solution, a 1:1 solution of NaC18S and C18naph over a 10^{-2} M G_2CO_3 aqueous subphase, as the control (**G**)C18S:C18naph film. Deposition onto a silicon substrate occurred at a surface pressure of 20 mN/m. Upon completion of the deposition, the film was immediately immersed in the 20% THF:hexane mixture. XRR data was then taken upon removal from the 20% THF:hexane mixture to observe any changes in film thickness. The XRR data for the immersed slide were then compared to the data for the control (**G**)C18S:C18naph film, as illustrated in Figure 4.51.

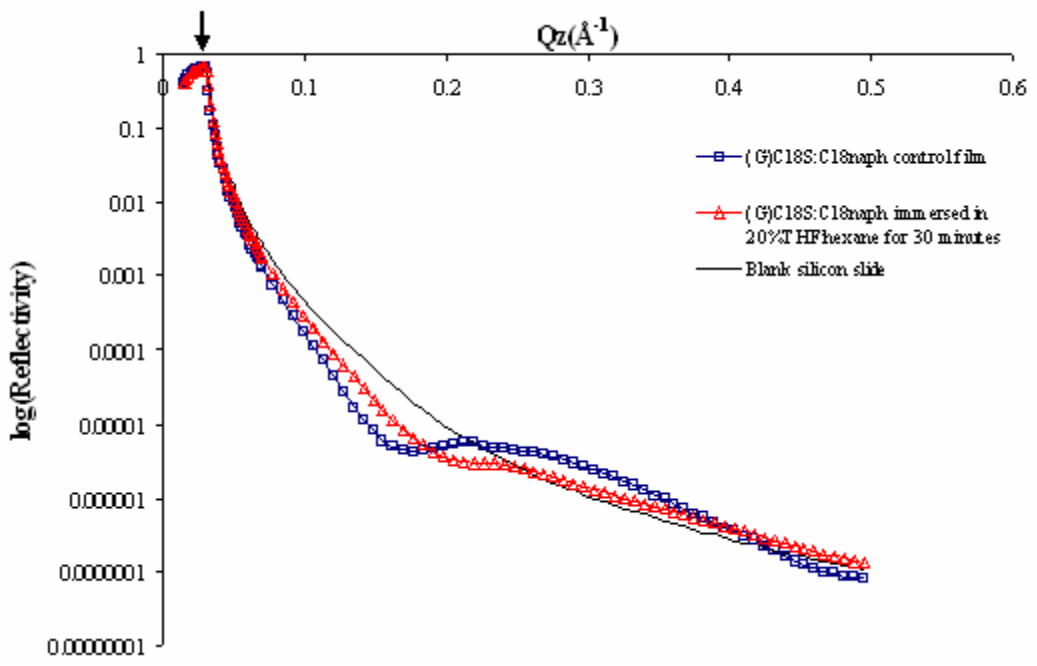

Figure 4.51. XRR data from a blank silicon slide (thin solid line), the (**G**)C18S:C18naph control film (squares), and the (**G**)C18S:C18naph film immersed in 20% THF:hexane for 30 minutes (triangles). A significant increase in the oscillation in the XRR data suggests that thickness of the (**G**)C18S:C18naph decreased substantially as a result of immersion in hexane.

From Figure 4.51, it can be seen that the immersion of the (**G**)C18S:C18naph film in the 20% THF:hexane mixture for 30 minutes resulted in a significant increase in the oscillation period, implying that the total film thickness significantly decreased. The oscillations in the XRR data become more apparent in Figure 4.52 where the XRR for the films are normalized by the blank silicon XRR data.

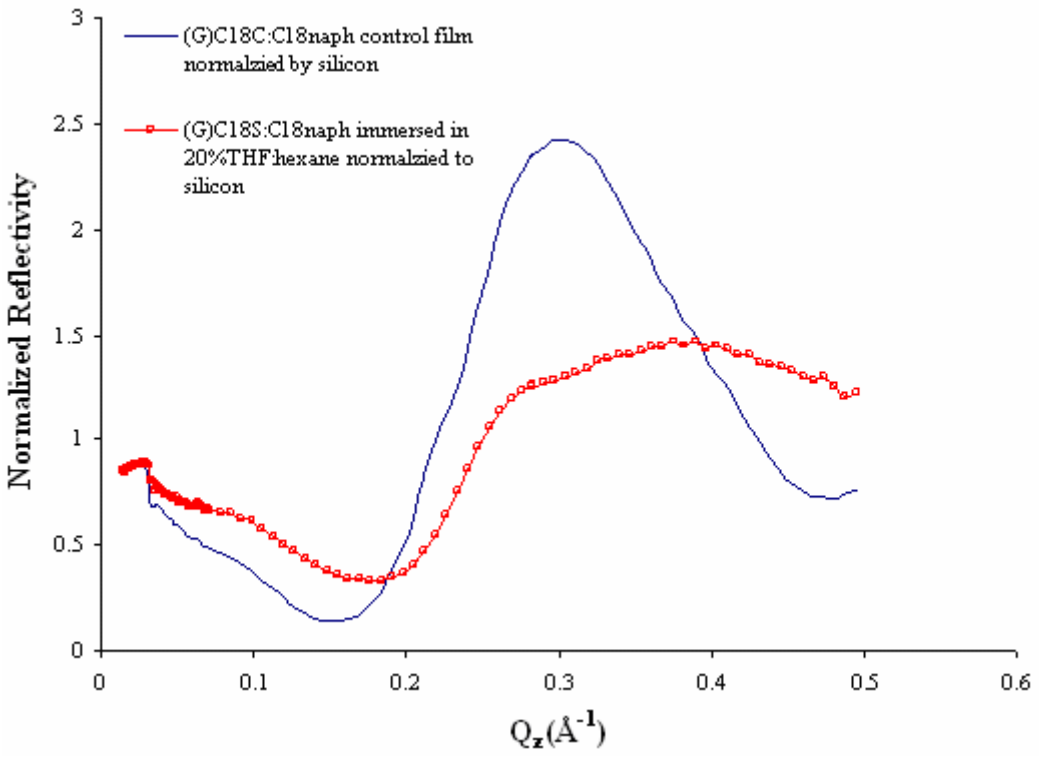

Figure 4.52. Normalized to the intensity of the blank silicon slide, shifts in the XRR data in Figure 4.51 for the (**G**)C18S:C18naph control film (solid line) and the (**G**)C18S:C18naph film immersed in 20%THF:hexane 30 minutes (squares), become more apparent. This graph supports the suggestion that immersion in the 20% THF:hexane resulted in a significant decrease in the film thickness.

Both Figure 4.51 and Figure 4.52 exhibited a significant increase in oscillation of the XRR data resulting from the immersion of the (**G**)C18S:C18naph film in the 20% THF:hexane mixture. To calculate the total decrease in film thickness resulting from the 20% THF:hexane mixture, the XRR data was modeled using the best-fit nonlinear least-squares regression model and the electron density was extracted. The best-fit model for XRR data for the control slide was illustrated earlier in this chapter in and the calculated electron density was shown in. The following plots are for the (**G**)C18S:C18naph film immersed in 20% THF:hexane.

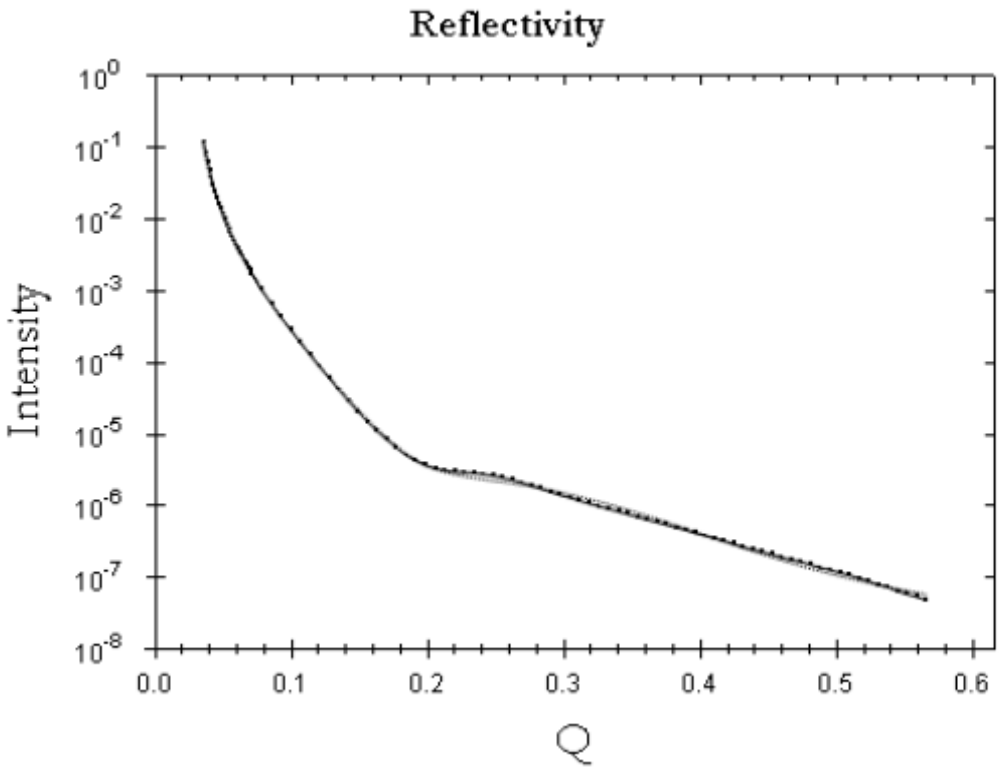

Figure 4.53. XRR from a (**G**)C18S:C18naph film on silicon immersed in 20% THF:hexane for 30 minutes. The data are shown with the heavy dotted line and the best nonlinear least-squares fit by the dashed lines. χ^2 for the fit was $2.083E^{-3}$.

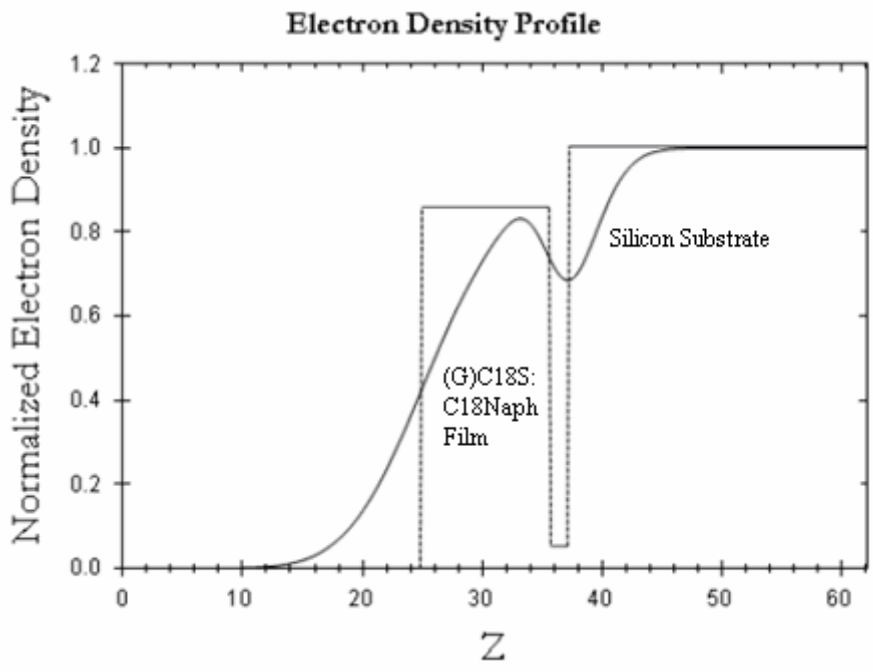

Figure 4.54. Electron density profile calculated from the best fit shown in Figure 4.53 for (**G**)C18S:C18naph immersed in 20% THF:hexane for 30 minutes. The dashed line is the 2 box fit model fitted to the data and the solid line is the electron density extracted from the best fit. The overall calculated film thickness was ~ 12 Å.

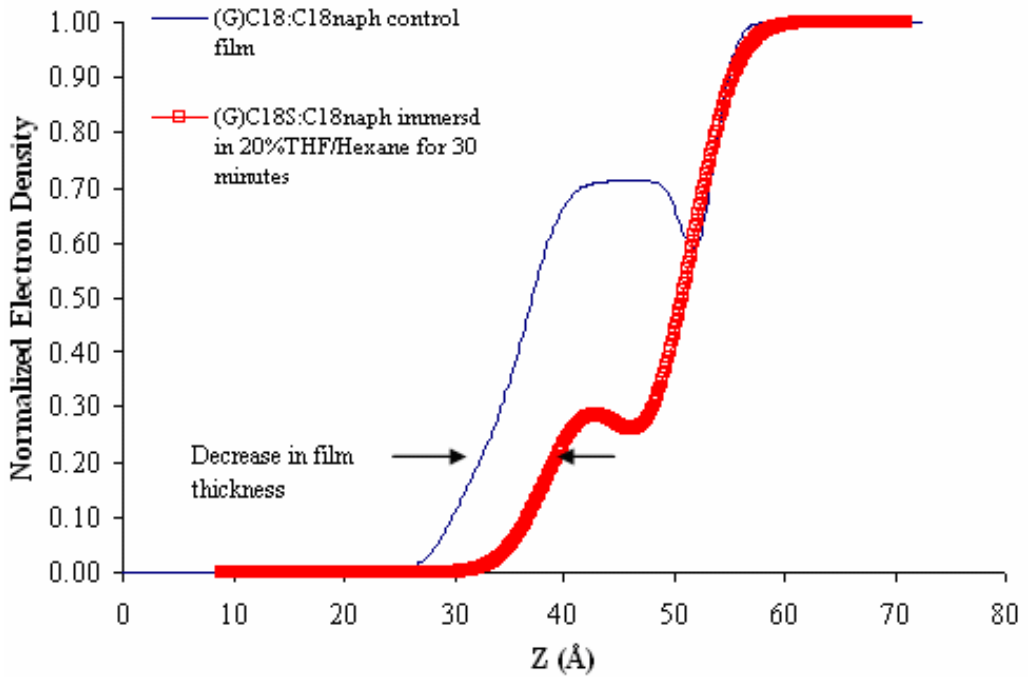

Figure 4.55. Electron density profilers calculated from the best fits for (**G**)C18S:C18naph control and (**G**)C18S:C18naph after immersion in 20% THF:hexane show in Figure 4.22 and Figure 4.54 respectively. The solid line is for the profile from the (**G**)C18S:C18naph control slide and the squares are for the (**G**)C18S:C18naph immersed in the solvent. The decrease in the film thickness is indicated by arrows and is ~ 10 Å.

Figure 4.55 shows the best-fit electron density profiles for the (**G**)C18S:C18naph control film (solid line) and for the (**G**)C18S:C18naph immersed in the 20% THF:hexane (square). Important things to note about these profiles are: a dip in density still occurs at the silicon substrate/film interface after immersion, which is attributed to the remaining film molecules physisorbed onto the silicon surface, and the film thickness is significantly decreased from ~22.7 Å to ~12 Å. The reduction in the film thickness further supports the suggestion that THF disrupts the hydrogen bonding between the host molecules and the spacer molecules and the hydrogen bonding between the hydrocarbon chains. The decrease in the film thickness can also be attributed to the physisorption between the film and silicon substrate being disrupted, resulting in the film being

removed from the substrate and causing a large shift in the XRR data and in the electron density. One other cause for the thickness decrease can be hexane replacing the C18naph guest molecules.

4.3.7 (G)C18S:C18naph immersed in DI Water for 30 minutes

Immersion in a environment more polar than the 20% THF:hexane mixture was conducted using DI water, which has a polarity index of ~ 9.0. The (**G**)C18S:C18naph slide was immersed in DI water for 30 minutes. Upon removal, the slide was immediately subjected to XRR. The film immersed in DI water did not exhibit any reflectivity, as illustrated in Figure 4.56, which suggests that the film had been completely removed from the silicon substrate. This suggests that the hydrogen bonds needed to keep the film intact and attached to the substrate were completely disrupted by the DI water.

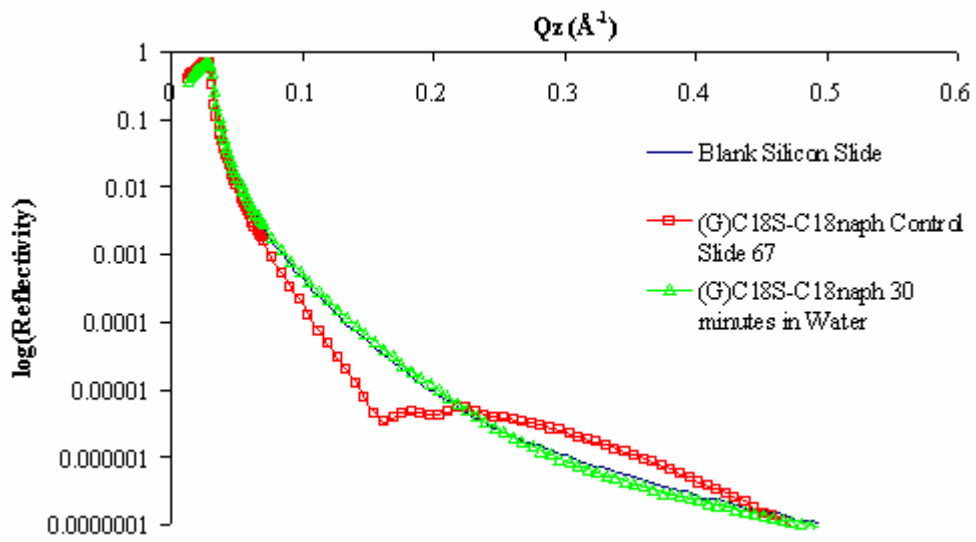

Figure 4.56. XRR data from a blank silicon slide (thin solid line), the (**G**)C18S:C18naph control film (squares), and the (**G**)C18S:C18naph film immersed in DI water for 30 minutes (triangles). As seen from the graph, the film was completely removed from the silicon surface suggesting that the hydrogen bonds between the host and spacer molecules were broken and physisorption is not strong enough to keep the film attached in a polar environment.

4.3.8 (G)C18S:C18chol immersed in hexane for 30 minutes and 5 hours

The last 'host-guest' film system studied was (**G**)C18S:C18chol. The first stability test conducted on the films was the immersion in a nonpolar environment. The films were created using the same spreading solution for the control film, a 1:1 solution of NaC18S and C18chol over a 10^{-2} M G_2CO_3 aqueous subphase, and deposited at a surface pressure of 20 mN/m. The (**G**)C18S:C18chol films were then immersed in hexane for 30 minutes and 5 hours. Upon removal, the slides were immediately subjected to XRR to observe any changes in film thickness. The XRR data for the immersed slide were then compared to the data for the control (**G**)C18S:C18chol film, as illustrated in Figure 4.57.

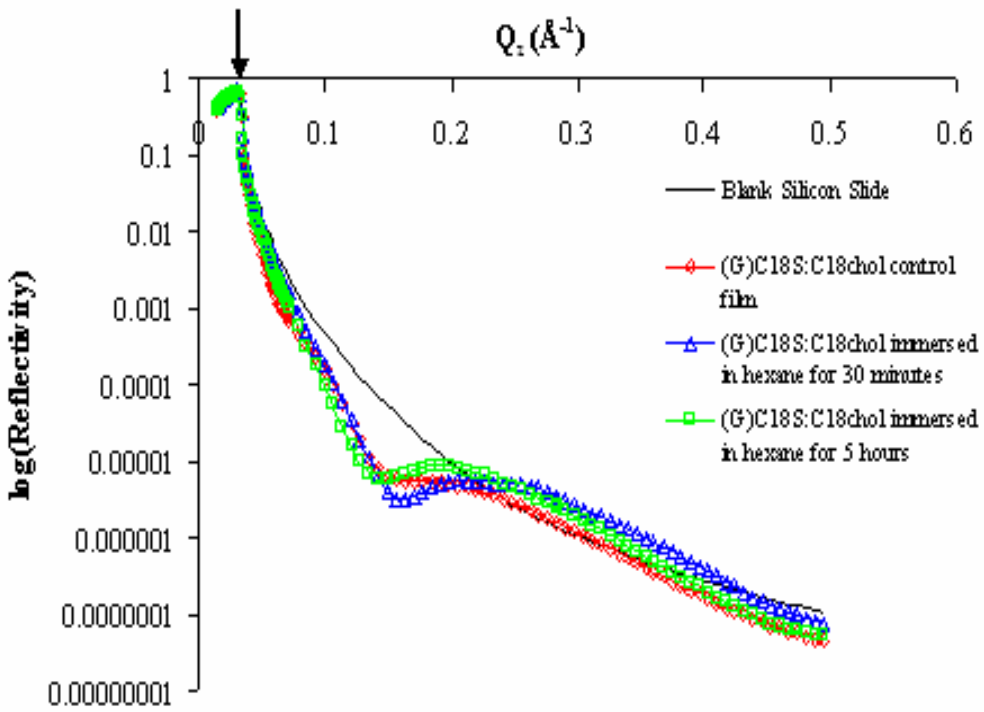

Figure 4.57. XRR data from a blank silicon slide (thin solid line), the (**G**)C18S:C18chol control film (circles), and the (**G**)C18S:C18chol films immersed in hexane for 30 minutes (triangles) and 5 hours (squares). No significant increase in the oscillation in the XRR data from immersion in hexane suggests that thickness of the (**G**)C18S:C18chol did not decrease as a result of immersion in hexane.

From Figure 4.57, it can be seen that the immersion of the (**G**)C18S:C18chol film in hexane for 30 minutes and 5 hours resulted in an increase in the oscillation period, implying that the total film thickness decreased. The oscillations in the XRR data become more apparent in Figure 4.58 where the XRR for the films are normalized by the blank silicon XRR data.

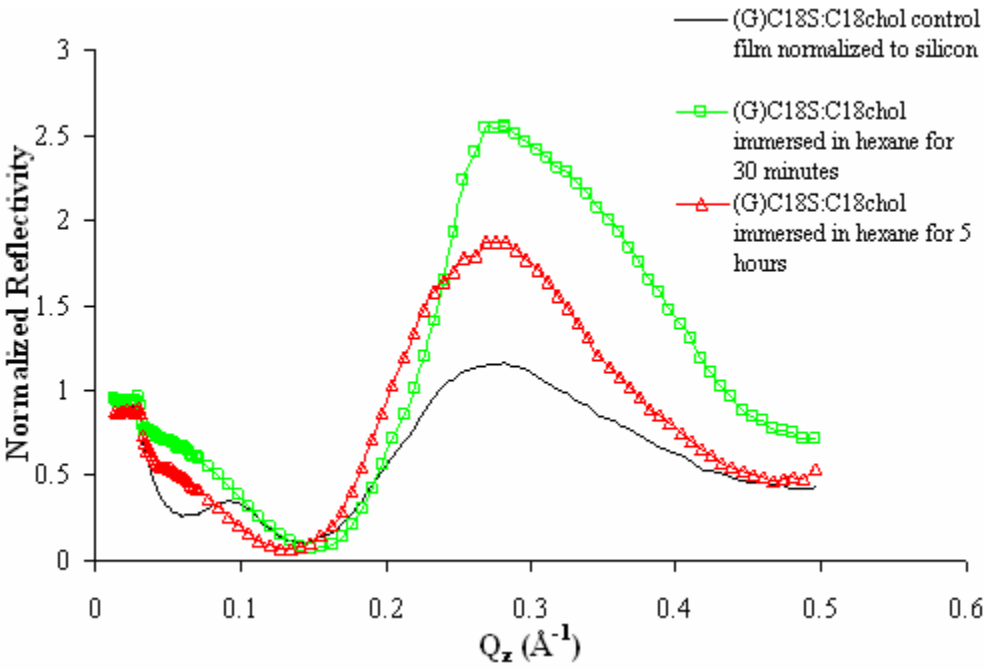

Figure 4.58. Normalized to the intensity of the blank silicon slide, shifts in the XRR data in Figure 4.57 for the (**G**)C18S:C18chol control film (solid line) and the (**G**)C18S:C18chol films immersed in hexane for 30 minutes (squares) and 5 hours (triangles), become more apparent. This graph supports the suggestion that immersion in the hexane did result in a significant decrease in the film thickness.

Both Figure 4.57 and Figure 4.58 exhibited a gradual increase in the oscillation of the XRR data resulting from the increase immersion time of the (**G**)C18S:C18chol films in hexane. The decrease in film thickness for the (**G**)C18S:C18chol films were determined from the electron densities extracted from the best-fit nonlinear least-squares regression model for their respective XRR data. The best-fit model for XRR data for the control slide was illustrated earlier in this chapter in Figure 4.16 and the calculated electron density was shown in Figure 4.17. The following plots are for the (**G**)C18S:C18naph films immersed in hexane for 30 minutes.

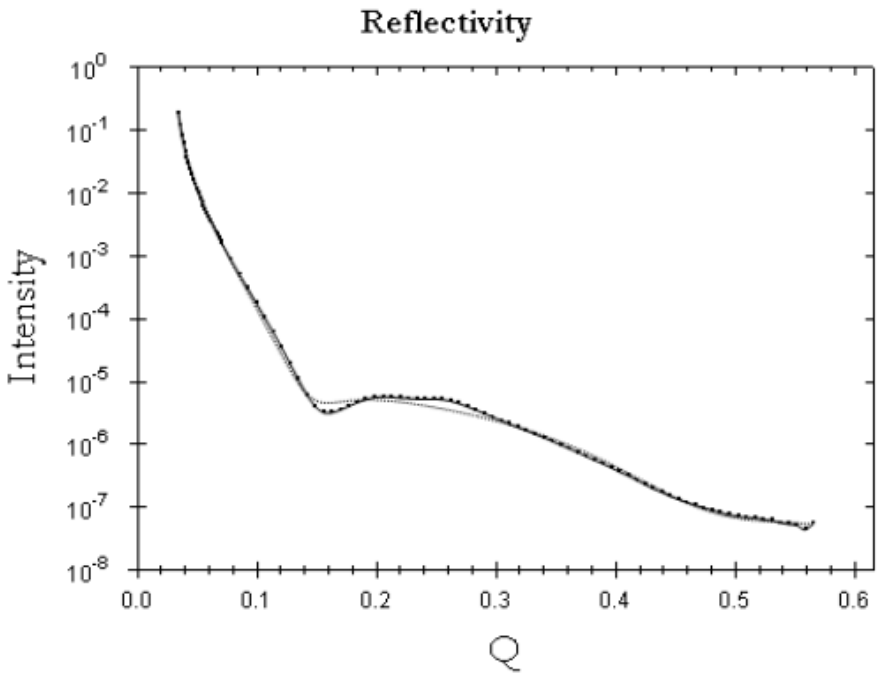

Figure 4.59. XRR from a (**G**)C18S:C18chol film on silicon immersed in hexane for 30 minutes. The data are shown with the heavy dotted line and the best nonlinear least-squares fit by the dashed lines. χ^2 for the fit was 5.056 E^{-3}.

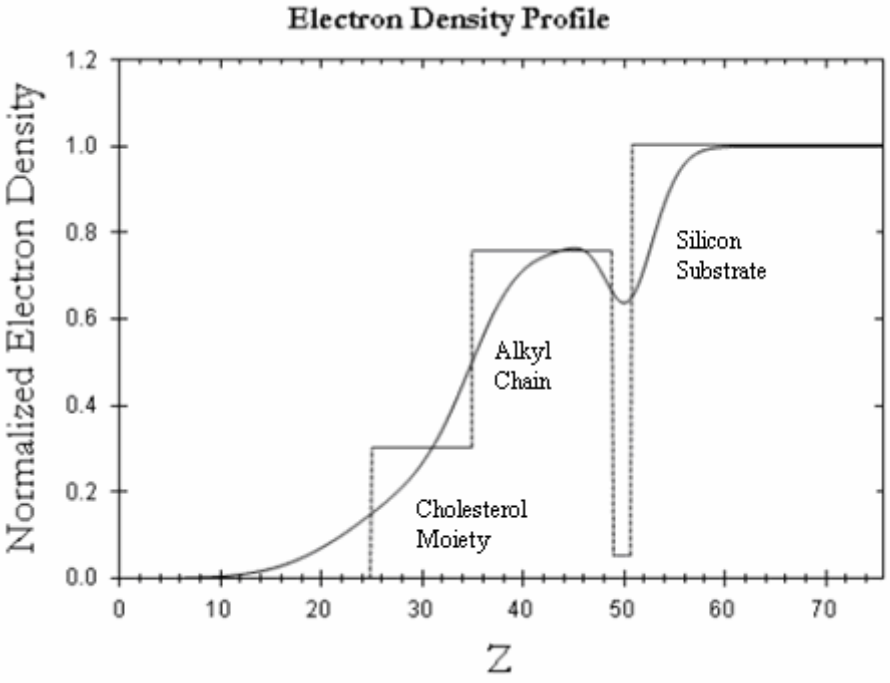

Figure 4.60. Electron density profile calculated from the best fit shown in Figure 4.59 for (**G**)C18S:C18chol immersed in hexane for 30 minutes. The dashed line is the 3 box fit model fitted to the data and the solid line is the electron density extracted from the best fit. The overall calculated film thickness was ~ 26 Å.

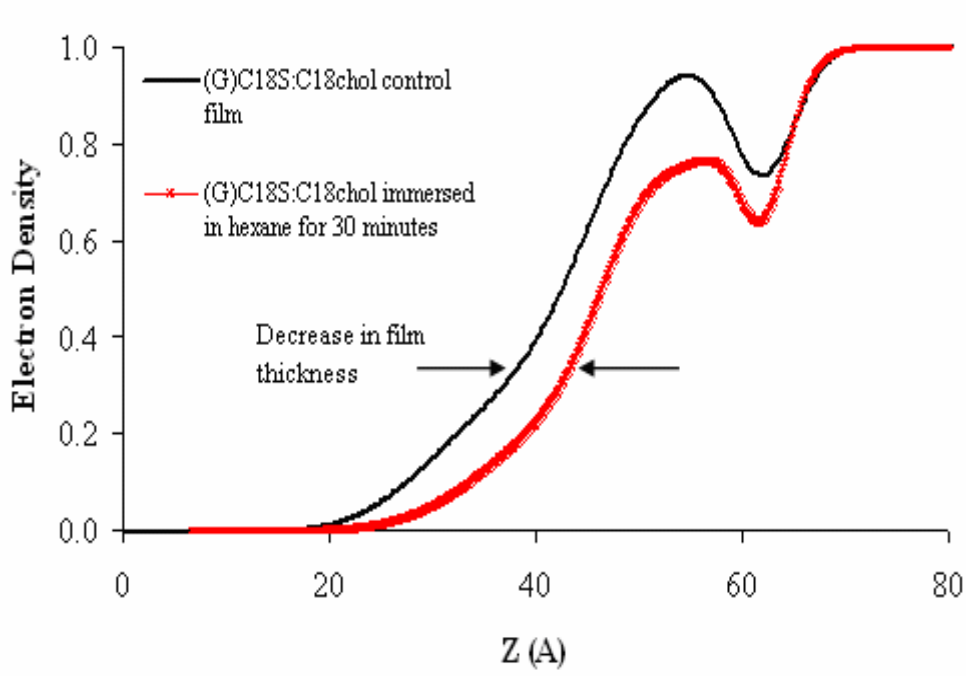

Figure 4.61. Electron density profilers calculated from the best fits for (**G**)C18S:C18chol (solid line) and (**G**)C18S:C18chol after immersion in hexane for 30 minutes (crosses). The decrease in the film thickness is indicated by arrows and is ~ 6.5 Å.

Figure 4.61 shows the best-fit electron density profiles for the (**G**)C18S:C18chol control film (solid line) and for the (**G**)C18S:C18chol immersed in hexane for 30 minutes (squares). An important feature of the profiles is the presence of the dip in the electron density after immersion in hexane for 30 minutes. This indicates that the film was not removed from the silicon surface by the hexane. Another important feature is the decrease in film thickness, as indicated by the arrows. The film thickness significantly decreased from ~ 33 Å for the control film to ~ 26 Å for the film immersed in hexane. A film thickness of 26 Å suggests that the C18naph molecules were starting to be replaced by the hexane, which creates large height changes in the film causing a lower electron density.

The next three plots are for the (**G**)C18S:C18nchol films immersed in hexane for 5 hours.

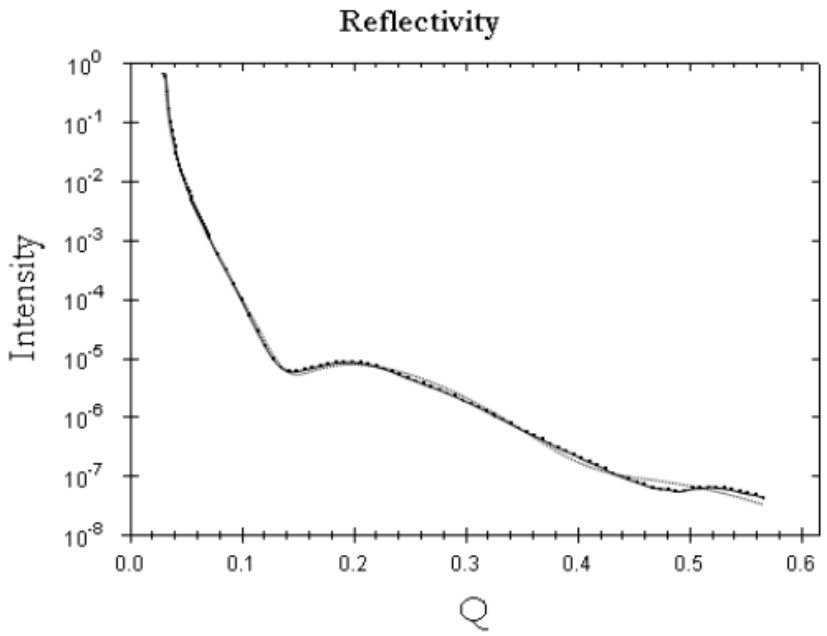

Figure 4.62. XRR from a (**G**)C18S:C18chol film on silicon immersed in hexane for 30 minutes. The data are shown with the heavy dotted line and the best nonlinear least-squares fit by the dashed lines. χ^2 for the fit was 5.056 E^{-3}.

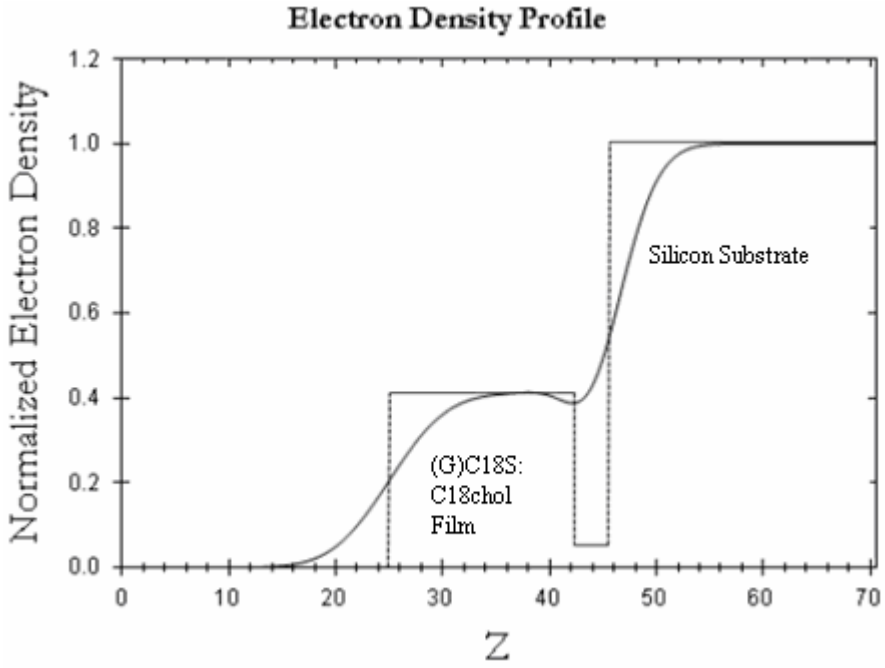

Figure 4.63. Electron density profile calculated from the best fit shown in Figure 4.62 for (**G**)C18S:C18chol immersed in hexane for 5 hours. The dashed line is the 2 box fit model fitted to the data and the solid line is the electron density extracted from the best fit. The overall calculated film thickness was ~ 20.5 Å.

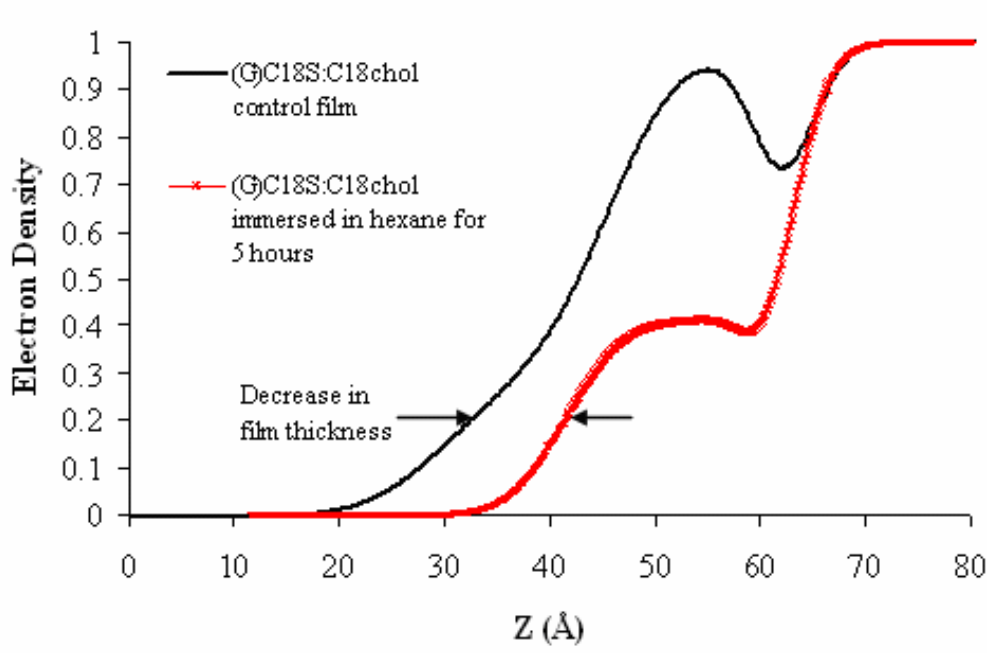

Figure 4.64. Electron density profilers calculated from the best fits for (**G**)C18S:C18chol (solid line) and (**G**)C18S:C18chol after immersion in hexane for 5 hours (crosses). The decrease in the film thickness is indicated by arrows and is ~ 11.5 Å.

Figure 4.64 shows the best-fit electron density profiles for the (**G**)C18S:C18chol control film (solid line) and for the (**G**)C18S:C18chol immersed in hexane for 5 hours (crosses). An important feature of the profiles is the presence of the dip in the electron density significantly decreased resulting from the film being immersed in hexane for 5 hours. Another important feature is the decrease in film thickness, as indicated by the arrows. The film thickness significantly decreased from ~ 33 Å for the control film to ~ 20.5 Å for the film immersed in hexane for 5 hours. The observed drop in film thickness and the decrease in the dip in electron density at the film/silicon interface suggest that the C18naph molecules were being replaced by the hexane, which creates large height changes in the film causing a lower electron density, and that part of the film could have been removed by the hexane.

4.4 Summary of LB Stability Results

The guanidinium (**G**) ions were necessary to create the space in which the guest molecules can interdigitate into. They interacted with the polar head groups of octadecanesulfonic acid (C18S) to create the inclusion gaps necessary for the interdigitatation of the guest molecules, which included linear alkane guest molecules (C18 and C18OH), guests with large functional groups (C18naph and C18chol) and guests with polar functional groups (2-HSA) were used. With the absence of diffraction peaks from the host-guest film created using 2-HSA, it can be concluded that guest molecules with a polar functional group will prevent the formation of a crystalline monolayer by disrupting the hydrogen-bonded host network of **G** and C18S.

To further investigate what can affect the stability of the (**G**)C18S host network, the deposited films that exhibited diffraction peaks were subjected to stability tests. The films were exposed to a nonpolar (hexane) or polar solvent mixture (20% THF:hexane, 40% THF:hexane, or DI water) for predetermined time periods. The immersion of the films into pure hexane resulted in a decrease in the film thickness measured from XRR despite the original guest molecules. This reduction in film thickness is attributed to hexane replacing the desired guest molecule. The electron densities of all the films immersed in hexane are illustrated in Figure 4.65.

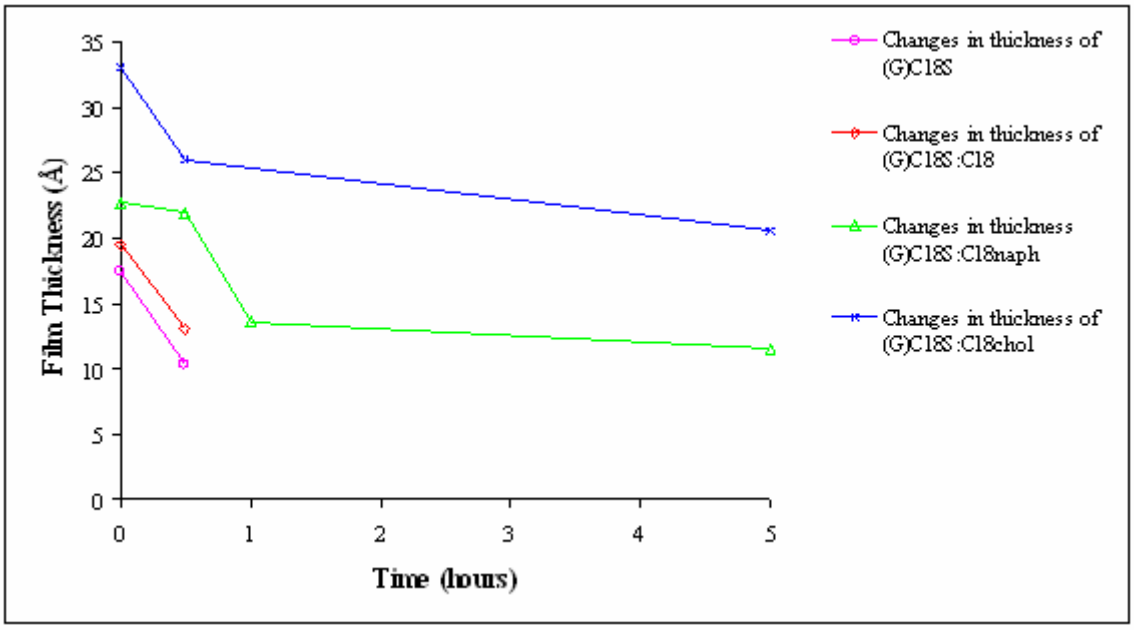

Figure 4.65. A comparison of the changes in film thickness calculated from the electron densities for all the films subjected to immersion in hexane for 30 minutes, 1 hour and 5 hours.

Figure 4.65 displays the trends in the reduction of film thickness resulting from immersion in hexane, which supports the suggestion that the hexane molecules are removing the original guest molecule and inserting themselves into the inclusion gaps. As seen from the figure, the majority of the linear alkane guest molecules (C18) were replaced by hexane within a 30 minute time period while it over an hour to for the hexane to replace the guest molecules with the large functional group (C18naph and C18chol). These trends support the idea that the large functional groups stabilize the film and prevent the hexane from readily replacing the guest molecules. Further studies using more sensitive surface measurements, such as X-ray photoelectron spectroscopy (XPS) and infrared spectroscopy (IRS), are needed to fully understand the mechanism of substitution.

When the films were immersed in a 20%THF:hexane, 40% THF:hexane and DI water, a significant reduction in the film thickness was observed from XRR measurements or no films were observed at the surface. This suggests that the THF in the mixture dissolves the thin film off the silicon surface. Due to the lack of stability of the (**G**)C18S 'host-guest' films, SAMs were explored and create the desired 'host-guest' system for the functionalization of surfaces.

4.5 Self-Assembled Monolayer Results

Self-assembled monolayers (SAMs) were investigated due to the instability of the (G)C18S LB films in polar environments. The goal of working with SAMs was to create a more stable thin film by eliminating the dependence on hydrogen bonds to create an inclusion gap in the host film for insertion of desired guest molecules. Initial experiments on the stability of SAMs were performed using octadecyltrichlorosilane (OTS) monolayer on hydroxylated silicon oxide (SiO_2) wafers. 9-octadecyl,10-trichlorosilyl anthracene was chosen as the initial synthetic target for the production of sterically hindered SAMs. The methods used for forming the self-assembled monolayer films and synthetic pathways are found in the Chapter 3. Figure 4.66 illustrates the end goal for 'host-guest' self-assembled monolayers.

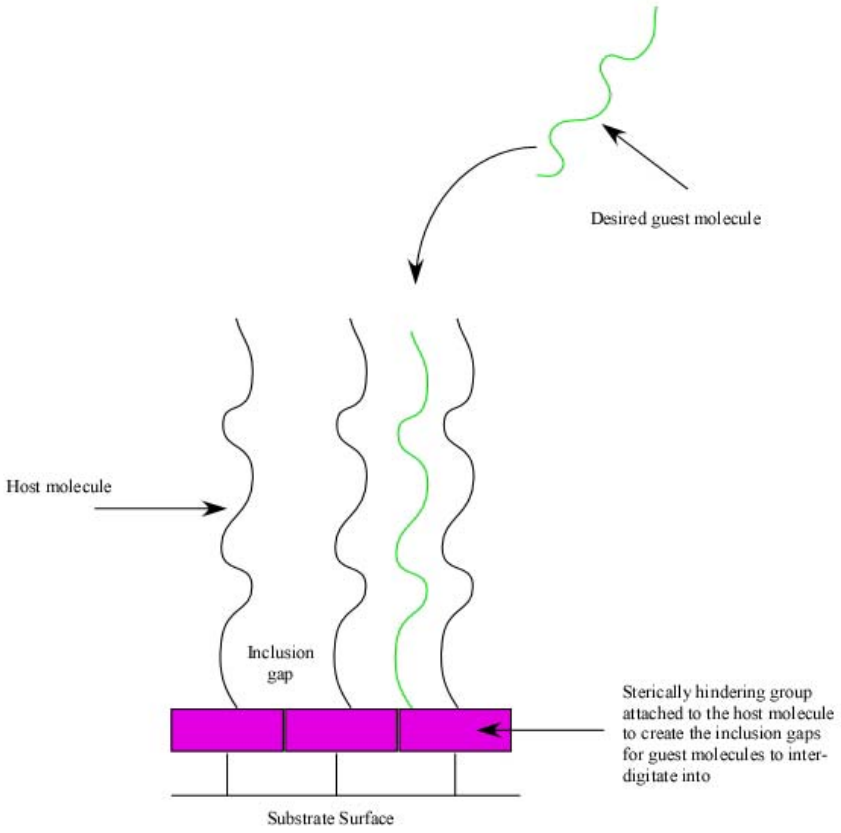

Figure 4.66. The end goal of working with SAMs is illustrate in this figure. The goal was the creation of a host molecule with a sterically hindering head group, which would create an inclusion gap for insertion of desired guest molecules without relying on hydrogen bonding.

4.5.1 Octadecyltrichlorosilane Self-Assembled Monolayers

Contact angle measurements are an effective method to determine the wetting behavior of a monolayer deposited on a surface. Considering that the OTS molecules do not contain a polar functional group ($-CH_3$), as illustrated in Figure 4.67, the coated surface would be hydrophobic preventing water from wetting the surface.

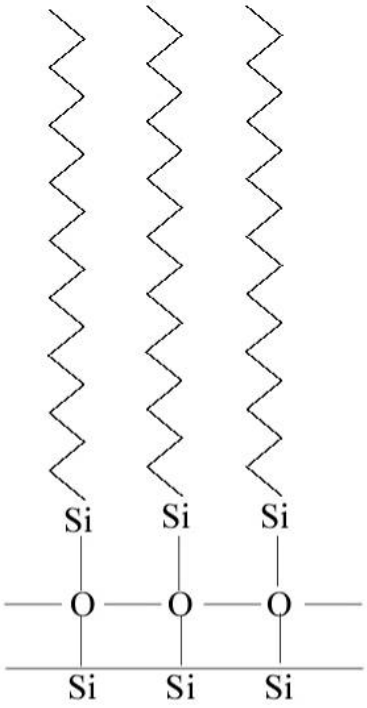

Figure 4.67. A schematic drawing of OTS SAMs deposited on a hydrolyzed silicon surface.

Contact angle measurement results of OTS SAMs were 106 °± 4°. These results were in good agreement with the angles reported in literature [4].

In order to compare the stability of the OTS SAMs to (**G**)C18S LB films, the OTS SAMs were also subjected to immersion in polar and nonpolar solvents for 30 minute time periods. Contact angle measurements were taken with water before and after immersion of the OTS SAMs in hexane and THF. For the OTS SAM immersed in hexane, the contact angle prior to immersion was 107° while the contact angle after immersion for 30 minutes was 108°± 2°. This slight increase in the contact angle suggests that not all the hexane was removed from the OTS SAM from drying under vacuum, thus causing an increase the hydrophobicity of the surface. For the OTS SAMs immersed in pure THF, the contact angle prior to immersion was 104° while the contact

angle after immersion for 30 minutes was 101°± 2°. The slight decrease in contact angle from immersion in THF suggests that trace amount of THF remained on the surface resulting in a slight increase in hydrophilicity. However, unlike the stability test results for the (**G**)C18S LB films, neither stability test resulted in the removal of the film from THF or the replacement of OTS molecules with hexane.

4.5.2 9-octadecyl,10-trichloroanthracene silane TLC and ^{1}H NMR Results

Prior to undertaking the present work, the synthetic pathway to create 9-octadecyl,10-trichloroanthracene silane was not known. The pathway was complied from different sources, as listed in the experimental section, and adapted for this synthesis. Refer to the experimental chapter for the setup, the quantities used, the purification methods employed and ^{1}HNMR results.

^{1}HNMR analysis of 9-octadecylanthracene indicated the presence of a ringed structure from the higher order shifts in the protons, which are attributed to ringed structures and the successful attachment of the carbon chain to the 9-bromoanthracene from the lower order shift attributed to carbon chains.

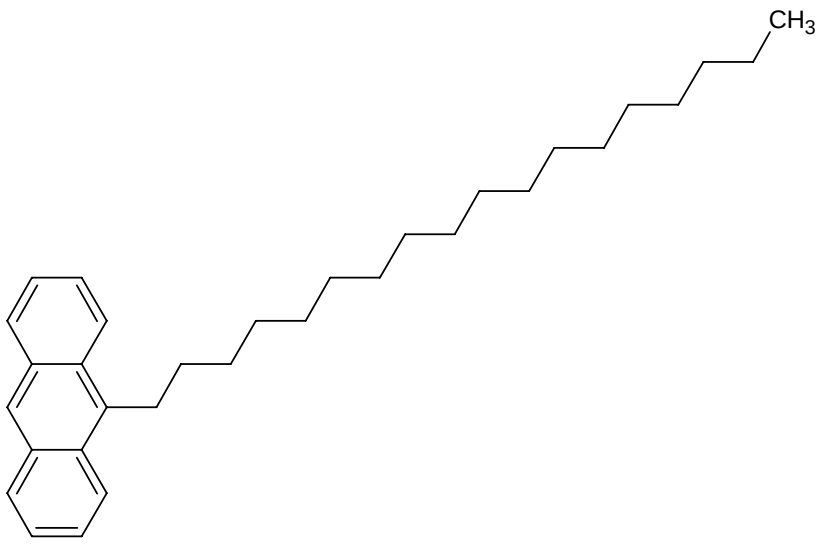

Figure 4.68. A schematic illustrating the desired product from reacting 9-bromoanthracene with 1-octadecylmagnesium bromide.

The percent yield of 9-octadecylanthracene was determined to be 4.83%, which is drastically low. This is the result of the creation of a side product that is more energetically favorable and not all the starting material reacting.

From the comparison of predicted and actual ^{1}HNMR data for 9-octadecyl,10-trichloroanthracene silane, the absences of the higher order shifts (the 2.88ppm shift) in the alkyl chain suggests that the ring structure became detached from the alkyl chain during the synthesis process.

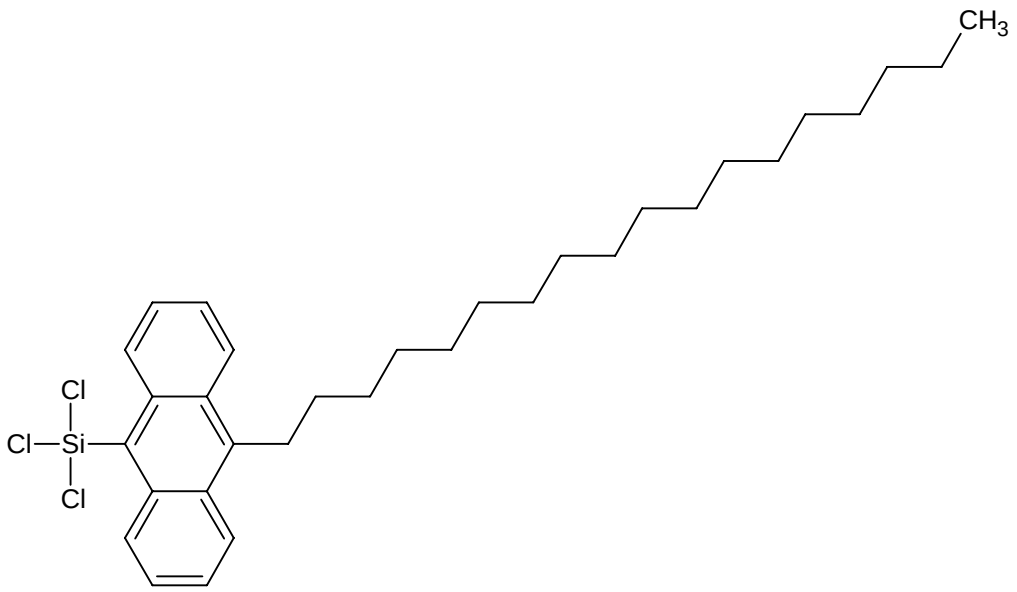

Figure 4.69. A schematic of the 9-octadecyl,10-trichloroanthracene silane, the desired end product of the synthetic pathway. Inclusion gaps for the insertion of guest molecules are build into this molecule, thus eliminating the dependence on hydrogen bonding between spacer molecules and host molecules for the formation of an inclusion gap.

Once the trichlorosilane is successfully attached, 9-octadecyl,10-trichloroanthracene silane will be used in the creation of a sterically hindering self-assembled monolayer with the guest molecule inclusion gaps already present. This will eliminate the dependence of formation of the inclusion gap on hydrogen bonding and enhancing the overall stability of the 'host-guest' thin film.

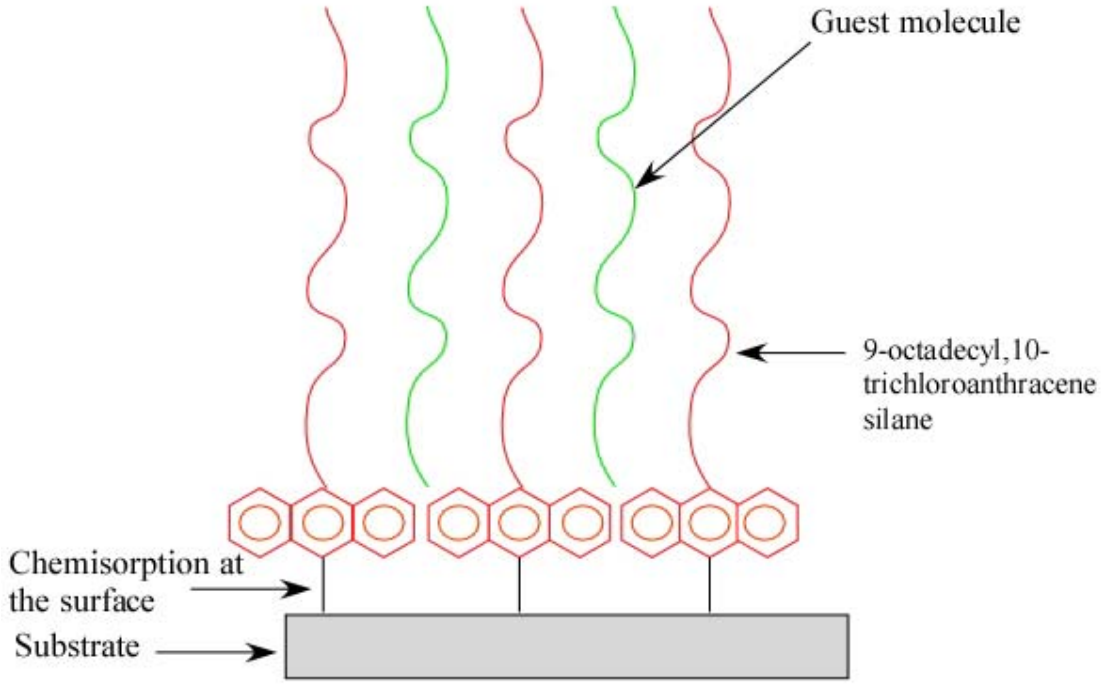

Figure 4.70. A schematic of the 'host-guest' self-assembled monolayer created using the 9-octadecyl,10-trichloroanthracene silane as the host film. The aromatic rings in the anthracene would create a gap in which the guest molecules would be able to interdigitate into.

4.6 Summary of OTS Stability Test Results and Synthesis of 9-octadecyl,10-trichlorosilanthracne

Initial experiments on the stability of SAMs were performed using octadecyltrichlorosilane (OTS) monolayer on hydroxylated silicon oxide (SiO_2) wafers. The OTS SAMs were subjected to stability tests by immersing them in pure hexane and THF in order to compare the results to LB film stability tests. The slight changes in the contact angles taken before and after the immersion were attributed to solvent remaining on the surface after being dried and not to the dissolution of the thin film. The increase in stability from the LB films to the OTS SAMs is attributed to the SAMs being

chemisorbed to the substrate surface instead of physisorbed and the SAMs not relying on a hydrogen-bonding network to generate a stable film.

9-octadecyl,10-trichlorosilyl anthracene was chosen as the synthetic target for the production of sterically hindering SAMs with the anthracene moiety acting as a spacer in the formation of host-guest monolayers 9-octadecylanthracene was successfully synthesized, but the final trichlorosilane substituted product has not yet been produced. The problems with the substitution of the trichlorosilane are attributed to the rapid polymerization of 9-octadecyl,10-trichlorosilyl anthracene upon contact with air and the introduction of contaminants during the synthetic pathway that interfered with the attachment of the trichlorosilane.

4.7 References

1. *StochFit*. 2008. p. StochFit utilizes stochastic fitting methods to model specular x-ray reflectivity or neutron reflectivity data. It provides an easy to use graphical user interface for both model dependent and model independent methods.

2. Martin, S.M., *Structure and properties of organic materials reinforced by hydrogen-bonding*, in *Chemical Engineering*. 2004, University of Minnesota.

3. Toney, M.F., et al., Thickness Measurements of Thin Perfluoropolyether Polymer Films on Silicon and Amorphous-Hydrogenated Carbon with X-ray Reflectivity, ESCA and Optical Ellipsometry. Journal of Colloid and Interface Science, 2000. **255**: p. 219-226.
4. DePalma, V. and N. Tillman, *Friction and Wear of Self-Assembled Trichlorosilane Monlayer Films on Silicon.* Langmuir, 1989. **5**: p. 868-872.

5. Summary and Future Work

Sodium octadecanesulfonate (NaC18S) amphiphiles have been reported to form crystalline monolayers when spread on an aqueous subphase containing **G** counterions, which cooperatively hydrogen bond with the sulfonate moieties and act as spacers between the amphiphiles. The formation of a crystalline monolayer is attributed to the close-packed structured formed by tilted alkyl chains in the C18S amphiphile and the **GS** intermolecular hydrogen-bonding in the monolayer [1]. GIXD studies indicated that (**G**)C18S monolayers were unable to maintain the crystalline structure when transferred from the air-water interface to a hydrophilic substrate. This is likely due to the alkyl chains being unable to tilt enough to achieve close-packing, thus producing an amorphous film.

Crystalline inclusion monolayers consisting of the host network of **G** ions and C18S amphiphiles, and various intercalated guests, can be generated at the air-water interface and transferred to a hydrophilic substrate as long as the guests are structurally homologous with the C18S [1]. Linear alkane guest molecules (Octadecane - C18, Octadecanol - C18OH), guests with large functional groups (naphthyl stearate - C18naph, cholesteryl stearate - C18chol) and guests with polar functional groups (2-hydroxystearic acid - 2-HSA) were used. The (G)C18S:2-HAS disrupted the hydrogen-bonding in the guanidinium sulfonate host network and prevented the formation of a crystalline monolayer from forming. The other guest molecules were found to form crystalline monolayers. X-ray specular reflectivity results did, however, indicate the presence of a monolayer, most likely amorphous, for these systems. Transfer of (**G**)C18S Langmuir monolayers containing C18, C18naph and C18chol guest molecules to a hydrophilic

substrate resulted in crystalline inclusion monolayers. The (**G**)C18S:C18 monolayers formed a hexagonally packed crystal structure with the alkane chains aligned perpendicular to the substrate surface, a structure that is different than those reported for (**G**)C18S:C18 monolayers at the air-water interface. The (**G**)C18S:C18naph and (G)C18S:C18chol monolayers exhibited more complex structures, suggesting that the larger functional groups play an important role in the organization of the host-guest monolayers. These results suggest a possible approach for the creation of functionalized surfaces in which non-amphiphilic molecules with a desired functionality can be attached to a surface through physisorption; however, it is clear that the reliance on the hydrogen-bonded **G**S network for the formation of host-guest monolayers limits their applications to non-polar, non-hydrogen-bonding functionalities.

To further investigate the possibility of forming a functionalized surface using a 'host-guest' LB monolayers, the stability of deposited films were studied by exposure to either a nonpolar (hexane) or polar (THF or water) solvents for various periods of time. Immersion of the (**G**)C18S, (**G**)C18S:C18, (**G**)C18S:C18naph and (**G**)C18S:C18chol films into hexane resulted in a decrease in film thickness, as determined from XRR data. The resulting altered structures are similar regardless of the initial film. These results suggest that the original guest molecule is being extracted and replaced by hexane. When the films were immersed in a 20%THF:hexane mixture, a significant reduction in the film thickness measured from XRR suggests that the THF in the mixture dissolved the thin film off the silicon surface. Films immersed in pure THF of in aqueous solutions were also removed from the surface. Due to the lack of stability of the (G)C18S 'host-guest' films, sterically hindered self-assembled monolayers (SAMs) are being explored as a

means to create a more stable host-guest monolayer system for the surface functionalization.

Initial experiments on the stability of SAMs were performed using octadecyltrichlorosilane (OTS) monolayer on hydroxylated silicon oxide (SiO_2) wafers. In order to compare the stability of the OTS SAMs to that of the (**G**)C18S LB films, the SAMs were subjected to stability tests by immersing them in pure hexane and THF. Contact angles taken before and after the immersion showed little change suggesting that the film structure is not altered by exposure to either polar or non-polar solvents. The increased stability is due to the fact that SAMs are chemisorbed to the substrate surface whereas the **G**S LB films are only physisorbed and rely on a hydrogen-bonding network to generate a stable films.

9-octadecyl,10-trichlorosilyl anthracene was chosen as the initial synthetic target for the production of sterically hindered SAMs. The integral anthracene moiety is expected to act as a spacer in the formation of host monolayer containing cavities into which functional guest molecules can be intercalated. 9-octadecylanthracene was successfully synthesized, but the final trichlorosilane substituted product has not been produced at this time. The problems with the substitution of the trichlorosilane are attributed to the rapid polymerization of 9-octadecyl,10-trichlorosilyl anthracene upon contact with air and the introduction of contaminants during the synthetic pathway that interfered with the attachment of the trichlorosilane. Suggested future efforts for the synthesis of this and other related molecules are described in the next section.

Future Work

To confirm the replacement of guest molecules by hexane in the **G**S films, GIXD patterns of the resulting films should be taken and compared to the GIXD of the control film to observe a change in unit cell parameters. It may also be instructive to perform the stability studies using a non straight-chain alkane solvent, such as cyclohexane, which should not readily intercalate into the (**G**)C18S host monolayer.

In order to observe the mechanism of hexane guest substitution in the (**G**)C18S films, alternative surface characterization methods need to be explored. Fourier-transform infrared spectroscopy (FTIR) can be used to observe the film structure by looking at the interaction of electromagnetic waves with dielectric media [2]. This takes into account the wavelength character of the light and treats the phase interference between different media in thin films samples [2]. The data acquired through FTIR measurements would allow the study of the mechanism of hexane substitution by viewing the changes of film structure as in real time.

Another characterization method that can be used is X-ray photoelectron spectroscopy (XPS), which is the tool of choice when surface composition and its depth profile are being studied [2]. In XPS, X-rays bombard the sample material, causing electrons to be ejected allowing the identification of the elements present in the sample [3]. The strengths of XPS are semiquantitative elemental analysis of surfaces without standards and chemical state analysis [3]. An XPS study would provide information on chemical composition, depth profiling, compositional distribution and thickness [4]. This data gathered from XPS measurements would provide the necessary information to fully understand the mechanism of hexane guest substitution.

In order to avoid the rapid polymerization of 9-octadecyl,10-trichlorosilyl anthracene upon contact with air, a trimethylsilane or trimethylsilane can be used instead of a tetrachlorosilane. Also, a thiol group can be attached instead, which involves the substitution of a halogen atom on an unactivated aryl halide with a –SH group using sodium thiomethoxide (NaSMe) [5]. The formation of a thiol monolayer would require the deposition of a thin film on the substrate surface. In addition, a hydrophilic headgroup, like SO_3, can be attached to the 9-octadecylanthracence molecule for studies at the air-water interface and fabrication of Langmuir-Blodgett films.

References

1. Martin, S.M., *Structure and properties of organic materials reinforced by hydrogen-bonding*, in *Chemical Engineering*. 2004, University of Minnesota.
2. *Characterization of Organic Thin Films*. Materials Characterization Series, ed. A. Ulman. 1995, Boston: Butterworth-Heinemann.
3. *Encyclopedia of Materials Characterization*. Materials Characterization Series, ed. C.R. Brundle, C.A. Evans, and S. Wilson. 1992, Boston: Butterworth-Heinemann.
4. Geng, S., S. Zhang, and H. Onishi, *XPS Applications in Thin Films Research.* Materials Technology, 2002. **17***(4): p. 234.*
5. *Dou, R.-F., et al., Self-Assembled Monolayers of Aromatic Thiols Stabilized by Parallel-Displaced π−π Stacking Interactions.* Langmuir, 2006. **22**(7): p. 3049-3056.

Appendix A – Sample calculation for 1:1 molar LB film solution

Composition of NaC18S "stock" solution:

Mass of NaC18S:	0.0104 g
Mass of $CHCl_3$:	23.62 g
Mass of Methanol:	3.38 g
Concentration:	$0.000289 \frac{g\ NaC18S}{g\ CHCl_3}$

Composition of C18S "stock" solution:

Mass of C18:	0.0120 g
Mass of $CHCl_3$:	23.00 g
Concentration:	$0.000522 \frac{g\ C18}{g\ CHCl_3}$

For a 1:1 molar mixture of NaC18S(C18):

Target solution of $0.1 \frac{mg\ NaC18S}{mL}$

$$10\text{mL} * 0.1 \frac{mg\ NaC18S}{mL\ CHCl_3} * \frac{1g}{1000mg} * \frac{1g\ CHCl_3}{0.000289g\ NaC18S} = \boxed{\textbf{3.4g of NaC18S "stock"}}$$

1.0 mg NaC18S = $2.805 * 10^{-6}$ moles (using its molecular weight)

$$2.805 * 10^{-6}\text{moles} * 254.5 \frac{\text{g C18}}{\text{mol}} * \frac{g\ \text{CHCl}_3}{0.000522\text{g C18}} = \boxed{\textbf{1.367g of C18 "stock"}}$$

These quantities were then weighed out into a vial and 10 mL of $CHCl_3$ was added. The vials were then sonicated for at least 20 minutes to produce a uniform dispersion of the mixed monolayer.